Study of Physiological Parameters of the Human Body for Variability: Case Study of Heart

Thesis submitted to Goa University

for the award of the degree of

`

DOCTOR OF PHILOSOPHY

In

Electronics

By

Mr. NOEL GERVASIO TAVARES

UNDER THE GUIDANCE OF

Dr. RAJENDRA S. GAD

Department of Electronics

Goa University, Goa- 403206

August 2019

Dedicated

To my parents

Nicholas Natividade Tavares

&

Effie Gretty Tavares

DECLARATION

I state that the present thesis entitled "Study of Physiological Parameters of the Human Body for Variability: Case study of heart", is my original contribution and the same has not been submitted on any occasion for any other degree or diploma of this or any other University or Institute to the best of my knowledge the present study is the 1st comprehensive work of its kind in the area mentioned. The literature related to the problem investigated has been cited. Due acknowledgments have been made whenever facilities and suggestions have been availed of.

Place: Goa University

Research Candidate

Date: August 2019
Mr. Noel Gervasio Tavares

CERTIFICATE

This is to certify that the thesis entitled, "Study Of Physiological Parameters Of The Human Body For Variability: Case Study Of Heart" submitted by Mr. Noel Gervasio Tavares for the award of degree for doctor of philosophy in electronics, is based on his original and independent research work carried out by him during the period of study, under my supervision. The thesis or any part thereof has not been previously submitted for any other degree or diploma of this or any other university or institute.

(Dr. Rajendra S. Gad)   **(External Examiner)**

Research Guide

Place: Goa University

Date: August 2019

ACKNOWLEDGEMENT

ABSTRACT

The accurate measurement of human blood pressure, is a growing need in recent years, to obtain prior information about heart-related risks. The blood pressure measurement is based on the principle of oscillometric and auscultatory methods. The currently available devices use one of these principles or combined information of both the principle to compute systolic and diastolic pressure. In this work, we have developed a pressure meter that is based on the principle of the oscillometric and auscultatory method. Further, to combine the information from the oscillometric and auscultatory signal, we present a complementary data fusion approach that fuses the data to improve the accuracy of the measurement. However, the parameters for our complementary information fusion are optimized for systolic and diastolic pressure sample data points generated using the Windkessel approach. The experimental results were obtained to measure the systolic and diastolic pressure for three types of patients that include Normal, Hypertension, and Hypotension. The better accuracy measurement of around 90% is obtained using our approach of complementary information fusion for α = 0.5 value. Further, the proposed data fusion scheme compliments the information from various sensors, that enables the potential scope in a health care facility to improve the completeness of the system under observation.

Human body physiology is regulated through the central neural control (CNS) which takes the signal from the respiratory system and ambiance which signifies atmospheric pressure, temperature and various gases in the environment. The central nervous system then controls the metabolic control of various organs through the afferent nerves and the efferent nerves reflecting the various reflex of the organs to the CNS, which regulates the cardiovascular system (CVS) for the stroke volume (SV) of the blood and heart rate (HR). The SV and HR collectively synthesize the cardiac output of the heart balancing the body for the coherence or non-coherence states. We have defined and simulated here in this work the Neural Mass Model (NMM), which is one of the components which feeds the CNS and controls the cardiovascular system for the human blood pressure (ABP) and heart rate. We have defined and simulated arterial blood pressure model, i.e., Windkessel model; describing the arterial blood pressure for the particular input volume of the blood and ECG

model for the computing heart rate and heart rate variability (HRV). The integration of CNS, Windkessel and EEG model has thrown light on some aspects of sympathetic and parasympathetic of ANS for further improvisation and experimentations. Brain-Computer Interface (BCI) provides an alternative way for humans to communicate with the external environment. BCI systems can be of great help to people with severe motor disabilities who cannot perform normal daily activities. In this work, we introduce a novel steady-state visual evoked potential (SSVEP)-based brain-computer interface system that controls home appliances like an electric fan, tube light, etc. The designed system aim is to extract the SSVEP signal and then classify them using multiclass SVM. We confirmed the generation of SSVEP frequencies in the online analysis using Fast Fourier Transform. The classification of SSVEP signals is done using multiclass SVM.

Finally, a preliminary study was done on the use of SSVEP BCI paradigm for biometric studies and the results were found to be promising.

List of Publications

1. Tavares N.G., Gad R.S., 'Steady-state visual evoked potential-based real-time BCI for smart appliance control', Cognitive Informatics and Soft Computing, Ed. by: Mallick, P.; Balas, V.; Bhoi, A. and Zobaa, A. Advances in Intelligent Systems and Computing, 768. Springer, Singapore. 768; 2019; 795-805.

2. Tavares N. G., Gad R.S., Hernandez A. M., Kakodkar U., Naik G. M., 'Autonomic Nervous System for Sympathetic and Parasympathetic for Cardiac Event Coherence. In: Mallick P., Balas V., Bhoi A., Zobaa A. (eds) Cognitive Informatics and Soft Computing. Advances in Intelligent Systems and Computing, Vol 768.   Springer, Singapore, 768; 2019; 795-805.

3. Noel Tavares, Kenneth S. Lobo and R. S. Gad, "Steady-State Visual Evoked Potential-Based Real-Time BCI for Smart Appliance Control", International Journal of Pure and Applied Mathematics, Volume 118 No. 19 2018, 177-189.

4. Noel Tavares and R.S, Gad, "Steady State Visually Evoked Potentials(SSVEP) Review in Cognitive Neuroscience" in 11th Annual National Symposium on "VLSI and Embedded System", Goa University, March 2018.

5. Wilbert Cardoso, Arjun Pednekar, Noel Tavares, R.S. Gad, "Biometric System Using Brain Waves" in 11th Annual National Symposium on "VLSI and Embedded System", Goa University, March 2018.

6. Lobo, K.; Palni, M.; Naik, N.; Tavares, N.; Gad, R.S., "Mind Controlled Automation with P300 Waves", Proc. Nat. Conf. On Science Education and Research (NCSER 2016), Bangalore, India, Dec 2016. 2016; 5pp.

7. Fernandes, I.; Tavares, N.; Vetrekar, N.T.; Gad, R.S.; Naik, G.M.: Design of human blood pressure meter based on oscillometric and auscultation. Poster. 4. Bharatiya Vigyan Sammelan and Expo (BVS-2015),5-8 Feb 2015.

8. Noel, T.; Gad, R.S.: Human physiological parameters analysis using EEG heat maps. 9. Indian Conf. on Computer Vision, Graphics and Image processing, ICVGIP-2015. IISc, Bangalore. 14 Dec 2015-17 Dec 2014.

Table of Contents

List of Figures

List of Tables

List of Symbols and Abbreviations

AAMI   Association for the Advancement of Medical Instrumentation

ABP   Arterial Blood Pressure

AC   Alternating current

ADC   Analog-to-digital converter

ANS   Autonomic nervous system

ANSI   American National Standards Institute

ARM   Advanced RISC Machines

AV   Atrioventricular node

BCI   Brain–computer interface

BHS   British Hypetension Society

BP   Blood pressure

Bpm   Beats per minute

CCA   Canonical Correlation Analysis

CNN   Convolutional Neural Network

CNS   Central Nervous System

CV   Cardiovascular

CVS   Cardiovascular system

dB   Decibels

DBP   Diastolic blood pressure

DC   Direct current

DFT   Discrete Fourier Transform

DTF   Directed Transfer Function

DALY   Disability-adjusted life year

ECG   Electrocardiogram

ECoG   Electrocorticography

EEG   Electroencephalogram

EOG   Electrooculography

EPSP   Excitatory post synaptic potentials

FIR   Finite Impulse Response

FFT   Fast Fourier transform

FMRI   Functional Magnetic Resonance Imaging

GABA γ-aminobutyric acid

HF   High frequency

HR   Hear Rate

HRV   Heart Rate Variability

Hz   Hertz

IPSP   Inhibitory post synaptic potentials

ISO   International Organization for Standardization

kPa   kilopascal

LPM	Liter per minute
LCD	Liquid Crystal Display
LED	Light Emitting Diode
LF	Low frequency
LFP	Local Field Potentials
LPC	Linear Programming Control
LPF	Low pass filter
MAP	Mean Arterial Pressure
MATLAB	Matrix Laboratory
MCU	Microcontroller unit
MEG	Magnetoencephalography
MLP	Multi-layer perceptron
MRI	Magnetic Resonance Imaging
mA	Milliamperes
ml	Milliliter
mV	Millivolts
mmHg	Millimetre of mercury
NIBP	Non-invasive blood pressure
NMM	Neural Mass Model
NTS	Nucleus Tractus Solitarius

OAA	One against all
OAO	One against one
P300	Positive peak occurring 300ms after an infrequent stimulus
PET	Positron Emission Tomography
PNS	Parasympathetic nervous system
PPG	Photoplethysmography
PSP	Post synaptic potentials
PTT	Pulse Transit Time
RK-4	Runge-Kutta 4th order
ReLU	Rectified Linear unit
ROI	Region of interest
SA	Sinoatrial node
SBP	Systolic blood pressure
SCP	Slow cortical potentials
SD	Standard deviation
SNR	Signal-To-Noise-Ratio
SNS	Sympathetic nervous system
SRT	Stress Reduction Theory
SSEP	Steady State evoked potentials
SSVEP	Steady-state visually evoked potentials

SV	Stroke volume
SVM	Support Vector Machines
SVR	Systemic vascular resistance
TPR	Total peripheral resistance
ULF	Ultra low frequency
VEP	Visually evoked potentials
VLF	Very low frequency
WHO	World Health organization
π	pi
CarOP	Cardiac output
C_1	lumped compliance of the proximal large arteries
C_2	lumped compliance of the distal muscular arteries
L	inertance of flowing blood
p_1	pressure in chamber one
p_2	pressure in chamber two
q_{in}	left ventricular stroke volume per beat
q_0	maximum input amplitude w.r.t cardiac output
q_{out}	output stroke volume per beat
R	peripheral resistance
T_{sys}	duration of left ventricle ejection

Time   duration of cardiac cycle

u   average membrane potential

v_1 volume in chamber one

v_2 volume in chamber two

f_c cut off frequency

Chapter 1

Introduction

1.1   ORIGIN OF RESEARCH PROBLEM

In general, it has been discovered that people with access to neighboring natural environments are healthier than other people. Long-term, indirect effects also include enhanced rates of satisfaction with one's home, one's job, and life in general [1]. City authorities had a powerful faith in the potential health benefits that would result from open space when parks were first built in the nineteenth century [2,3]. Parks were expected to decrease disease, crime, and social unrest and provide the town with' green lungs' and leisure places [3]. These assumptions were used to justify offering urban parks and other natural regions and maintaining wilderness areas outside towns for government use [4,5]. Contact with nature in an urban park environment can be experienced through a variety of means, including viewing natural scenes, being in natural settings, encountering plants and animals, taking part in recreational activities, undertaking environmental conservation work, and participating in nature-based therapy programs. A broad range of study findings indicate that exposure to nature may affect the functioning of physiology. For instance, researchers have discovered that greater levels of well-being and life satisfaction were associated with window opinions of nature from the office and home [6,7].Some researchers[8] showed that among kids residing in urban settings, those who had daily opin ions of nature (e.g., a tree outside their apartment window, rather than a concrete perspecti ve) performed better on assignments that measured working memory (backward digit span, backward alphabet span), impulse inhibition (fitting familiar figures task), selective attenti on (Stroop color-word span) and concentration (pattern control assignment for Necker Cube). These findings indicate that there may be a variety of significant benefits connected with increased exposure to natural settings. Benefits from exposure to nature were also noted over different exposure durations; from a few minutes of viewing pictures, to hour-

long or multi-day wildlife experiences, to life-long proximity to greenspace. The variety of findings indicates that the psychological functioning effect of nature experience can be both prevalent and robust.Two significant theories were suggested to explain the restorative advantages of nature. They indicate that one helpful way to categorize the literature's empirical findings is to differentiate between the affective and cognitive benefits of the experience of nature.

1.2   Complexity in the Human Physiological System

Increased consistency is correlated with beneficial modifications in multiple physiological functional dimensions, which in turn are associated with psychological advantages. We present this debate by explaining how the quantity of data traveling through the afferent nerves rises during coherence, and then we examine the role that cardiac afferent input plays in pain perception, pulmonary function, emotional processing, and cognitive performance of neural pathways.

Over the previous several centuries, several lines of scientific evidence have shown that the heart works as a sensory organ and as a complicated encoding and processing center of data far more than a mechanical pump.In the comparatively new field of neurocardiology, groundbreaking research has shown that the heart has an enormous intrinsic nervous system that is sufficiently advanced to qualify as a "little brain" on its own. In 1991, Pioneer neurocardiology researcher Dr. J. Andrew Armour first defined the heart brain's anatomical organization and function [9]. It's complicated circuitry, which contains over 40,000 neurons, allows it to sense, control and remember. In addition, the heart brain can process data and make choices independently of the central nervous system about cardiac control [10,11]. The heart brain senses, translates hormonal, heart rate, and blood pressure signals into neurological impulses, and processes this data internally. It then sends the data in the vagus nerves and spinal column via afferent pathways to the central brain. When the sensory neurites in the core detect distinct hormones or neurotransmitters in the bloodstream, the pattern in the afferent cell output sent to the brain is changed [12].In other words, in relation to its better known tasks, the heart is also a sensory center that detects and transmits data about the regional blood flow's biochemical content. In controlling the function of organs and structures throughout the body, neurological signals originating in the core have a significant and widespread impact. For

instance, it is now recognized that in relation to modulating nervous and endocrine system activity, cardiac input affects digestive tract activity, urinary bladder, spleen, respiratory and lymph systems, and skeletal muscle activity [13].Cardiovascular afferent signals in more particular terms control efferent outflow of ANS [14] modulate pain perception [15] and hormone manufacturing [16]. The activity of the locus coeruleus and pyramidal tract cells in the motor cortex is influenced [17,18]. Also, excitability of the spinal cord differs directly with the heart pulse, as does in ordinary skeletal muscle physiological tremor [19]. An important fact is the impact of the heart on perceptual and cognitive function through its input into greater brain centers beyond the main role of cardiac afferent signals in physiological regulation. So far, we have discussed behavioral information indicating a connection between the input of the heart and cognitive performance as well as demonic electrophysiological studies. Psychophysiologist Rainer Schandry's experiments in Germany have shown that afferent heart input evokes similar cortical reactions to 'classical' sensory event-related potentials. These studies have shown that cardiovascular afferent input is accompanied by particular modifications in the electrical activity of the brain. Schandry and peers have discovered that this activity is most pronounced in the frontocortical fields, a region that is particularly engaged in the processing of visceral afferent data. In addition, psychological factors such as cardiac sensitivity, sensitivity to perception, and motivation were discovered to modulate cortical heartbeat evoked potentials in a manner similar to the cortical processing of external stimuli [20,21,22,23]. In another study it was examined that the electrophysiology of the processing of information in relation to intuition, and also it was found that the afferent input of the heart significantly modulates frontocortical activity. The observation that the afferent contribution of the core modulates frontal activity is consistent with other results that activity covaries with modifications in heart rhythm in the prefrontal cortex [24]. This is compatible with the reciprocal links in neural systems biological principle. Thus, in relation to well-established paths (e.g., the thalamic pathway) through which cardiovascular afferent signals modulate greater cortical function, extra paths from the core to the prefrontal cortex may well be available.

1.2.1 Complexity of Cardiac Afferent Signals

One of the micro-pattern hypothesis fundamental assumptions is that there is a one-to-one correspondence between each heartbeat and the neural activity bursting from cardiac mechanosensory neurites into the brain. However, the dynamics of generating and transmitting cardiovascular afferent input require many kinds of neurons and a multiplicity of processes working over distinct moment scales at the stage of the macro-scale heart brain interactions studied here. About 40,000 sensory neurites are engaged in transmitting afferent data to the brain in the human core. Only 20 percent of these are mechanosensory cells. Of this 20%, only a small proportion actually fire in unison with each heartbeat. Moreover, there are at least five different types of mechanosensory neurons. Nearly all mechanosensory neurons are susceptible to change frequency, as their concentrations of activity rise in reaction to system change in a nonlinear way. Some only improve their firing rate when blood pressure drops, while others only increase during increased pressure. Others are only susceptible to big heart rate or blood pressure change rate motions [25]. Thus, there is only a minority of sensory neurites whose output activity shows a one-to-one connection to heartbeat and regional changes in blood pressure. To add to the complexity, the intrinsic nervous system of the heart has both short and long-term memory that affects cardiac (and therefore afferent) function over two different time scales: (1) changes in patterns of activity resulting from rapid changes in local mechanical status over milliseconds; and (2) variations in patterns of worldwide activity operating over time scales of seconds to minutes [25,26]. Therefore, in relation to data linked to a single cardiac cycle, there is also rhythmic data that can modulate brain activity over longer time scales. The fact that many of the neurons mainly react to change frequency and that changes in activity patterns can last for minutes is significant considerations in knowing how cohesion affects heart-brain interactions and can have an expanded carry-over impact. This is because the rate of change in beat-to-beat variation of both heart rate and blood pressure is increased in the coherence mode, in relation to the enhanced order in the cardiovascular system's spatial activity patterns. While the overall amount of afferent neural activity reaching the brain is likely to be the same or nearly the same from one heartbeat to the next under normal pressure variations and heart rates, it is our contention that the macro-scale patterns of neural activity may be quite different. Wölk and Velden

produced a significant observation in this respect in noting that the frequency and stability of the afferent input were significant variables influencing the efficiency of the sensory motor [27,28]. However, in this context, we recommend that the activity pattern idea is more suitable than the frequency idea. This is because data is encoded in the interspike interval (the temporal space between successive neural activity spikes). Thus, the significance of the data embedded in the signals is contained in the general pattern of activity and not simply its frequency. In addition, we consider the pattern's stability over longer time scales, from seconds to minutes. Therefore, in order to comprehend the impacts of cardiovascular afferent signals on the brain, in relation to stimulus intensity, heart rate and pressure, the rhythmic pattern of the heart over longer time scales must also be regarded as a significant factor in itself. As we have seen, the macro-scale pattern of the operation of the heart is likely to have a much higher impact on performance than the effects of the internal cardiac cycle.
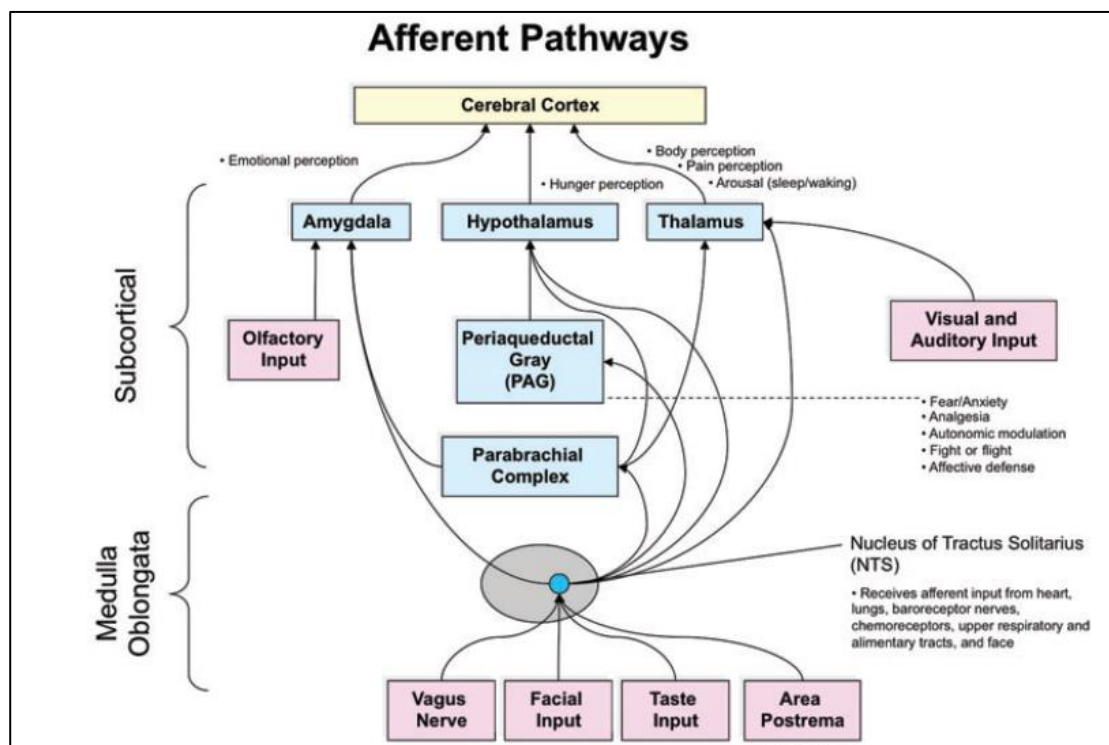
Figure 1.1: Different afferent pathways

1.2.2   Afferent Input to Brain Centers other than the Thalamus

Another significant factor in relation to heart-brain relations is that while the micro-pattern model focuses exclusively on cardiovascular thalamus input, there are other neural pathways through which the input of the heart can modulate cortical activity and therefore performance. As shown in Figure 1.1, cardiovascular inputs from the vagal afferent nerves first reach the tractus solitarius nucleus (NTS) and then travel straight to the parabrasive complex, periacqueductal gray, thalamus, hypothalamus, and amygdala. The afferent inputs then migrate from the amygdala, hypothalamus, and thalamus to the cerebral cortex through links. The presence of afferent pathways from the medulla straight to the prefrontal cortex is also suggested [29]. While this diagram demonstrates mainly the afferent pathways one-way input flow to the brain, in most instances the areas are interconnected reciprocally so that data flows in both directions. This reciprocally interconnected network enables ongoing positive and negative feedback interactions and autonomous reactions to be integrated with the processing of perceptual and sensory data. Moreover, the various parallel distributed pathways allow various ways to process a specified response. The third way the image is more complex is that while the hypothesis of Wölk and Velden considers only the alpha rhythm, there are other brain rhythms linked to the core as well. These include both beta rhythm and reduced brain activity frequency. Therefore, the impacts of macro-scale cardiovascular dynamics on other elements of brain activity are also likely to be crucial in contributing to greater performance changes.

1.2.3   Vagal Afferent Traffic

However, the vagus nerve is a significant duct which is relayed to the brain by afferent neurological signals from the core and other visceral organs. Psychophysiologist Paul Lehrer has shown that a lasting increase in baroreflex gain is achieved independently of respiratory and cardiovascular changes by using heart rhythm feedback to facilitate a state of physiological coherence (which he calls "resonance"), demonstrating the neuroplasticity of the baroreflex system [30].This change in baroreflex gain shows that the activation threshold of some of the mechanosensory neurons in the baroreflex scheme is reset with repeated episodes of consistency and consequently these neurons boost their production accordingly. Furthermore, a fundamental property of mechanosensory neurons is that they usually boost their output in reaction to a rise in the pace of change in the function to which they are tuned (heart rate, blood pressure, etc.).There is an increase in beat-to-beat

variation in both heart rate and blood pressure during heart rhythm consistency, which is equal to a rise in change rate. As a result, the vagal afferent traffic sent to the brain from the core and cardiovascular system will boost. With frequent exercise in keeping the mode of consistency, it is also probable that increased vagal afferent traffic would be observed even if one is not in this mode. This is due to the reality that the threshold of the mechanosensory neurons is reset as a consequence of the exercise of consistency building, thus creating a fresh level of afferent traffic baseline. There are a number of potential advantages to generating an increase in vagal afferent traffic through non-invasive methods such as heart-based emotion refocusing methods and heart rhythm coherence feedback. A number of clinical apps have been identified in latest years to boost vagal afferent traffic; however, the rise in afferent activity is generally produced by implanted or external instruments that boost vagal afferent pathways, typically in the left vagus nerve. An increase in ordinary inherent concentrations of vagal afferent traffic has been discovered to inhibit pain pathways at the stage of the spinal cord from the body to the thalamus and a latest research discovered that stimulation of afferent vagal cells considerably decreases cluster and headaches of migraine [31].It has also been shown that vagal nerve stimulation improves cognitive processing and memory [32] findings consistent with those of several latest individual research using cohesion-building methods for heart rhythm.

1.2.4   Emotional Processing

Afferent heart input, and especially the heart rhythm pattern, also plays a main role in emotional experience. One researcher in his study proposed a basic connection between feelings and changes in patterns of both efferent and afferent autonomous activity, as well as changes in ANS activation that are obviously reflected in changes in patterns of heart rhythm. The experience of adverse feelings is represented in more erratic or disordered heart rhythms, suggesting less synchronization in both the operation of parasympathetic outflow-regulating brain structures and the reciprocal action between the parasympathetic and sympathetic branches of the ANS. In comparison, a strongly ordered or consistent pattern in the heart rhythms is connected with continuous favorable feelings, reflecting higher general synchronization in these same systems. However, it is essential to stress that the rhythmic running patterns of the heart not only represent the emotional state of the

individual, but also play a direct part in determining mental experience. At the physiological stage, as shown in Figure 1.1, afferent heart input is transmitted to several subcortical brain areas engaged in emotional processing, including thalamus, hypothalamus, and amygdala. In addition, cardiac afferent input has an important impact on brain center activity [32,33,34,35,36,37]. For instance, amygdala activity is discovered to be synchronized with the cardiac cycle [35,37]. These understandings support the claim that afferent heart data is directly engaged in emotional processing and emotional experience.

1.3   Coherence in Cognition for Nature Experience

The theory of stress reduction (SRT) offers an explanation for the effect on the effect of nature experience. This theory suggests that the restorative benefit of natural settings over artificial settings is due to the role they played in our species development [38]. More specifically, according to this perspective, because of our inherent attachment to the natural world, nature scenes activate our parasympathetic nervous system in ways that decrease stress and autonomic excitement. Particular natural landscapes tended to provide 'possibilities' for benefit for human beings and safe locations of 'shelter'. The viewing of these kinds of landscapes activates our physiology in affectively beneficial ways, according to Ulrich et al. [39], helps to develop an inherent preference for these kinds of settings. In support of SRT, it has been shown that viewing photographic pictures and videos of natural landscapes reduces skin behavior, heart rate and other physiological stress indices [39,40,41]. Likewise, walking through trees and other natural scenery decreases concentrations of cortisol [42,43]. Besides these changes in physiological stress measures, a 50-minute walk through a natural environment may have a beneficial effect [44,45,46]. After monitoring for population and socioeconomic variables [47,48,49], proximity to green space has been shown in other cross-sectional and longitudinal research to encourage reduced rates of "mental distress" and stress, as well as higher psychological well-being. For instance, many psychological disorders are correlated with modifications in other effect dimensions, including anxiety, rumination, and negative mood rises. Importantly, previous studies did not specifically assess anxiety or rumination, although

some used scales that may partially reflect anxiety changes [47]. Ulrich's theory provides a number of testable hypotheses about the impact of nature on the autonomic nervous system, and these were tested during their exposure to various settings through the use of individual physiological measurements. These results show that extensive nature exposure can decrease stress and increase positive impacts. If improvements in mental health result from decreased exposure to nature could be expected to extend beyond stress and positive mood the affective impacts.

According to ART, natural environments invoke a distinct kind of attention from individuals – a feeling of "fascination," "being away," "extent," and "compatibility" – which can lead to a replenishment of focused attention because they are less taxed in these alternative settings. This, in turn, may lead to improved performance on tests that measure memory and attention. Consistent with ART, [50] found that dormitory students who had views of nature through their windows performed better on tasks that require concentration (Necker Cube pattern test) than students without such views. Some researcher's [51] proved nature's restorative influence on suspended attention, demonstrating that respondents who viewed nature pictures performed better on the assignment than those who saw urban environment pictures.

1.3.1 Effects of Yoga on Human Health

Yoga is an ancient Indian science that, with its different methods, designs the way of life. It is performed by professionals in a variety of techniques and styles in the form of Asana (Posture), Pranayama (breathing manipulation), Meditation (concentration method), etc.Pranayama is one practice discovered to be efficient in many respects for human physiology. The Sanskrit term Pranayama includes two sections namely Prana (means essential force) and Yama (means control). It literally implies a yogic act conducted to control the flow of essential energy that governs the body's entire physiological cycle.Pranayama is one practice discovered to be efficient in many respects for human physiology.In humans, the breath is an active link between body and mind, while the Pranayama is deemed to manipulate one-time own breathing. Different kinds of pranayama generate specific physiological responses and are highly dependent on the practice type and length. Among them are well established Nadisuddhi, Savitri,

Kapalbhati, Bhasrika, BhramariPra-nayama, etc. [52,53,54]. Pranayama reduces dead space ventilation by ongoing exercise and decreases breathing job. In comparison to the shallow breathing that only refreshes the base of the lung, the entire lung is ventilated. Practicing pranayama frequently has a beneficial effect on cardiovascular and respiratory functions, demonstrates the parasympathetic (vagal tone) dominance of the autonomous system. This increases general physical and mental health. Yoga practice has also been reported to be efficient in correcting circumstances of hormonal imbalance and other illnesses such as hypertension, anxiety, and depression. It's calming impact also helps in overcoming drug addiction.

1.3.2   HRV in Physical Activities

Research has shown the impact of somatic and cognitive anxiety on sports result measures. Competitive stress method includes the perception of a significant imbalance between environmental demand and the ability to respond. This imbalance is seen to have significant effects on the outcome [55].It has been shown that elevation in sympathetic tone as marked by anxiety and decreased heart rate variability patterns are controlled by breathing regulation [56]. In addition, to boost efficiency, cognitive behavioral therapy directed at decreasing anxiety has been documented [57]. The ability to overcome pressure and anxiety is an integral part of sports, particularly among elite athletes [58,59].

1.4 Coherence in Physiological System of Body

Organizing the many interconnected neural networks within the brain enables maximum flexibility to adapt to evolving requirements, such as focusing on an external sensory input or an inner process. The degree of coupling, however, which controls synchronized network activity, differs depending on the moment's requirements. The system is less willing to dynamically employ the suitable neural support mechanisms that it requires to react to a specific demand when the network is either excessively coupled or too loosely coupled. For example, when the neural populations in the brain are more closely linked, the alpha rhythm increases in amplitude and distribution, which occurs when the brain regions involved do not process information. Cognitive efficiency is decreased under these conditions, in particular that involves processing external sensory data. This generally implies that one should not be too relaxed (enhanced coupling) or overly stimulated

(reduced coupling) in terms of optimizing efficiency. Thus, taking into account the outcomes of our cognitive performance and heart-brain synchronization research mentioned above, the psychophysiological coherence mode appears to be a condition under which optimal coupling and thus enhanced performance happens across a variety of body structures. This is important in understanding the relationship between global coherence, emotional stability, and optimal performance. Whatever the mechanisms that enable synchronous activity in distant cell assemblies turn out to be, it is evident that input from the core to the brain impacts the thalamus ' activity and its capacity to synchronize cortical activity. The procedures that are accountable for the synchronization of remote cells in the brain are even more complex as there are local and global synchronization levels as well as interactions at local and global level.

1.5   Motivation

It is estimated that increased blood pressure is causing 7.5 million fatalities worldwide, about 12.8 percent of all fatalities. This represents 57 million life years adjusted for disability (DALYS) or 3.7% of total DALYS. Heightened blood pressure is a significant risk factor for heart disease and ischemic and hemorrhagic stroke. It has been shown that blood pressure levels are favorably and continually associated with the danger of stroke and coronary heart disease. For each 20/10 mmHg increase in blood pressure, the danger of cardiovascular disease doubles in some age groups, beginning as low as 115/75 mmHg. Complications of increased blood pressure include heart failure, peripheral vascular disease, kidney deficiency, retinal hemorrhage, and visual impairment in relation to coronary heart disease and stroke. A decrease in cardiovascular complications is connected with the treatment of systolic blood pressure and diastolic blood pressure up to 140/90 mmHg. Overall, in 2008, the overall incidence of increased blood pressure in adolescents aged 25 years and older was about 40%. Between 1980 and 2008, the percentage of the world's high blood pressure population, or uncontrolled hypertension, dropped modestly. However, the proportion of individuals with uncontrolled hypertension grew from 600 million in 1980 to nearly 1 billion in 20 due to population growth and ageing. In Africa, where it was 46 percent for both sexes coupled, the incidence of

increased blood pressure was highest across the WHO areas. Both males and females in the African area have elevated levels of increased blood pressure, with prevalence rates above 40%. For both sexes, the lowest prevalence of increased blood pressure was 35 percent in the WHO Region of the Americas. The incidence of males in this area was greater than that of females (39% for males and 32% for females). Men have a significantly greater incidence of elevated blood pressure in all WHO regions than females. This distinction in the Americas and Europe was only statistically important.
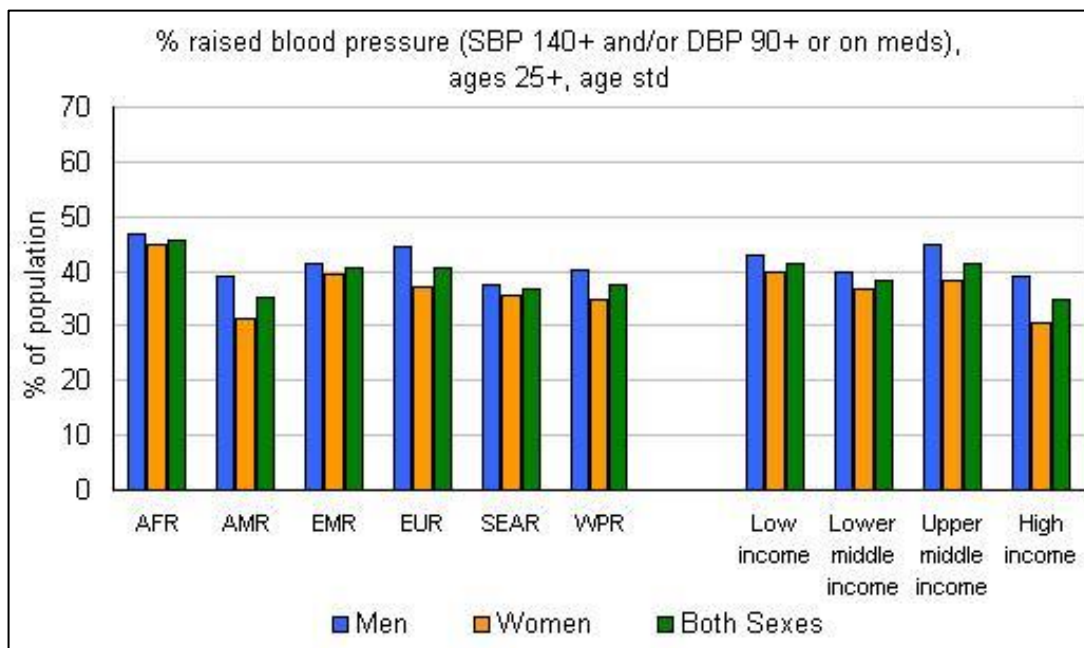
Figure 1.2:   Prevalence of blood pressure across the globe in different income categories

The incidence of increased blood pressure was constantly high across countries revenue groups, with low, lower middle and upper middle nations all at levels of around 40% as shown in in Figure 1.2. The incidence was smaller in high-income nations at 35%. Here based on the above understanding the research problem was framed with following objectives.

1.6   Objectives of Research:

➢ Collect the database of various modalities available.

- ➢ Modeling the system for the HRV using parameters like ECG, Human blood pressure and EEG (Neural Mass Model).

- ➢ Integrating the setup for the measurement of ECG, Human blood pressure and EEG (Neural Mass Model).

- ➢ Establishing data acquisition for the said system.

- ➢ Establish the time domain analysis for the modalities.

- ➢ Establish the frequency domain analysis for the modalities.

- ➢ Exploring the relation with the Sympathetic and parasympathetic system of body.

1.7 Thesis organization

Chapter 2 discusses the various state of the art techniques used to measure human physiological parameters like arterial blood pressure EEG, ECG etc. Also literature survey is discussed on SSVEP paradigms. Finally, we conclude the chapter by mention the work done to achieve coherent state of body.

Chapter 3 discusses about the design and implementation of a human arterial blood pressure meter based on auscultation and oscillometric principles. It talks about modelling Windkessel blood pressure model to find out which fusion gives the least standard deviation error. It also covers the implementation of the Windkeseel model in detail.

Chapter 4 discusses about the design and implementation of a human neural mass model which mimics the EEG activities of the brain

 Chapter5 discusses about the design and implementation of a Heart Rate Variability model which mimics the ECG activities of the heart. It mentions about the integration of the above NMM, HRV and Arterial blood pressure model for coherence studies.

Chapter 6 discusses about the design and implementation of a SSVEP based Brain Computer Interface.

Chapter 7 discusses about the various conclusion made and the scope of future work

Chapter 2

Related Work in the Reseach Area

2.1 Human Physiological Monitors

Measurement of human physiological parameters is not only useful for diagnosis but also for prognosis of a human being. This chapter discusses the various state of the art techniques used to measure various physiological parameters of the human body like blood pressure, respiration rate, blood-oxygen saturation, ECG, EEG and so on. Also a thorough literature survey on the use of SSVEP for BCI paradigms and for biometrics studies has been done.

Finally, the chapter concludes with a literature review on the various multimodal biometrics based on human physiological traits.

2.1.1 Pulse oximeter

Measurement of blood-oxygen saturation (SpO2) is another method used to monitor the effects of abnormal ventilation. When air enters the lungs, it connects its oxygen in red blood cells to the hemoglobin. The oxygen is then transferred in arterial blood throughout the body. The proportion of hemoglobin in the blood that is saturated with oxygen is determined by a pulse oximeter using the red and infrared frequencies. This proportion is known as saturation of blood, or SpO2. The SpO2 level as well as the pulse rate and plethysmogram are displayed at the same time by an oximeter [61].

2.1.2 Respiration rate monitor

Respiratory rate is a vital sign used to monitor disease progression and an abnormal breathing rate is a significant indicator of severe disease. There is significant proof that respiratory changes can be used to forecast possibly severe clinical occurrences such as cardiac arrest or admission to the intensive care unit. The gold standard for monitoring exhaled air is still to position a thermistor in a nostril. A range of contact and non-contact breathing devices have been developed like, Noncontact respiratory monitoring methods include radar based respiration rate monitoring, optical based respiration rate monitoring, thermal sensor and thermal imaging based respiration rate monitoring [62]. The other contact respiratory monitoring methods are Electrocardiogram derived respiration rate, oximetry probe (SpO2), transcutaneous CO2 monitoring, chest and abdominal movement detection, airflow based methods and acoustic based methods [63].

2.1.3 Central Nervous System

2.1.3.1 Functional Magnetic Resonance Imaging (fMRI)

It operates by detecting changes in blood oxygenation and flow in reaction to neural activity when a brain region is more active, it consumes more oxygen and raises the blood flow to the active region in order to satisfy this enhanced requirement. FMRI can dynamically detect changes in regional blood flow and concentration of oxyhemoglobin and reflect changes in brain activity with excellent spatial resolution through these measures [64]

2.1.3.2 Magnetoencephalography (MEG)

Magnetoencephalography (MEG) is the magnetic field measurement produced by neuronal electrical activity. It is normally mixed with magnetic resonance imaging to form magnetic source imaging. The technology that helped record these minute magnetic fields

is a superconductive detector of quantum interference that is like an extremely delicate magnetic field meter. The MEG is housed in a magnetically protected space to attenuate the internal magnetic noise. Magnetometers and/or gradiometers are the real sensors that record magnetic fields. Without distortion, MEG fields pass through the head. This is a major benefit of MEG over electroencephalography. MEG offers a high resolution in space and time [65-66].

2.1.3.3 Electroencephalography (EEG)

Human brain is made up of millions of neurons that play a significant role in regulating the human body's conduct towards internal / external motor / sensory stimulation. These neurons are going to behave as carriers of data between human body and brain. It is possible to understand cognitive brain conduct by analyzing either signals or brain pictures. In terms of motor and sensory conditions such as eye movement, lip motion, memory, attention, hand squeezing, etc., human behavior can be visualized. These states are associated with particular frequency of the signal that helps to comprehend the functional behavior of complicated brain structure. Electroencephalography (EEG) is an efficient way of obtaining brain signals that corresponds to different states from the surface of the scalp [67-68]. These signals are usually classified as delta, theta, alpha, beta, and gamma based on the range of signal frequencies from 0.1 Hz to over 100 Hz.

2.2 Cardiovascular related Monitors for Human Blood Pressure

There are two approach to measure the blood pressure in human subject. The invasive and non-invasive measurement.

2.2.1 Arterial Blood Pressure

Arterial pressure measurement is a compulsory step in evaluating the hemodynamics of patients as it provides main data on cardiovascular system efficiency and tissue perfusion. Direct intra-arterial pressure measurement invasive blood pressure is regarded the gold standard in critically ill patients and in patients experiencing high-risk and significant surgery. The option to invasive blood pressure is the (oscillometric) non-invasive (NIBP) system [69-70]. However, NIBP measurement is not continuous and this technique is expected to be less accurate than the invasive one during hemodynamic

instability, severe hypotension, under conditions of increased arterial stiffness and in obese patients.

2.2.1.1 Invasive blood pressure measurement

Arterial blood pressure through an arterial line is most correctly assessed invasively. Invasive intravascular cannula arterial pressure measurement includes direct arterial pressure measurement by putting a cannula needle (generally radial or brachial) in an artery as shown in in Figure 2.1.It is necessary to connect the cannula to a sterile, fluid-filled device linked to an electronic pressure transducer. The benefit of this scheme is the constant beat-by-beat monitoring of pressure. A brief, parallel-sided cannula made up of teflon or polyurethane, like the radial artery, is transmitted into a non-end artery. The cannula is connected to a system of tubing that offers a steady saline infusion. The pressure waveform is transferred to a diaphragm in reaction to the stress through the fluid within the infusion tube. The displacement is then converted to an electrical signal by a transducer. The invasive BP measurement method is generally limited to a hospital environment and has the inconvenience of complexity, patient risk, and inconvenience.
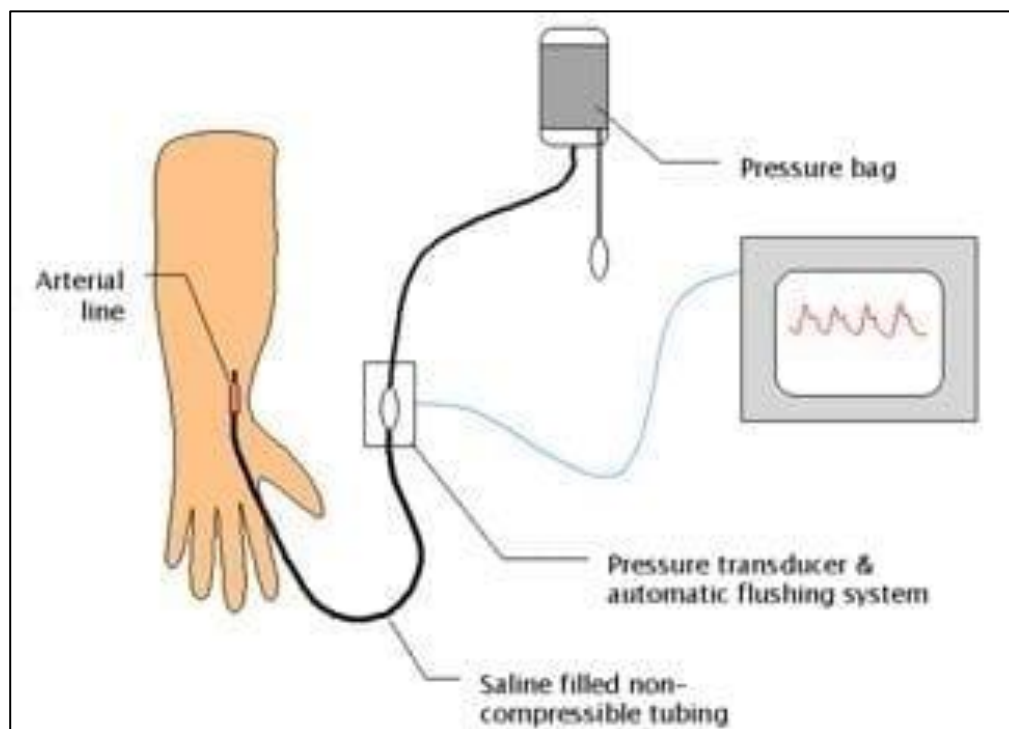
Figure2.1: Invasive blood pressure measurement via a catheter or cannula

2.2.1.2 Non-invasive blood pressure measurement

2.2.1.2.1 Palpatory

Alternatively, several non-invasive BP estimation techniques that are safer, faster, and involve less knowledge have been created. The methods of non-invasive BP estimation are either manual or automated. This technique does not have the disadvantage of being able to assess diastolic pressure. These are the two popular BP estimation manual techniques. In both manual techniques, a sphygmomanometer consisting of an inflatable cuff and a manometer is used, traditionally filled with mercury. The inflatable brace is put at the same height as the core around the upper arm of the subject. The cuff is inflated so that the artery is totally occluded to the supra-systolic pressure.
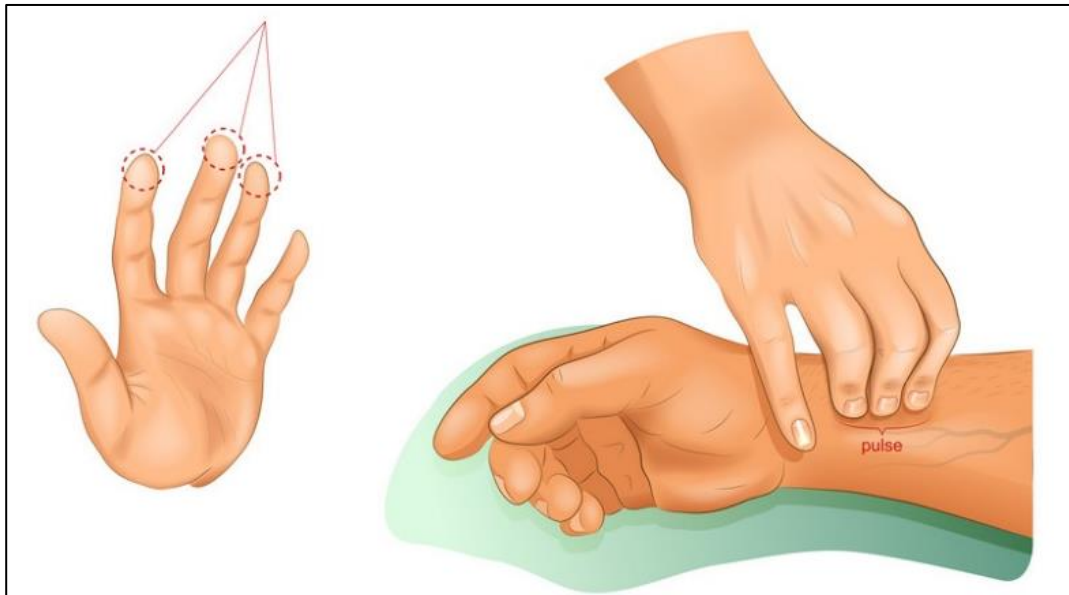
Figure2.2: Non-Invasive blood pressure measurement via palpitation method

The cuff is then released slowly. The method of palpation is shown in Figure. 2.2. A qualified examiner palpates the radial pulse at the neck of the subject in the palpatory technique [71-72]. During inflation, the stress at which the pulse falls and then reappears during deflation will be the SBP. Palpation is used only in emergency situations and the DBP and MAP cannot be estimated.

2.2.1.2.2 Auscultation (Korotkoff sounds)

The auscultative method was first described by the Russian physician "Korotkoff" in 1905 [73]. The cuff is inflated to a point above arterial pressure in this technique (as stated by pulse obliteration). The stress at which sounds generated by the arterial pulse waves (Korotkoff sounds) appear and vanish again as flow through the artery resumes is mentioned as the cuff is gradually deflated. The first Korotkoff sound's appearance is the highest pressure produced during each heart cycle: the systolic pressure. The pressure level at which the sounds permanently vanish when the artery is no longer compressed and the blood flow is fully restored is the resting pressure between the heart contractions: the diastolic pressure. As the pressure is reduced during deflation of the occluding cuff, the Korotkoff sounds change in quality and intensity. The five phases of this change are characterized as follows:

Phase 1: First appearance of clear, repetitive, tapping sounds. This coincides approximately with the reappearance of a palpable pulse.

Phase 2: Sounds with the quality of an intermittent murmur are softer and longer.

Phase 3: Sounds become louder and crisper again.

 Phase 4: Muffled sounds, less separate, softer sounds.

 Phase 5: Sounds totally disappear.

The pressure at which the sounds first appear (Phase 1) corresponds to the systolic pressure, sound disappearance (Phase 5) best corresponds to diastolic blood pressure and also better correlates with intra-arterial pressure [74,75]. If an auscultative gap exists, the identification of systolic blood pressure by palpatory technique enables one prevent a reduced systolic reading by auscultative technique.

Zhi Zhang et al [76] introduced a smartphone-based method to check the precision of BPMs. During readings of electronic oscillometric BPMs, Korotkoff sounds were gathered concurrently using a stethoscope head under a smartphone-connected cuff, and an App called AccutensionStetho could then be used as a reference for an auscultatory BP reading.

Next, differences were identified in BP between the various BPMs and AccutensionStetho. The precision could differ in the same person if, under distinct physiological circumstances, the BP values differ, which requires regular validation. The limitation of this research was that no study was done to verify whether the accuracy obtained by the oscillometric method was influenced by the deflation rate. However, although a slow pace of deflation in this research appeared to contribute to the precision of the BPMs. The amplitude of Korotkoff sounds was evaluated in one of the research works to give an understanding of the nature of the arterial wall as shown by a reduction in amplitude in elderly people compared to younger people and the quantity of blood flowing through the artery as shown by the greater amplitudes found in men compared with females [77].In order to standardize the values of the Korotkoff sounds amplitudes for healthy individuals in each category-young males, young females, old males and old females-a study with a larger sample size can be taken up.

Another researcher quantitatively evaluated the variety of Korotkoff sounds during BP measurement from above systole to below diastole, as well as the variability of Korotkoff sounds within the subject between repeats [78]. To classify whether stethoscope sounds could be recognized as Korotkoff sounds (KorS), a deep learning based CNN technique was created and implemented at beat-by-beat stage. The author has claimed that it was a first study to use the CNN technique to evaluate the variety of Korotkoff sounds during BP measurement. Subjects with a higher heart rate may result in mistaken outcomes. Therefore, it is necessary to develop more sophisticated signal processing strategy to prevent its potential impact at higher heart rate. In addition, there was no investigation into the efficacy of the CNN technique on certain particular cardiovascular patients, such as patients with ectopic beats and atrial fibrillation, to verify its efficacy. The authors looked at quantifying the impacts of cuff stress and stethoscope position on the measured features of the KorS waveform in the study work [79]. Under most conditions, the stethoscope above the artery (m1) produced the largest amplitude of RMS intensity and the shortest high-level duration, whereas the stethoscope at the opposite location of m1 produced the smallest amplitude of RMS intensity. The stethoscopes below the center of the cuff always generated KorS recordings with higher intensity amplitude and shorter high-level duration in terms of the impact of longitudinal position. Their research quantified and presented

scientific evidence that cuff stress, longitudinal and circumferential positions of the stethoscope are significant variables that affect the features of the KorS waveform. No comparative trials were conducted to explore the distinctive waveform distinction between the cuff microphones and the cuff. A computerized data acquisition and analysis scheme was developed by Yuqi Wang et al to provide observers with more objective information about an auscultatory measurement so that adequate information can be accessible to create measurements with higher prospective objectivity and precision [80]. Their system could obtain and store Korotkoff sound, cuff pressure, and oscillometric pulse signals as well as the sphygmomanometer picture, and it also showed the waveforms of the three signals and the sphygmomanometer video while playing Korotkoff synchronous sounds. Due to this scheme, observers can use the visual auscultation technique to create their readings, i.e. by observing these waveforms instead of the sphygmomanometer while listening to synchronized Korotkoff sounds. The scheme was validated under the International Protocol (IP). No modern digital signal processing algorithms have been implemented to improve the accuracy of the system.
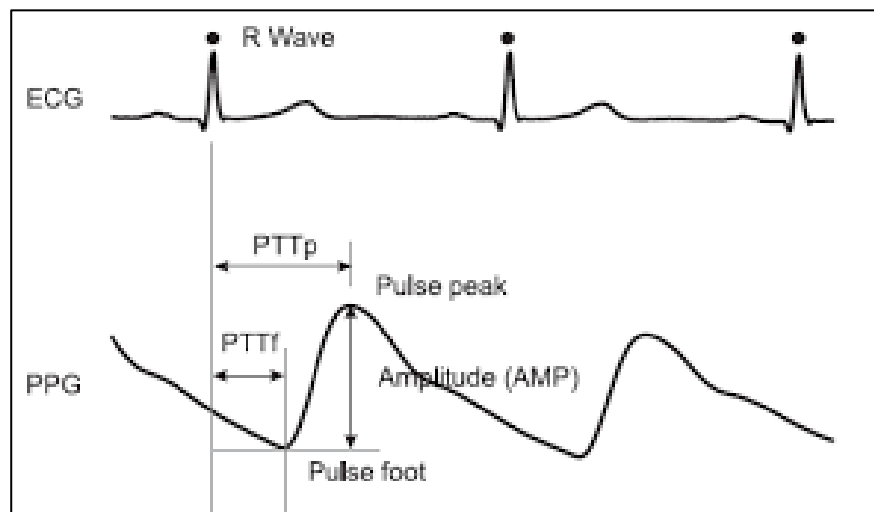
Figure2.3: Non-Invasive blood pressure measurement via PTT

2.2.1.2.3 Oscillometric method

This method utilizes manometer or sensor appearance and disappearance of oscillation. The word NIBP is often used to define oscillometric surveillance devices (automated electronic blood pressure monitoring devices) for non-invasive blood pressure.

Charles Babbs has developed a mathematical model integrating artery anatomy, physiology, and biomechanics, which predicts cuff pressure oscillations generated by the oscillometric technique during non-invasive blood pressure measurements. In his work he has explored the fundamental processes that contribute to a model-based algorithm for correctly deducting systolic and diastolic pressures from cuff pressure oscillations in the presence of varying arterial rigidity or pulse pressure [81]. Here, future proof of real-world precision will involve information comparing human oscillometric and intra-arterial pressure over a variety of test circumstances including variable cuff size, arm diameter, cuff tightness, cuff deflation rate, etc. In another research study, the author [82] has suggested a novel strategy on information corrupted with motion artifact to estimate SBP and DBP using variable feature ratios derived from oscillometric waveform envelope characteristics. An automatic algorithm was suggested to remove outlier points before the curve fitting method based on modifications in the oscillometric pulses relative to their corresponding neighboring pulses. Though there was an improvement in the SBP in the mean and standard deviation with respect to the reference system, negligible improvement was accomplished in the estimation of DBP. One researcher has used Bayesian method for fusing of various oscillometric estimation algorithms' in order to achieve more accurate and stable results [83]. Though the author has claimed improved accuracy no validation has been done as suggested by AAMI. Soojeong Lee has proposed a profound learning-based regression estimator with asymptotic methods and provides a technique that can reduce uncertainty for oscillometric blood pressure (BP) measurements using the Monte-Carlo and bootstrap approach. Although the former is used to assess SBP and DBP, the latter tries to determine SBP and DBP confidence intervals (CIs) based on oscillometric BP [84]. Clinical testing was done on a small subject population and protocols suggested by AAMI/ANSI were not followed. In another research work the author [85] has introduced a Hammerstein–Windkessel model to represent the central blood pressure system. It is a very simple representation capturing the low frequency dynamics of the cardiovascular system which was extended by an amplitude modulation representing the inflating and deflating cuff. A Kalman filter estimated the time varying Fourier series representing the Windkessel model's output signal. The Fourier coefficients of this output signal was then used in a next step to drive a logistic regression analysis. He showed that a logistic regression analysis based on the signal features of the oscillometric signal can

detect hyper and hypotension and correct the blood pressures accordingly. Validation was not done as suggested by AAMI/ANSI protocol.

2.2.1.2.4 Pulse Transit Time and PPG

One of the most commonly used methods for acquiring BP is Pulse Transit Time (PTT) [86] is shown in Figure 2.4. PTT is generally defined as the time taken to propagate from the heart to the peripherals of the body by the heart beat pulse. In most cases, to measure this parameter, researchers use signals from Electrocardiograph(ECG) and Photoplethysmography (PPG). One ECG sensor and one PPG sensor or two PPG sensors can be used to measure PTT [86,87].Proper ECG signal recording needs the positioning of at least three electrodes at three distinct body points. Motion artifacts and non-contact of the electrode with the skin surface and the long-term recording cables of the electrode may add noise to the signal, which are the limiting factors of BP estimation with this method [88,89].Two separate hardware is required at two different points in the body when recording two PPG signals to estimate BP. Therefore, it estimates BP using only one PPG signal. Because of the elasticity of the human blood vessels, the diameter of the vessels and then the quantity of blood inside them shifts when the pressure pulse moves through them [90].
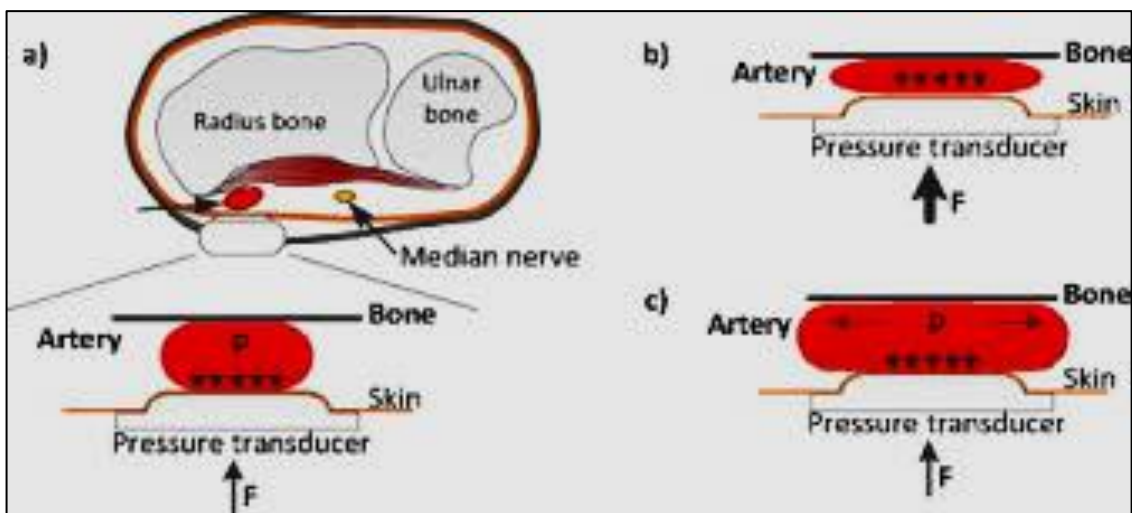
Figure2.4: Non-Invasive blood pressure measurement via Pulse Transit Time

Plethysmography is a technique to record changes in blood volume per heart drop in the body, whereas PPG is a non-invasive optical technique for measuring changes in blood

volume per pulse as shown in Figure 2.3 [91].In this technique, a Light Emitting Diode (LED) emits light into a portion of the body's tissue and changes in light absorption are evaluated over a period of time using a photo detector [92]. If the blood volume modifications are measured correctly, PPG has a wave-like shape and its frequency would be the same as the heart's operating frequency [93].It is possible to divide the PPG signal into two components. The upper portion of the signal has to do with heart or systole contraction while the bottom of the signal has to do with heart growth or diastole. There is a time-split variable in the PPG signal between systolic and diastolic cardiac stages called dicrotic notch. The dicrotic notch is not detectable in many recorded specimens of PPG signals from patients with hypertension. Fig. 1(a) demonstrates an instance of a PPG signal and its significant points belonging to a healthy individual, while Fig. 1(b) shows the hypertension patient's PPG signal. In this research, if detectable at the three points of systole peak, dicrotic notch, and diastolic peak, a PPG signal is called suitable. Otherwise, inappropriate is called the signal.

2.2.1.2.5 Other alternative methods

Several automated methods for ongoing and home BP surveillance have been created as an option to the manual BP estimation methods. These methods can be divided into two kinds: (i) ongoing recording methods that provide beat-to-beat arterial BP differences, and (ii) sampling methods that estimate only SBP, DBP, and sometimes MAP in less than one minute [94]. Tonometry [95] and vascular unloading [96] are the most prevalent ongoing methods. These methods are of low precision and involve frequent calibration. Automated auscultative [97], Doppler ultrasound sphygmomanometry[98] and oscillometry [99],[100] are the most popular sampling techniques. Among these methods, oscillometry is the most popular for SBP, DBP, and MAP assessment as it can be applied comparatively readily in automated BP measuring devices [99,100,101].

2.3 Human Blood Pressure Meter Survey

Most of the available non-invasive measurement of blood pressure systems are either based on oscillometric signals or auscultatory signals or fusion of both the signals.Both these methods of blood pressure measurement are complementary and provide enough information to accurately measure the pressure if both the devices are

associated together. Some of the related works conducted based on the oscillometric and auscultatory methods are listed in the follows: The previous literature has shown more attention towards the comparison of oscillometric and auscultatory methods. For instance, Heinemann et al. performed a comparison of these two methods in computing the systolic and diastolic pressure. The observed output results have indicated the poor estimation by the oscillometric method in extracting systolic and diastolic pressure [102]. Further, the lower blood pressure measurement is estimated by the oscillometric method compared to the auscultatory method of measurement using mercury manometer[103,104]. Several other studies have shown more focused on measuring blood pressure measurement in hemodialysis patients[105]. However, the interesting results have been obtained under this study, which has indicated the higher coefficents of variation in auscultatory method over the 23 hours of measurement.Although oscillometric and auscultatory methods are well studied in the literature, despite these facts, there is limited evidence that can experimentally validate the significance of one of this method over the other method. We will discuss in brief, some of the pros and cons of both the methods in measuring the pressure when it comes to the clinical applications. For instance, the auscultatory method can be implemented using a simple mechanical system like a sphygmomanometer which gives a more accurate detection of systolic and diastolic pressure based on the appearance and disappearance of 'Korotkoff' sounds. But this method performs poorly in the presence of artifacts such as movements, exercise, talking, background noise, difficulties in the signal analysis due to physiological variations of the 'Korotkoff' sound patterns or low Signal-To-Noise-Ratio (SNR) due to ambient temperature change, alcohol/nicotine consumption, bladder distension, etc. [106]. On the other hand, the oscillometric method has shown great potential to measure blood pressure, under the circumstances when the 'Korotkoff' signal strength is poor. However, the major drawback of this method is that it is very sensitive to movements due to the bandwidth of signals, so the arm must be immobile and also the accuracy of systolic and diastolic blood pressure is highly dependent on the algorithms used for the estimation [107]. Further, the accurate measurement in the different categories of patients such as Normal, Hypertension, Hypotension is always a challenging task, hence it is required to integrate information from both the methods to get an accurate measurement.

2.4   Heart Rate, HRV & RR measurement

Computer modeling of a human physiologic system centered around the Autonomic Nervous System (ANS) is discussed. Autonomic nervous system is a control system that involuntarily controls the body organs. It consists of two major subdivisions Sympathetic and Parasympathetic system. Sympathetic system controls the body during emergencies, stress or exercise. It is known as the flight or fight mode. Parasympathetic system is responsible for basal autonomic activities like digestion, heart and respiration under normal conditions. It is also sometimes called as the rest or digest mode. The ANS usually consists of two major components Central Nervous System(CNS) and cardiovascular system which collectively generate body blood pressure indirectly dictated by the heart rate variability(HRV) of the ECG signals generated at the sinoatrial node (SA) of the heart. The HRV gives a reflection of how well the heart is performing. A flat HRV line will suggest that the subject is not being able to adapt to different external conditions whereas variability suggests that the heart is in a heathy state and is being able to adapt to according to the situation. Here, we have developed CNS, Cardiovascular and ECG signal mathematical models and further present the interaction of them to demonstrate the sympathetic and parasympathetic signal of the ganglion which regulated the body physiology through the control of various organs.
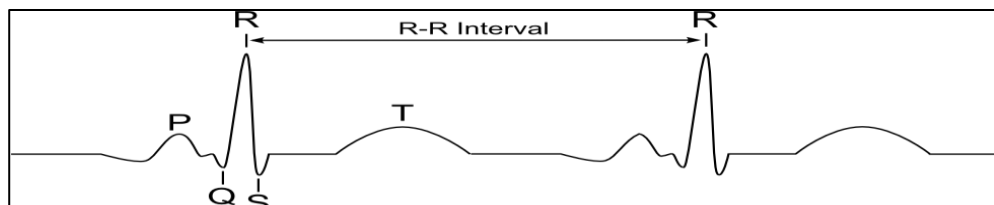
Figure 2.5: One Cardiac cycle
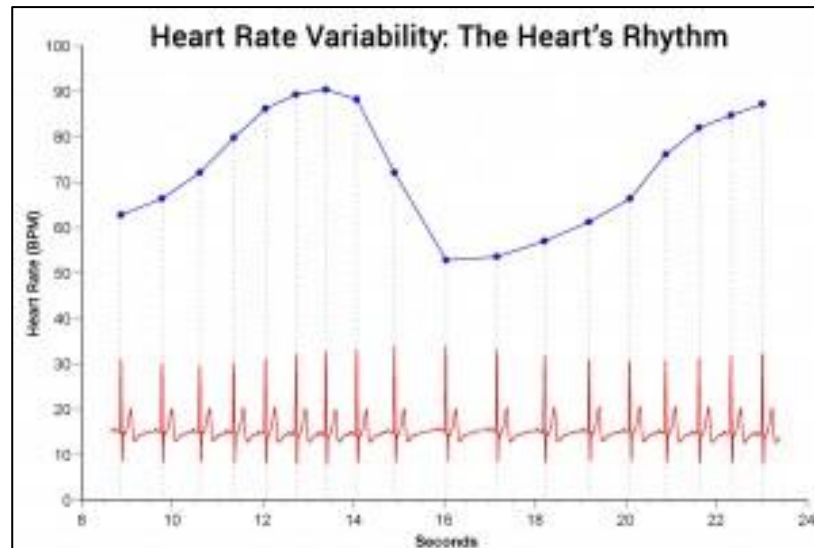
Figure 2.6: HRV over time of a healthy subject (Image Source: Heart Math Institute)

A normal one-cycle electrocardiogram (ECG) signal consists of several waves, as shown in Figure 2.5. RR intervals show the variation between consecutive heartbeats. Heart rate variability (HRV) measurements analyze how these RR intervals change over time. The sinoatrial(SA) node and atrioventricular(AV) nodes are responsible for the repeated contraction of the heart. They are known as the pacemakers of the heart. The SA node is located in the upper wall of the right atrium. The firing rate of the SA node is usually around 60-100 action potentials per minute. The sympathetic nervous system(SNS) and parasympathetic nervous system(PNS) compete with each other to maintain overall sympathovagal balance. The PNS is dominant during state off rest or relaxation which generates an average heart rate of 75 beats per minute(bpm). This is comparatively lower than the SA node actual heart rate of about 107 bpm at 20 years to 90 bpm at 50 years [1]. The PNS can decrease the heart rate to as low as 20 bpm.

Heart rate variation (HRV), a non-invasive technique used to assess the modulation of the autonomous nervous system on the cardiac sinus node, explains the oscillations between successive R-R intervals of electrocardiogram (R-Ri), (Figure 2.6). There is currently increasing interest in knowing the processes associated with HRV, its clinical usefulness, and modifications in its norms that may imply impairment of health. High concentrations of HRV indices are usually indications of effective autonomic processes that characterize a healthy person, while low or decreased HRV often demonstrate an autonomous

malfunction of the nervous system and may result in impairment of health. However, cardiovascular defects such as conductive illnesses and atrial fibrillation (especially in the elderly) can also generate elevated HRV. It is heavily related to enhanced mortality danger in this situation. Therefore, a clinical assessment of the topics with an electrocardiogram and thorough interpretation of it is essential before obtaining HRV. Therefore, a clinical assessment of the topics, followed by an electrocardiogram and thorough interpretation of it, is essential before obtaining HRV. Various cardiology studies have shown the significance of this technique as an instrument for assessing patients following cardiac surgery, myocardial infarction, ventricular dysfunction patients, arrhythmias, predicting sudden cardiac death and evaluating patients receiving therapeutic exercise intervention. The assessment of HRV as a predictor of danger of cardiac illness was also provided special significance. In patients with left ventricular dysfunction or heart failure, or with previous myocardial infarction, or bypass surgery, low HRV index values have been shown to be a powerful predictor of low probability of survival. Considering that disseminating the findings of these and other research using HRV as a technique of assessment is crucial to the growth of health care and that many outcomes are clinically important, it is essential that this technique is used correctly. Hemanth Kapu et al., presented a method to estimate Resting Heart Rate (RHR) by a PIR sensor system [108]. The PIR-based system is an effective and low-cost cardiac monitoring alternative. Here, they have estimated the RHR from the 2nd order derivative of the analog PIR sensor signal which exhibits an almost periodic behavior due to the heart beat. Since the waveform acquired from the PIR detector depict the heart activity, it may be necessary to monitor the variation of heart rate from the zero-crossings or peaks of the second-order derivative signal. Parham Nooralishahi et al. suggested a novel algorithm for estimating heart rate compared to algorithms that function well on stationary topics under well-controlled circumstances and considerably degrade their efficiency under the movements and variations in illumination of the subject [109]. It can also distinguish between a photograph of a human face and a real human face, which means it can detect and skip fake signals. The technique obtains ROIs using facial landmarks, then rectifies lighting based on the adaptive filter Normalized Least Mean Square (NLMS) and eliminates non-rigid movements based on standard deviation of the sections of the signal's set length. The method uses the technique of RADICAL to obtain autonomous subcomponents. The heart

rate measurements for each subcomponent are predicted to locate the one with the largest magnitude by analyzing the frequency signal. A two-steps data fusion method is also introduced to combine current and previous measured heart rates to calculate a more accurate result. Researchers have also proposed a novel HR estimate from the PPG signal during treadmill practice using cascade hierarchical structure and adaptive filter parallel combinations [110]. For each window, they have estimated the HR through the PPG signal and the HR received from the ECG signal are contrasted and the estimated HR from the PPG signal is found to be precise with regard to the HR received from the ECG signal. Their proposed design of combining two distinct pairs of adaptive filters is extremely robust and has shown an enhanced HR estimation and monitoring efficiency. The efficiency of their suggested algorithm to the distinct situations has not been evaluated.A novel and low-complex PPG peak detection algorithm for HR estimation has been suggested in another research [111]. Results indicate that their technique can be a useful contribution to solid approaches that can dynamically adjust their peak detection technique to conditions where the PPG signal amplitude is anticipated to reduce. The restriction of their work was that they have not tested in order to conduct a strict validation under a broad spectrum of circumstances. Norihiro Sugita has suggested a new technique for measuring heart rate variability using a compact RF motion sensor that is tiny enough to fit in the shirt pocket of a user [112]. They used an algorithm to optimize a digital filter based on the signal's energy spectral density to extract a heart rate-related element from the sensor signal. During the resting state, they measured signals from the RF motion sensor for 29 subjects and their heart rate variability was estimated from the measured signals. A correlation coefficient estimated from their suggested technique between true heart rate and heart rate was 0.69.However, some improvements were needed for stable measurement, such as regulating the direction of sensing.

2.5 Brain Wave Monitors for EEG

A novel pin-shaped dry electrode for electroencephalography recording was provided in a document released by Kun-Peng Gao et al. To obtain low impedance and smooth characteristics, the pins on dry electrode were manufactured from carbon fibers [113].The tips of the pins were further processed to carbon fiber bristles to decrease the contact impedance between the skin and the dry electrode and could fill the unevenness on

the scalp. It could also achieve bigger contact area and better convenience with tiny pressure compared to the traditional pin tip without bristles. The characterization findings suggested a comparatively small skin-electrode contact impedance for the smooth dry electrodes with carbon fiber. In order to assess the electrode efficiency for EEG recording, the alpha rhythms from auditory evoked potential and steady-state visual evoked potential were evaluated. Moreover, the influences of dry electrode on skin showed there was no breakage and movement.Guger C, Krausz et al. have shown that dry electrodes with a P300 BCI can deliver similar output to gel electrodes [114]. This is a significant result giving both the promise and prominence of dry electrodes and P300 BCIs. The dry electrode decreased preparation time but may be more susceptible to artifact motion and electrostatic ambient charges. Despite elevated impedances, the dry electrode system enables excellent efficiency by using various gold-coated pins in each electrode and an integrated amplifier within each electrode. The average P300 amplitude peak was reduced and greater signal drifts were also shown below 3 Hz than electrodes based on gel. This may cause issues with other BCI types.

P. Kidmose et al. intended an over the-ear EEG and compared the standard on-scalp EEG rigorously [115]. This is accomplished over steady-state and transient paradigms and across a population of topics for both auditory and visual evoked responses. The corresponding steady-state answers were assessed in terms of signal-to-noise ratio and statistical significance, while the transient response qualitative analysis is conducted by considering large-scale event-related waveforms (ERP).The results of their research have shown conclusively that the ear-EEG signals are in line with standard EEG collected from electrodes positioned over the temporal region in terms of the signal-to-noise ratio. Ear-EEG provides a non-invasive and discrete way to record EEG and has the potential to be used in real-life environments for long-term brain monitoring. While ear-EEG recordings were earlier recorded using moist electrodes, Kappel et al. created and assessed ear-EEG dry-contact electrodes in their research [116]. They created a fresh ear-EEG platform to accomplish a well-functioning dry-contact interface. Their platform included actively protected and nanostructured electrodes integrated in a soft-earpiece that was individualized. The prototype built by the dry-contact ear-EEG platform reflects a significant user-friendly technological development of the technique as it eliminates the need for gel in the electrode-skin interface. Xiao Xing et al., introduced a high-

performance SSVEP-based BCI scheme using dry claw-like electrodes [117]. The study suggested dry electrode decreases the time required for system preparing and their flexibility increases wearing convenience and enhances user experience. The material as well as the dry electrode structure were elaborately constructed and adapted by them. It can comfortably be worn on the hair-covered head region and the electrode pins can readily go through the hair and touch the scalp. The electrode impedance is stable and the electrode is therefore capable of recording reliable and high-quality signals for subsequent signal processing. By fully considering the individual differences of SSVEPs, the adopted TRCA-based identification algorithm can attain high precision with brief information. By mixing these two features, their current dry-electrode-based BCI scheme achieves high classification precision (93.2 ± 5.74 percent) and elevated ITR (92.35 ± 12.08 bits / min) using a BCI paradigm of 12 classes. Chi-Chun Lo et al., have suggested that a new non-contact control system for disabled patients medical care and applied successfully in the hospital [118].Based on the benefit of the brain-computer interface method, the disabled patients brain can use the suggested scheme to regulate the hospital's nurse emergency call system, lights, air conditioners and TV sets without manual operation. A tablet is used in their study for the visual stimulus, and a specific coding scheme is proposed to provide the property of asynchronous operation to enhance the practicality of the proposed system and the convenience for use.In addition, this research also designs and implements a wearable EEG procurement device with non-contact dry EEG electrodes. With the benefits of tiny quantity, light weight and simple set-up in the suggested EEG sensor, the suggested scheme can readily be used in the hospital to measure EEG signals in the hairy site without conductive gel.

2.5.1   SSVEP Measurement

SSVEP is a type of BCI technology with a high speed of transfer of data. Because of its nature, however, frequencies may be used as stimuli are scarce. A stimuli encoding technique is created by Xing Zhao et al. to fix this issue, which encodes SSVEP signal using the Frequency Shift Keying (FSK) method [119]. In the technique used by them, each stimulus is governed by an FSK signal containing three distinct frequencies representing respectively "Bit 0," "Bit 1" and "Bit 2." Unlike common BFSK in digital

communication, the unique identifier of stimuli in binary bit stream form was composed by "Bit 0" and "Bit 1," while "Bit 2" indicates the end of a stimulus encoding. In order to study the function of sensory processing in the visual cortex, A. Zhigalov et al. have explored the feasibility of fast frequency tagging [120]. Our findings indicate that it is actually feasible to evaluate reactions at the tagging frequencies and that spatial attention modulates these reactions. The alpha energy modulation was inversely related to the gamma energy modulation. These findings provide significant proof of principle that fast frequency tagging can be used to assess visual cortex neuronal excitability in a stimulus-specific way to explore spatial attention. In addition, despite the frequency tagging, the dynamic properties of the alpha band oscillations have been preserved. Rapid frequency tagging is extremely advantageous for standard reduced frequency (< 20 Hz) tagging as it does not generate a noticeable flicker and the quicker frequencies also enable for better temporal resolution investigation of the tagged reaction. Alexander M. Dreyer et al., have attempted to enhance SSVEP's user experience by eliminating fatigue owing to flickering stimuli exposure [121]. To decrease this, the authors suggested high-frequency stimulation. They have adjusted auditory domain FM stimulation, where it is frequently used to evoke steady-state reactions, and compare the EEG and perceptibility scores of cognitive flicker. With rising FM carrier frequencies, subjective perceptibility ratings decline, while peak amplitude and signal-to-noise ratio (SNR) stay the same. They have adapted the FM stimulation of the auditory domain, where it is often used to evoke steady-state responses and compare the EEG and cognitive flicker perceptibility scores. Subjective perceptibility ratings decrease with increasing FM carrier frequencies, while peak amplitude and signal-to-noise ratio (SNR) remain the same. In another research, the scientists explored the correlation between EEG-based measures for the normal behavioral evaluation [122].

As their stimulus technique they used six gray-level natural pictures; in six stages of degradation produced by coding the pictures with the HM10.0 high-efficiency video coding (H.265/MPEG-HEVC) test model using six distinct compression rates. In fast alternation with the initial pictures, the degraded pictures were displayed. The existence of SSVEPs in this environment is a neural indicator that objectively shows the neural processing of the modifications in quality caused by video coding. They tested two distinct

techniques of machine learning, respectively, to classify such potentials based on brain rhythm modulation and time-locked elements. Their findings indicate elevated accuracy over the limit of perception of quality modifications in the classification of the neural signal. Accuracies in the standardized degradation category rating quality assessment of the same group of pictures were significantly associated with the mean opinion results provided by the respondents.

Their design could have been further enhanced by selecting subject-specific frequencies of stimuli, increasing the amount of quality concentrations evaluated, and tracking the alpha rhythm level during the experiment. In dealing with covariance matrices as classification characteristics, Emmanuel K. Kalunga et al. explored the efficiency of Riemannian geometry [123]. They created a new MDRM-based algorithm, improved by class probability and curve direction in the covariance EEG signals room, for a 4-class brain computer interface on a SSVEP classification assignment. Existing covariance matrix estimators have been explored and their robustness has been evaluated on multi-channel SSVEP signals to guarantee that the matrices collected are precise information covariance estimates, are well conditioned, and the positive-definite property is verified. They discovered the Schäfer shrinkage estimator to be the best because with the MDRM algorithm it yielded the greatest rating precision. Another research group attempted to explore whether a practical SSVEP speller could be created in the high-frequency range with Repetitive Visual Stimuli [124]. Using five flickering visual stimuli, they attempted to use an asynchronous high-frequency (35–40 Hz) speller for typing in Persian language. Despite very elevated general typing speed of 6.9 chars / min, average precision of 98.3 percent, and information transfer rate of 64.9 bpm for eight of the respondents, the other six respondents had severe problems with spelling the scheme and were unable to finish the typing experiment. According to some prior research, the findings of their research proposed that elevated illiteracy rates in high-frequency SSVEP-based BCI schemes. Perception of illusory contours have shown to be a consequence of neural activity related to spatial integration in early visual areas. Candidates for such filling-in phenomena are long-range horizontal connections of neurons in V1/V2, and feedback from higher order visual areas. To get a direct measure of spatial integration in early visual cortex, researchers have presented two differently flickering inducers, which evoked steady-state

visual evoked potentials (SSVEPs) while manipulating the formation of an illusory rectangle [125]. As a neural marker of integration they have tested differences in amplitudes of intermodulation frequencies i.e. linear combinations of the driving frequencies. These were significantly increased when an illusory rectangle was perceived. Increases were neither due to changes of any of the two driving frequencies nor in the frequency that tagged the processing of the compound object, indicating that results are not a consequence of paying more attention to inducers when the illusory rectangle was visible.

2.5.2 Using BCI paradigms for Biometric Applications

Table 2.1: Depicting literature survey of various BCI paradigms based biometrics

Author	Subjects	Electrodes	Stimulus	Sessions	CRR(%)
Su et al.[131]	40	1	Rested with eyes closed	One	97.5
Lee et al.[132]	4	1	Rested with eyes closed	One	98.33
Rocca et al.[133]	108	20	Resting with eyes open and eyes closed	One	100
Singhal et al.[134]	10	1	P300 VEP	One	78
Yearn et al.[135]	10	18	P300 VEP	Two	14.5
Palaniappan et al.[136,137]	10	61	P300 VEP	One	95
Marcel et al.[138]	9	8	Motor Imagery	One	92.9
Min et al.[139]	20	32	SSVEP	One	98.9

2.5.3 Literature survey of various physiological traits of human body used for biometrics.

In one of the earlier studies, Yogendra Narain Singh et al. [126] developed a multimodal biometric system comprising of face, fingerprint and ECG features. Their proposed FT-EER score level fusion scheme performed better with an EER of 0.22% as compared to the FT-MSD score fusion scheme attained an EER of 0.98%. The ROC curves of the fused ECG signal, face and fingerprint biometrics for the FT-EER and the FT-MSD fusion techniques showed that there was an improvement in the authentication rates of the biometric system in comparison to the unimodal systems. Marcin D. Bugdol et al. [127] has proposed a multimodal behavioral biometric system that involves the feature level fusion of ECG and sound signals. They have utilized heart rate variability (HR)features extracted from ECG beats and Mel-frequency cepstral coefficient and the voice timbre as features extracted from voice. These features are then fed individually to the Support vector machine classifier after feature reduction using principal component analysis. Average (arithmetic) identification accuracy was 77% using k- Nearest Neighbor as their classifier. In one of the research work, Belgacem, Noureddine, et al. [128] implemented a multimodal biometric system by fusion information from ECG and EMG to obtain a much more reliable biometric by the extra information give n by the EMG recordings. They extracted the spectral coefficients as features and used an optimum path classifier for classification. They achieve an accuracy of 99% for 120 subjects. More recently Mohamed Hammad et al. [129]have fused ECG and fingerprint information to identify human beings. They have generated biometric templates for both the biometric traits using a convolutional neural network and also have applied a cancellable biometric to secure the templates. Q-Gaussian multi support vector machine for authentication and fusion with an accuracy of 99.9%. In another recent work, KunSu et al. [130] developed a multimodal biometric system based on finger vein and ECG signals. They have made use of discriminant correlation analysis for the fusion of the two modalities. They achieved a Genuine Acceptance Rate of 94.86 % at False Acceptance Rate of 1% and an Equal Error Rate is 1.27 using sum rule-based fusion method which is a reflection of the complementary nature of the two biometrics. Figure 2.7 shows various biometrics based on physiological and behavioral traits of human body.
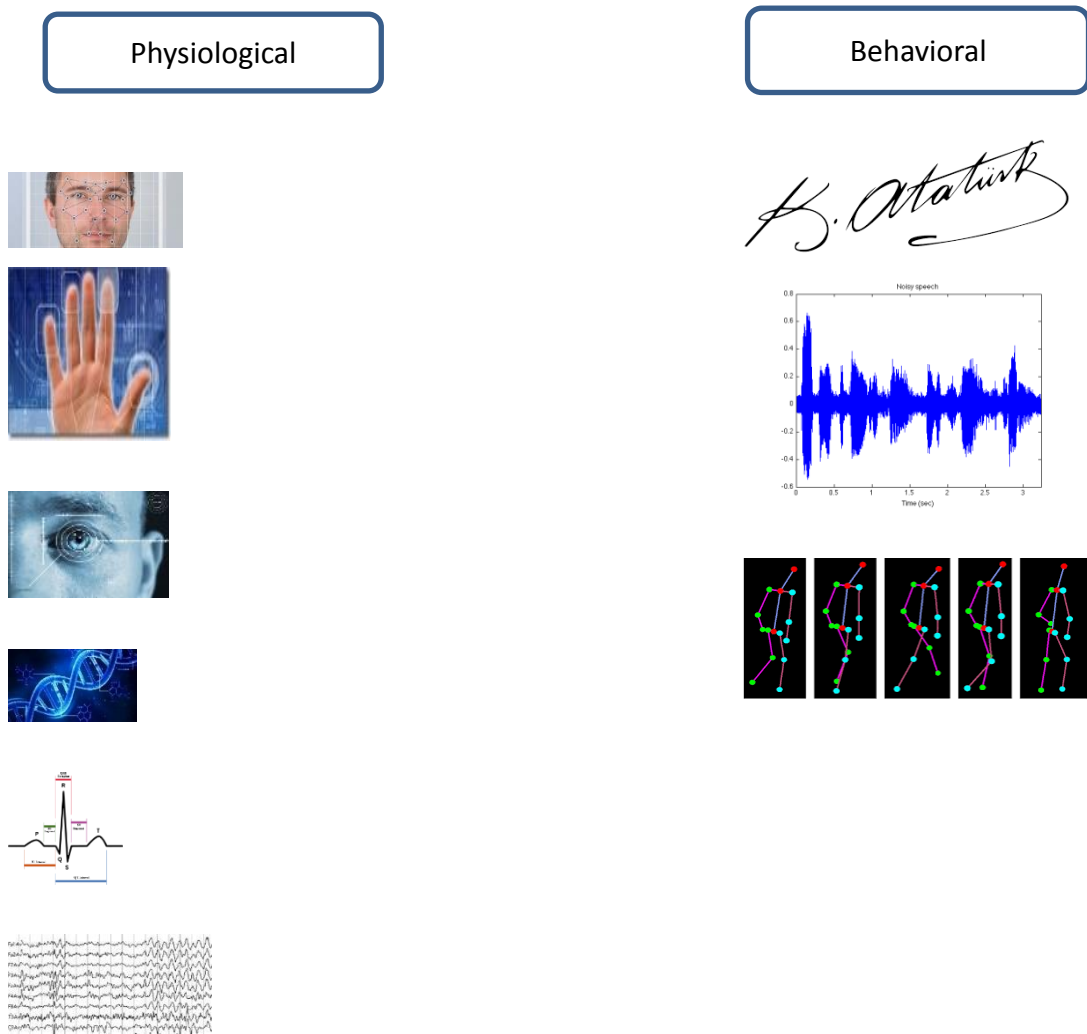
Figure 2.7: Different biometric traits at physiological and behavioral levels

2.6 Coherence in Physiology of Body

The study by Steinhubl SR examined inter-individual variations to meditation through continuous monitoring of EEG, blood pressure, heart rate and its variability (HRV) in novice and experienced meditators. They were able to show that meditation led to significant, measureable EEG changes even in individuals just beginning a meditation practice. The most unique finding was that they found that meditation was associated with a small, but statistically significant decrease in blood pressure in a normotensive population [140].In a study by Sze JA et al. it bridges two important areas of emotion

research, response coherence and body awareness. Using a within-individual approach for assessing coherence, their hypothesis was supported that body awareness training is associated with greater coherence between subjective emotional experience and heart period during film-induced emotional episodes. Moreover, they found that this association was strongest in those whose training emphasizes visceral awareness (Vipassana meditation), intermediate in those whose training emphasizes somatic awareness (modern dance and ballet), and weakest in those who have neither kind of training. These findings provided a more nuanced support for theories of emotion that posit that emotions help organize disparate response systems and for those that posit an important role for body sensations in the construction of emotional experience [141].Musicology is a branch very mush used to balance the sympathetic and parasympathetic activities of the body. The aim of such study is to evaluate the effects of music on autonomic nervous system activity in orthostatic tolerance after exercise. It is found that music increased parasympathetic activity and attenuated the exercise-induced decrease in parasympathetic activity without altering the orthostatic tolerance after exercise. Therefore, music may be an effective approach for improving post-exercise parasympathetic reactivation, resulting in a faster recovery and a reduction in cardiac stress after exercise [142].

Chapter 3

Exploring Design of Human BloodPressure Meter

3.1 Human Blood Pressure Meter System

Arterial blood pressure (ABP) is an important biomarker of the dynamics of blood flow and also organ perfusion. Pressure builds up as blood is ejected from the left ventricle into the aorta and other branching arteries. This pressure knows as the mean arterial pressure is governed by factors such as cardiac output and total peripheral resistance. The primary function of the heart is organ perfusion i.e. to make sure the important organs receive an adequate amount of blood to function. The heart accomplishes this job by contracting the heart muscle such that blood is ejaculated from the left ventricle into the aorta via the aortic valve and also from the right ventricle to the pulmonary arteries via the pulmonic valve. It has been seen that over time the amount of blood which is pumped from the right and left ventricle tends to be the same. This is known as the stroke volume and is expressed as ml per beat or in liters per beat. Cardiac output is the product of stroke volume and the beats per minute. It is expressed in ml/minute or liters per minute. Systemic vascular resistance (SVR) also known as total peripheral resistance (TPR) is the collection of systemic vasculature. Vasoconstriction and vasodilation increase and decrease SVR respectively.

3.2 Modeling Human Blood Pressure

3.2.1 Windkessel Arterial Blood Pressure(ABP)

The two elements lumped the Windkessel model developed by Otto Frank explained the dynamics of blood flow in the human arterial system [143]. The heart is considered as a current source which is replicated by a lumped resistance which represents the arterial resistance and compliance represents the elasticity of the arterial system parameters. But there was a limitation with this model that it could not explain the aortic pressure in systole [144,145]. Hence a third element called the characteristic impedance was introduced to overcome this shortcoming and it linked the Windkessel model to transmission phenomena. The capability of an arterial wall to compress or expand to accommodate changes in pressure is necessary for the proper functioning of the heart. This ability of the arterial walls to distend is called arterial compliance. This is similar to the compressibility of the air pocket and it simulates the elasticity and extensibility of the major artery. The capacitor is analogous to the compliance of the blood vessel. The resistance emulates the systemic vascular resistance to arterial blood flow.

N. Stergiopulos et al. found out that three-element Windkessel acted as a perfect load for isolated heart studies, but did not correctly estimate the total arterial parameters like the aortic characteristic impedance and total arterial compliance [146]. To solve this problem, they added a fourth element, the total arterial inertance to the Windkessel model. The inductance L represents the inertia of blood flow in the vascular system. They tested three and four-element Windkessel's that were tested against an extended model of the systemic circulation. The estimated lumped parameters were found to be within 10% of the arterial system. Their four-element Windkessel model also fitted well in vivo studies. We have adapted their model in our study and the equivalent circuit is shown in Fig. 3.1(a), here q_{in} represents the left ventricular stroke volume per beat, and the output stroke volume per beat is q_{out}. As shown in Fig. 3.1(a), the first elastic chamber represents the aortic arch and C_1 represents the lumped compliance of the proximal large arteries. The second elastic chamber represents the abdominal aorta and C_2 represents lumped compliance of the distal muscular arteries. R represents the peripheral resistance. The blood column L, which connects the two cavities, represents the inertance of the

flowing blood. The pressures and volumes in chamber one and chamber two are given by p_1, v_1, p_2, and v_2, respectively.

The arterial blood pressure model developed is based on Windkessel's model [147]. Blood flow occurs due to a pressure gradient(p_1-p_2) across the length of the systemic vasculature. p_1 is the pressure at the start of the artery and p_2 is at the end.

(a)

(b)
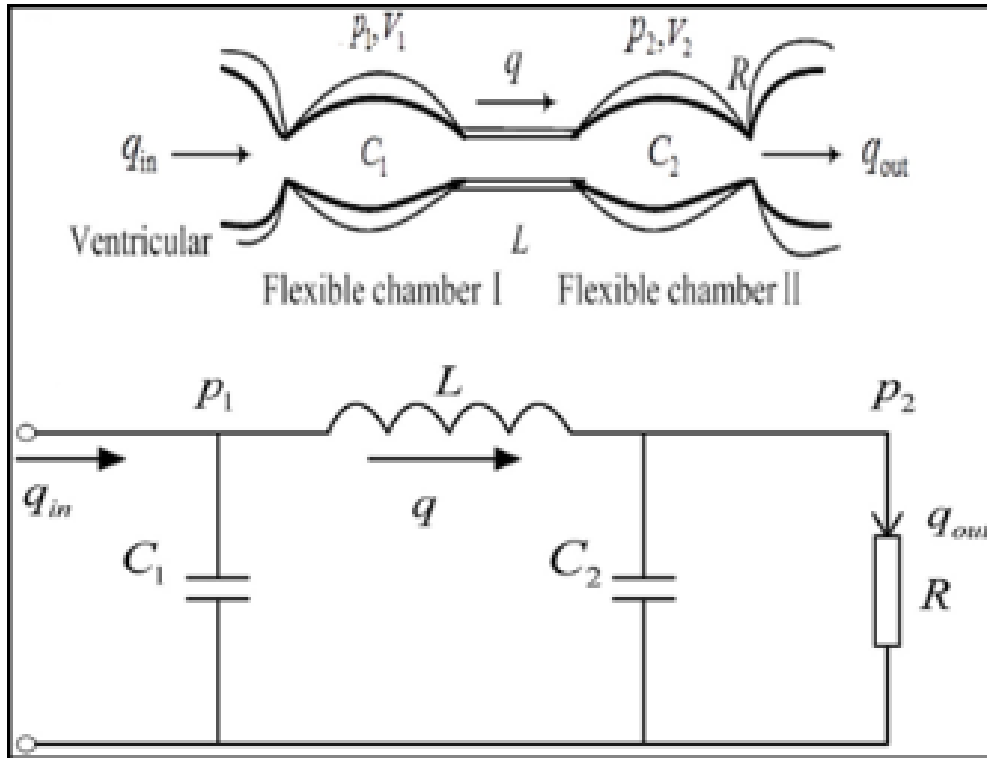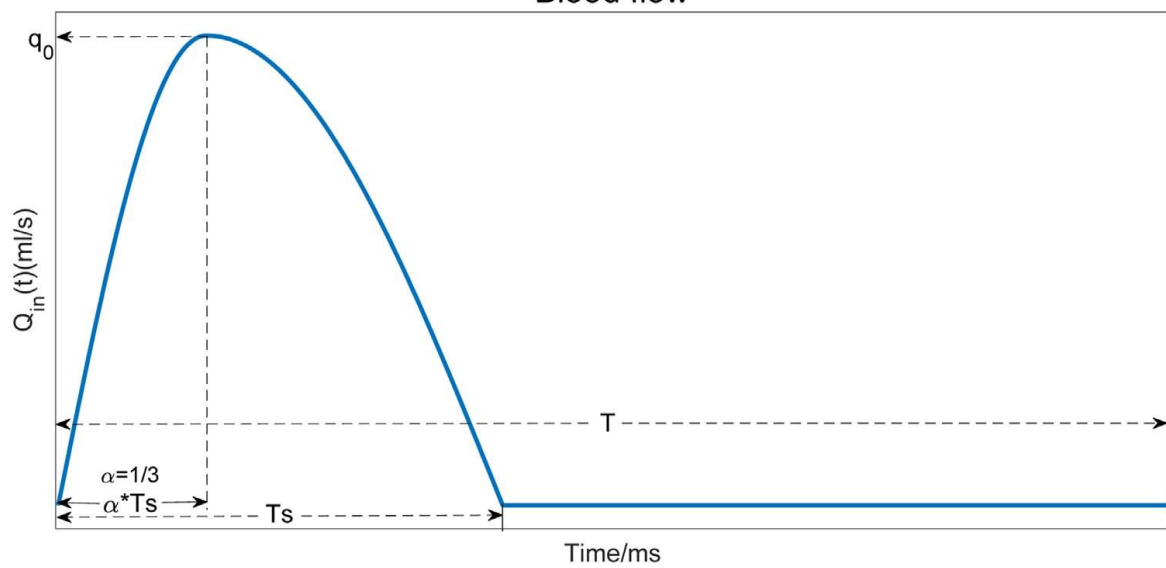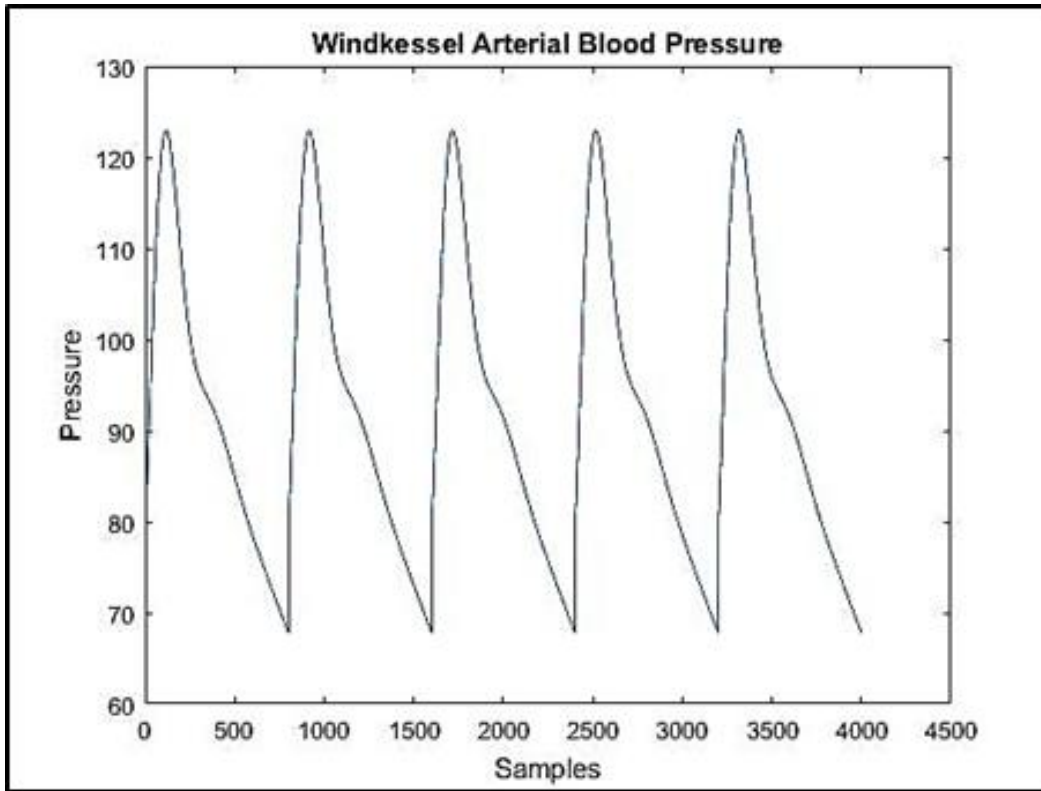
Figure 3.1 The Blood Pressure Modelling (a)Windkessel Model (b) Input Volume (c) Arterial blood pressure

The Windkessel arterial blood pressure is described by the following set of equations:

$$\frac{dq}{dt} = \frac{1}{L}(p_1 - p)$$

(3.1)

$$\frac{dp_1}{dt} = \frac{1}{C_1}(q_{in} - q)$$

(3.2)

$$\frac{dp_2}{dt} = \frac{1}{C_2}(q - \frac{p_2}{R})$$

(3.3)

The four element Windkessel model is shown in Figure3.1(a). The output arterial blood pressure waveform is shown in Figure 3.1(c) and the input volume to the model is shown in Figure 3.1(b) which is the left ventricular ejection in one cardiac cycle.

The input q_{in} is defined by the following equations:

$$qin(t) = \begin{cases} q_0 sin(\dfrac{\pi t}{2\alpha T_s}) & \text{...............} 0 \le t \le \alpha T_s \\ q_0 cos \dfrac{\pi}{4\alpha T_s}(t - \alpha T_s) & \text{..........} \alpha Ts \le t \le T \\ 0 & \text{.................................} Ts \le t \le T \end{cases} \quad (3.4)$$

$$q_0 = \frac{CarOP * Time * \pi}{120 * T_{sys}} (3.5)$$

The maximum input amplitude is given by q_0 with reference to the cardiac output; Tsys and Time represent the duration of left ventricle ejection and the cardiac cycle respectively. The time at which we get the maximum peak at systole is αT_{sys} where α is the ratio that varies form 0.1to 0.8.CarOP is the cardiac output and the left ventricular ejection plot $q_{in}(t)$ in one heartbeat is shown in Figure 3.1(b). All the differential equations (3.1-3.5) were solved using Runge-Kutta4th order method in MATLAB 2017.

3.3 Block diagram of the proposed system

This section describes the major system components and their significance in the development of our instrument. The developed pressure meter instrument is based on the oscillometric and auscultatory principle. Hence, before actually describing the instrumentation details, we will explain in brief, how systolic and diastolic pressure is obtained in the oscillometric and auscultatory principle. In the case of the oscillometric method, the cuff initially inflated above systolic pressure and then slowly starts to deflate until the systolic pressure is reached. Piezoresistive sensor detects the systolic pressure as soon as the oscillations start to appear due to the perturbation caused in the bronchial artery. The amplitude of oscillations increases and start to decrease as the pressure in the cuff starts to decrease due to deflation to match with brachial lower pressure. However, in this principle of measurement, it is always a difficult task to estimate the diastolic pressure due to a decrease in the amplitude of oscillations (Diastolic pressure is the lower arterial pressure at which the oscillations stop while the cuff pressure is deflated). Thus, diastolic pressure is then obtained from the Mean Arterial Pressure (MAP), i.e. the pressure at which the amplitude of the oscillometric signal is at its maximum (Figure 3.2).
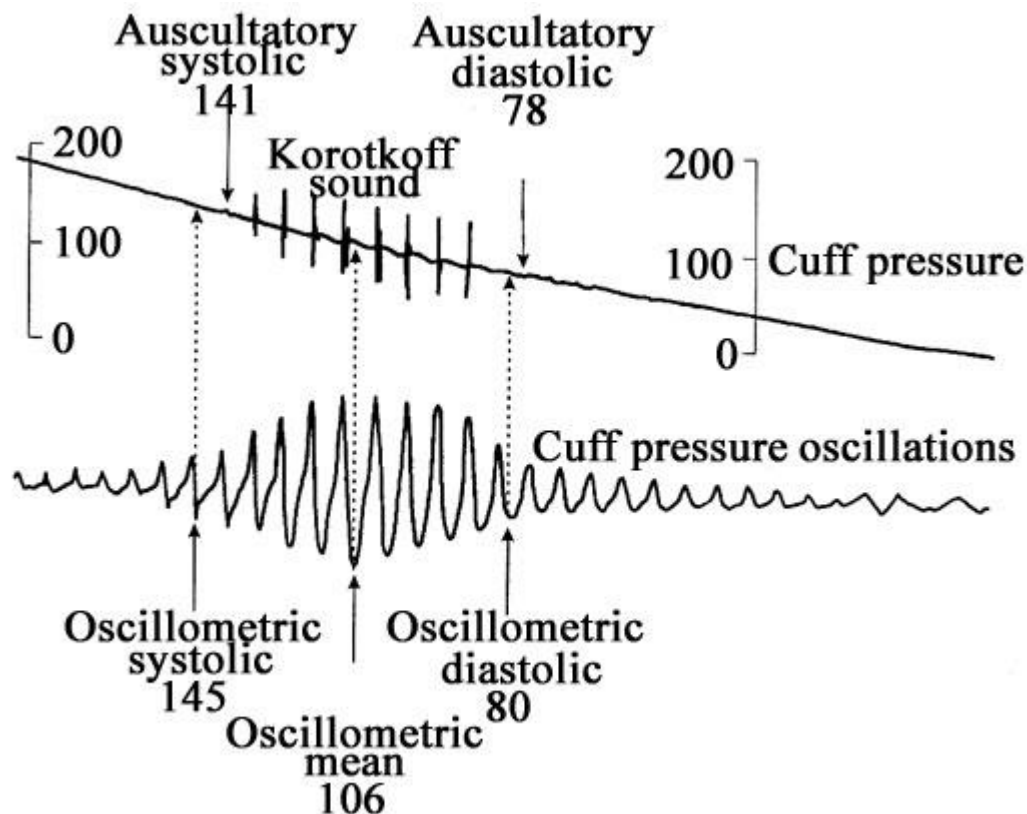
**Figure 3.2: Oscillometric and auscultatory signal during deflation of cuff pressure [a].
Where, xaxis corresponds to time in sec and y axis corresponds to pressure in
mmHg.**[a]www.accessanesthesiology.com

On the other hand, in the auscultatory method, the process of cuff inflation and then
deflation remains the same, but the measurement of systolic and diastolic pressure is based
on the 'Korotkoff' sounds. 'Korotkoff' sound is a kind of sound that results due to the
turbulence effect caused in the bronchial artery, when blood starts to flow through the
pressurized bronchial artery, after the pressure in the cuff is released. However, the systolic
pressure is indicated by the start of 'Korotkoff' sound, while diastolic pressure is detected
when 'Korotkoff' sound is stopped after the pressure build due to the cuff is released. We
employed the above standard protocol in our system to obtain systolic and diastolic
pressure based on oscillometric and auscultatory principle. To compute pressure, the
developed instrumentation device is subdivided into three main sections: Pneumatic
section, Analog section and a Microcontroller unit (MCU). Figure 3.3 illustrates the block
diagram of our developed pressure meter instrument and the developed system is shown in
Figure 3.13. The details description of each of the sections from the block diagram is
explained in the following subsections.
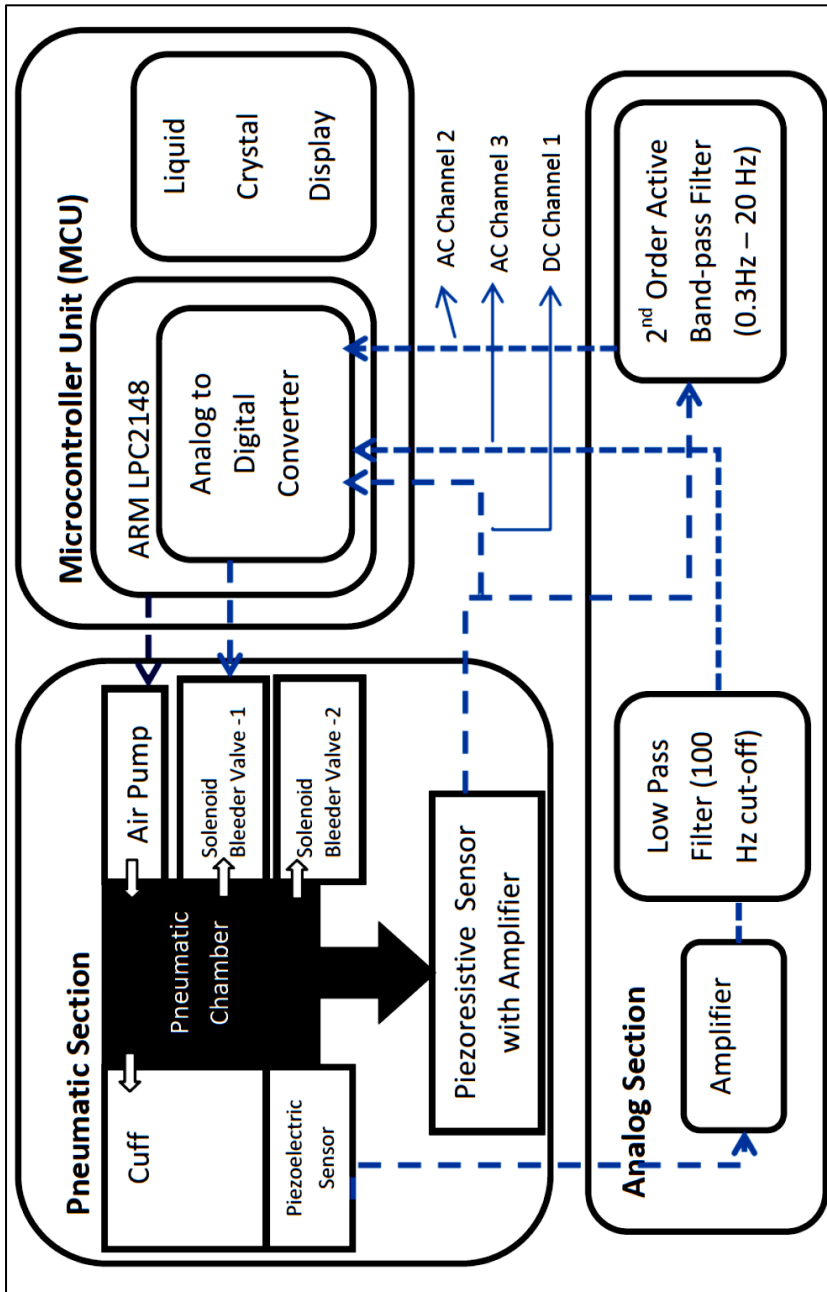
Figure 3.3: Block diagram of Blood Pressure Meter

3.3.1 Pneumatic section

The purpose of this section of the system is to maintain the cuff pressure above and below the systolic pressure and diastolic pressure respectively. We used CJP37-

D06A1 motor (V voltage: 9 Volt DC, Current:100mA, Flow Rate: 2 LPM) as an air pump to inflate cuff at the rate of 15mmHgs^{-1} to reach a pressure +15mmHg above the systolic pressure. The upper systolic cuff pressure is 285mmHg which covers the very severe stage 4 as per the standard human blood pressure chart [148]. A solenoid valve-1 with a bleeder is used to release the air pressure at a very low rate of 3mmHgs^{-1}, during the deflation, while it remains closed when the cuff is inflated. Further, a separate solenoid valve-2 is used to release the air pressure at the rate of 20mmHgs−1 at the time when the pressure in the cuff falls below the diastolic pressure. This second valve is used to improve the measurement time. Further, the size of the cuff selected is medium type (approximately 24 - 40cm). The selection of medium size cuff is because the majority of the population available are of the medium physique. The piezoelectric microphone sensor is embedded in the inner lining of the cuff at the central place in a separate pocket, so that it gets aligned with the bronchial artery during mounting of the cuff.

However, to measure the pressure based on the oscillometric method, a monolithic piezoresistive pressure sensor (Model: MPXV5050GP) is placed in the cuff. This sensor has a sensitivity of 90mV/kPa and an accuracy of 2.5% with an inbuilt instrumentation amplifier having a gain of 100 to sense the pressure from the cuff. Further, a piezoelectric microphone is used to sense the auscultatory signals and the signals captured in this section of the instrument is then further processed in the analog section.

3.3.2 Analog section

In this section, oscillometric and auscultatory signals are amplified and filtered before sending the signal to the microcontroller unit. The oscillometric signal obtained from the monolithic piezoresistive pressure sensor has a superimposed AC signal due to palpation dynamics of the bronchial artery along with the dc signal during the process of inflation and deflation of the cuff. The maximum pressure designed for smooth workingis

approximately 300mmHg which corresponds to approximately3.8 Volts DC level as per the sensitivity of the sensor. This signal is given as an input to a second order active bandpass filter with a roll-off factor of -40 dB/decade to filter the AC signal. The range of frequencies in the passband varies from 0.3 Hz to 20 Hz with 0.3Hz as the lower cutoff

frequency and 20 Hz as the upper cutoff frequency. The output of the second-order band-pass filter containing AC signal is then transferred to the microcontroller unit for further processing. However, on the other hand, auscultatory signal sensed from the piezoelectric microphones is first amplified in the analog section, which further passed through low pass filter before it reaches to the microcontroller section for further processing.

3.3.3 Microcontroller unit

The third section of our system is the Microcontroller unit. We have used ARM LPC2148 microcontroller in our developed pressure meter. This controller has two 10-bit ADC, which provides a total of 14 Analog inputs, with conversion time as low as 2.44 microseconds per channel. The following are the major work employed by the microcontroller section of the instrument.

First, work is to control the pneumatic section, which involves inflating and deflating the cuff using the motor and valve circuit. The second work is to process the AC and DC signals obtained from sensors over the analog section to quantify the oscillometric and auscultatory signals.
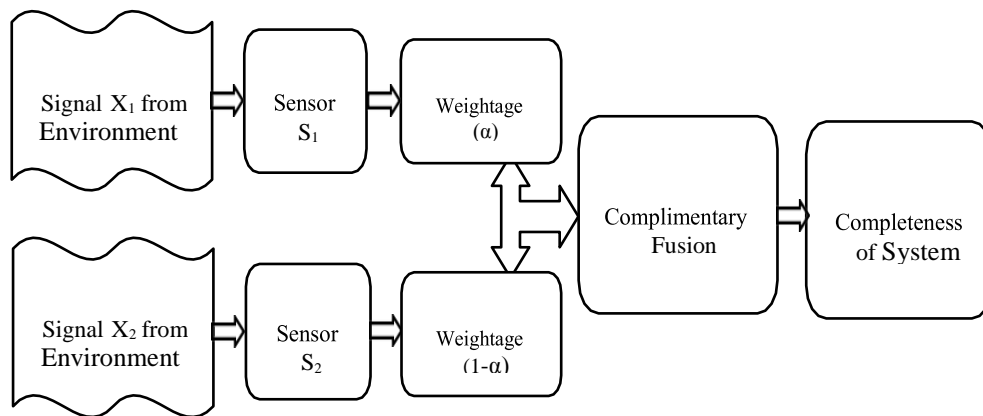
Figure 3.4: Illustration of Complementary sensor data fusion

Further, the details about the acquiring and processing of oscillometric and auscultatory signals are explained in section 3.4.1.2.1 and 3.4.1.2.2.

3.4 Data Fusion for Accuracy

As mentioned in the previous sections, the oscillometric and auscultatory method of pressure measurement depends on the various factors, that often lead to the variation in pressure value measured as compared to the actual value. Especially, in the case of oscillometric methods, most of the time sensors fail to provide the readings for Hypotension and Hypertension patients [149,150]. Hence, to avoid these errors, in recent times, instruments have been developed to have two separate sensors to capture oscillometric and auscultatory signals, such that even if one of the sensors fails, still the pressure can be measured with the other sensor. Moreover, very often complimentary fusion methods have been used where α is the variable and can be customized depending on the type of sensor operated. Equation for systolic pressure is given by Equation 3.6.

$$SBP = 3*MAP - 2*DBP \qquad (3.6)$$

Similarly, the equation for the diastolic pressure of oscillometric and auscultatory sensor can be easily deduced (For simplicity, we have not shown the equation diastolic pressure).

However, the fusion operator employed by most of the vendors is not known. Considering these above facts, we have introduced the complementary fusion approach for sensor data fusion. Figure 3.4, illustrates the block diagram for complementary data fusion. The mathematical details of the fusion are given as follows:

Let the $Oscillometric_{sys}$ and $Auscultatory_{sys}$ be the systolic pressure obtained from the oscillometric and auscultatory sensor. The complementary information fusion for systolic blood pressure measurement is given by the following Equation 3.7.

$$Pressure_{sys} = ((1 - \alpha) * Oscillometric_{sys}) + ((\alpha) * Auscultatory_{sys}) \text{ for } 0 \leq \alpha \leq 1 \quad (3.7)$$

Where α is the variable and can be customized depending on the type of sensor operated.

3.4.1 Experiments and Results

In this section, we present the experimental protocol and the results based on our developed instrument. The results were obtained independently for oscillometric and auscultatory method and fusion of these methods using complementary fusion operator.

3.4.1.1 Experiment 1

Table 3.1: Detail description of number of samples data generated based on Windkessel model.

No of subjects	Oscillometric		Auscultatory		No of measurements	Number of folds	Total samples
	Systolic	Diastolic	Systolic	Diastolic			
3	2		2		100	20	24000

Table 3.2: Comparison results for oscillometric, auscultation, complementary fusion at various values of α and state-of-the-art fusion methods such as min, max method.

Subjects	Pressure	Oscillometric	Auscultatory	Complementary fusion at α					MIN	MAX
				0.3	0.4	0.5	0.6	0.7		
Normal	Systolic	9.1435	8.8241	6.7059	6.2548	6.0656	6.1624	6.5326	7.139	7.094
	Diastolic	5.2236	6.0346	4.2148	4.1142	4.154	4.3304	4.6278	5.0959	4.4714
Hypotension	Systolic	4.2763	4.4635	3.1927	3.0217	2.9808	3.0753	3.2936	3.2359	3.6832
	Diastolic	4.3942	4.4377	3.321	3.1414	3.0833	3.1536	3.344	3.5086	3.7601
Hypertension	Systolic	5.77	5.856	4.0318	3.7254	3.6267	3.7521	4.0811	4.6385	4.1794
	Diastolic	5.2766	5.9671	4.1179	3.9807	3.9991	4.1711	4.4791	4.52	4.6693

The values of α selected are 0.3 and 0.7, to select higher and lower contribution from the sensors involved. Same contribution comes with 0.5 Value.

We present the results in three experiments: Experiment 1 presents the measurement errors in estimating oscillometric and auscultatory measurement based on the simulated sample

data (systolic and diastolic data) obtained using Windkessel model. Experiment 2 presents the blood pressure measurement for real subjects for various values of signal threshold. Experiment 3 is customizing the parameters α and threshold values from Experiment 1 and Experiment 2. The details of each of these experiments are discussed in the following sections.

In this experiment, we optimize the parameters for the complementary fusion method to combine oscillometric and auscultatory signals. Further, in the experiment, we present the systolic and diastolic pressure based on the optimized parameters. To perform this experiment, we introduced well known Windkessel model to randomly generate systolic and diastolic measurement by simulating the heart. The model is used to generate the measurement for three categories of patients: Normal, Hypertension and Hypotension categories having a standard deviation of ±10 about the reference pressure. The model is programmed to generate the reference measurement by considering the standard range of human blood pressure measurement chart for Normal, Hypertension, and Hypotension category. The reference reading for Normal, Hypertension, Hypotension is in the range of $50 - 82$ mmHg, $70 - 105$ mmHg, $110 - 170$ mmHg respectively. The total number of samples generated consists of 3CategoriesofSubjects x 2Oscillometricsignals x 2Auscultatorysignals x 100Measurement x 20 Folds of repetition = 24000 Total samples. Table 3.1 illustrates in more detail the classification of data in each category.After, generating the data using the Windkessel model, we processed the data to compute pressure using our complementary fusion method for various values of α shown in Equation 3.7. We present the validation results of complementary information fusion is illustrated in Figure 3.4
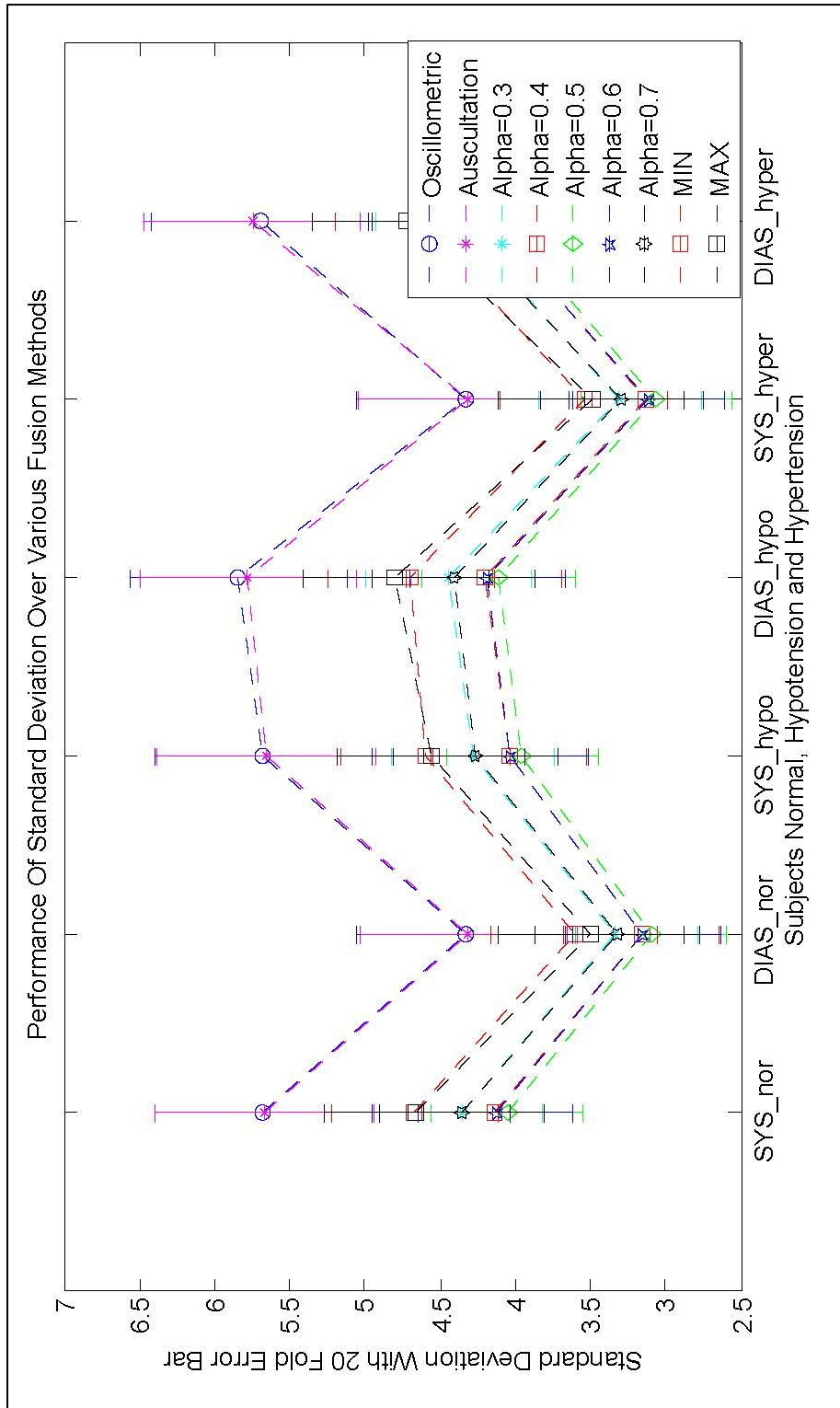
Figure3.5:Performance measurement in terms of standard deviation for oscillometric, auscultation, complementary fusion (α=0.3,0.4,0.5,0.6,0.7) , min fusion, and max fusion.

Observation 1 : Table 3.2 and Figure 3.5 presents the set of results estimating the errors in computing systolic and diastolic pressure for oscillometric, auscultation, using complementary fusion at various values of α and state-of-the-art fusion methods such as min, max method. Following major observation can be made:

The overall better measurement accuracy is obtained for fusion methods as compared to the oscillometric and auscultatory method operating independently. Specifically, our intuition of using complementary fusion method outperforms single method (Either, oscillometric and auscultatory method) and the state-of-the-art fusion methods such as min, max. Of the results obtained by a complementary fusion method, better measurement accuracy is obtained for α = 0.5 value for Normal, Hypertension, and Hypotension patients.

Observation 2: The British Hypetension Society (BHS) protocol classifies, the blood pressure monitoring devices into grades A to D, where, grade A shows the best accuracy and grade D is assigned to the device with the worst accuracy. Hence, to support such grading we have performed Clarkes Error Grid analysis to verify the percentage measurement accuracy over A and B quadrants. Figure 3.6 and Table 3.6represents graphically the accuracy independently for oscillometric and auscultatory method, and complementary fusion at various values of α such as 0.3,0.4,0.5,0.6,0.7 and state-of-the-art fusion such as min, max methods. Figure 3.10 demonstrates the fusion for various values of α.The results obtained for Normal, Hypertension and Hypotension categories, we make our following observations: The measurement accuracy for all values of α in complementary fusion method is around 90%, proving a reasonable accuracy in measurement. However, better measurement accuracy is obtained for min fusion method, but such method fails in the scenarios when either of the signal (oscillometric or auscultation) is deteriorates as in the case of Hypertension and Hypotension subjects.
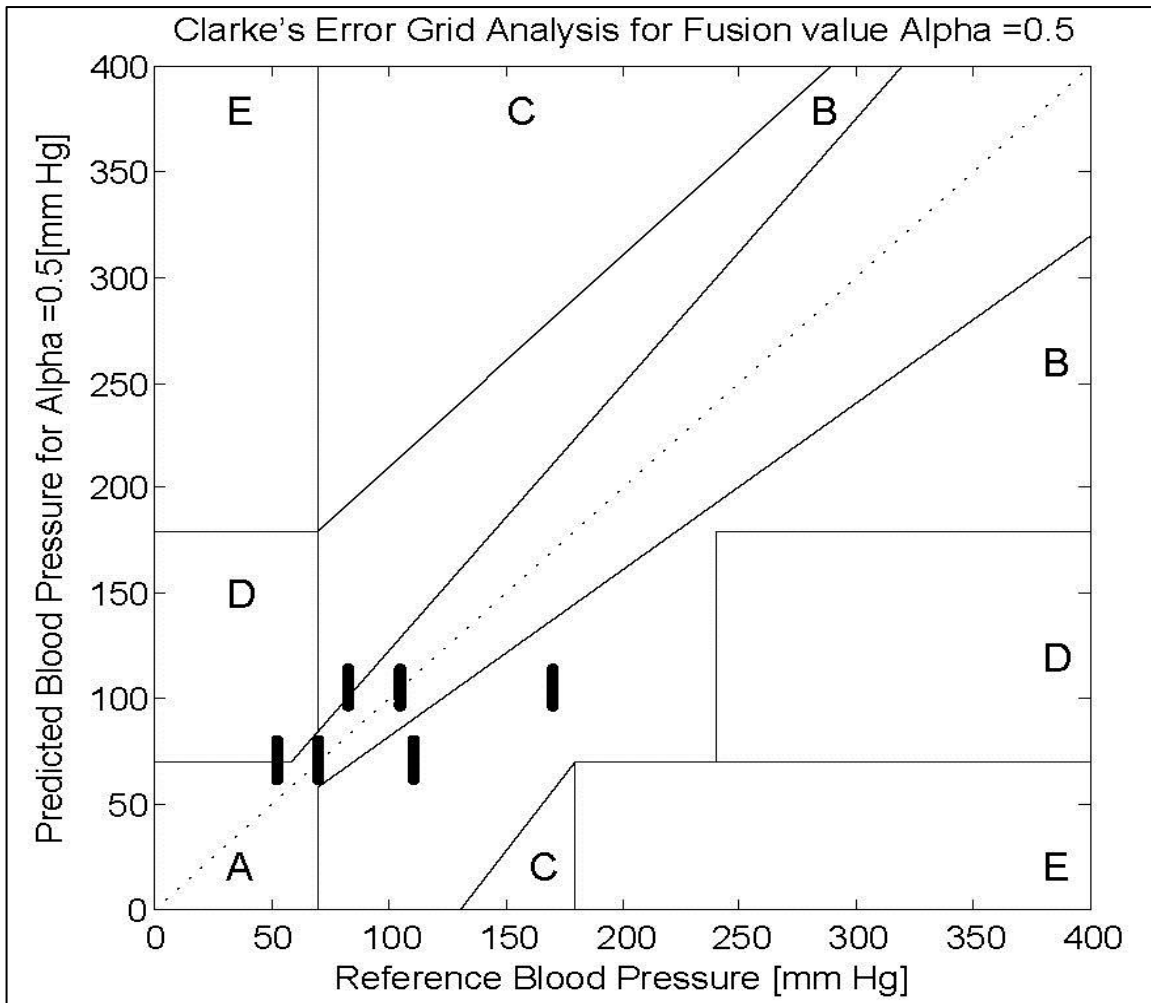
Figure 3.6: Clarks Grid chart illustrating complementary fusion method for measurement of systolic and diastolic values over Normal, Hypertension, and Hypotension categories. Here, we have shown the graphical results for $\alpha = 0.5$ for simplicity.

3.4.1.2 Experiment 2

This section, we present the experimental protocol and the results based on our developed instrument. The oscillometric and auscultation waveforms were fed into MATLAB via serial port for offline analysis. FIR filter was used to denoise the noisy waveforms as shown in Figure 3.7 and obtain cleaner waveforms as shown in Figure 3.8.
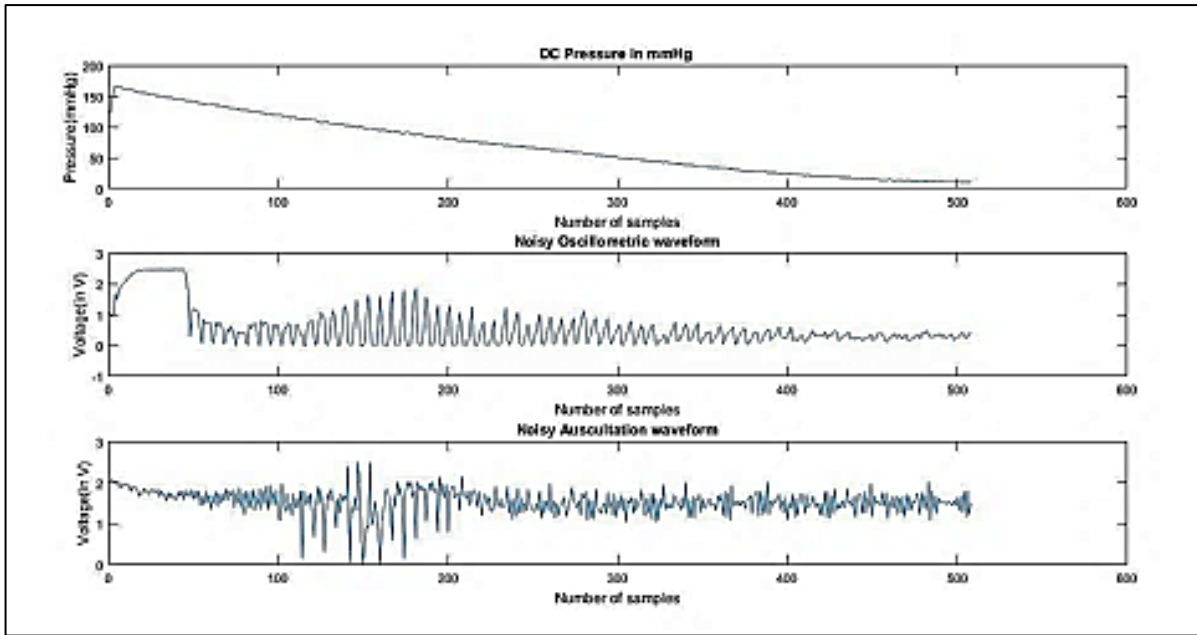
Figure 3.7: Noisy oscillometric and auscultation waveforms
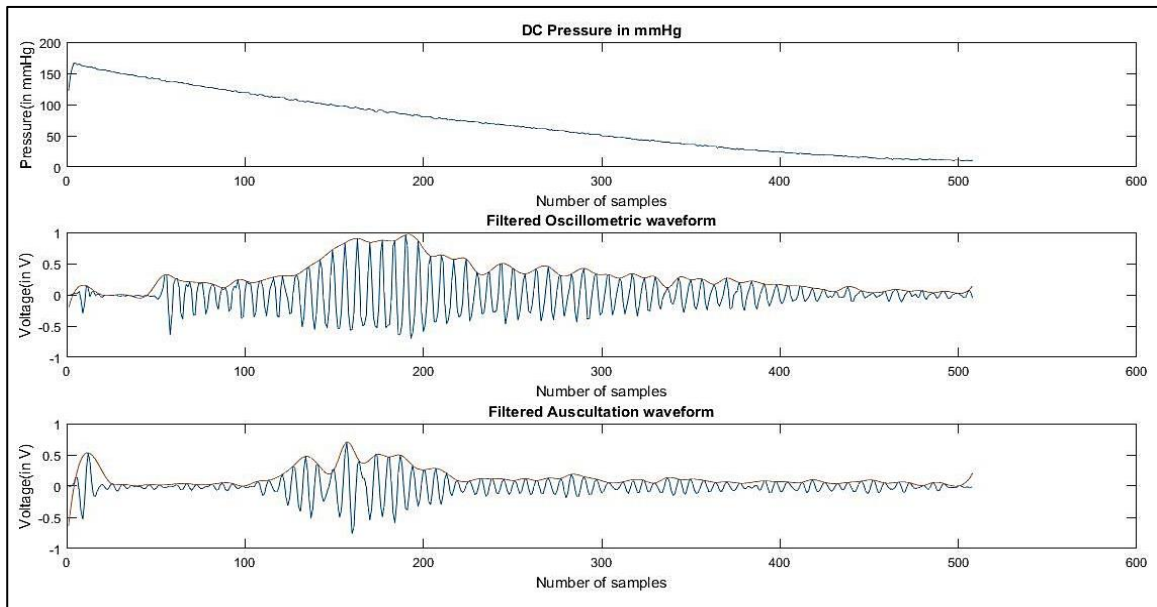
Figure 3.8: Filtered oscillometric and auscultation waveforms

3.4.1.2.1 Algorithm for Oscillometric Method

After filtering the next step is to find the envelope of the oscillometric waveform by using a moving average filter. Then we calculate the average of the envelope. The systolic pressure is the point at which the envelope crosses a certain threshold (100%,80% and 50% of average). The Mean Arterial Pressure is calculated by finding the maximum point

on the envelope obtained. Once we obtain the systolic and diastolic values the diastolic pressure is obtained by Equation 3.

3.4.1.2.2 Algorithm for Auscultation method

The first step is to find the envelope of the auscultation waveform by using a moving average filter. Calculate the average of the obtained envelope. The systolic pressure is the point at which the envelope crosses a certain threshold (100%,80% and 50% of average). The Diastolic Pressure is the point at which the envelope crosses the threshold (100%,80% and 50% of average) from the maximum point of the envelope.

Total ten readings of four subject was taken with simultaneous readings from Rossmax meter as shown in Table 3.3.Three values of threshold were used a) 100% of average b) 80% average c) 50% to find which gave the lowest standard deviation when compared to the reference RossmaxAC701k blood pressure meter as shown in Table 3.4. Standard deviation is the least when we choose the threshold as 80% of the average for the four subjects.

Table 3.3: Total ten readings of a subject with the blood pressure meter developed along with readings from Rossmax meter.

   a) **Threshold = 100% of average**

Our designed system			
Sys(Rossmax AC701k meter)	Sys(osc)	Sys(aus)	Sys(fusion)
113	136	124	130
122	125	121	123
126	123	133	128
124	114	132	123
120	135	137	136
124	128	128	128
122	124	117	120.5
119	111	122	116.5

118	119	115	117
118	127	127	127

Our designed system			
Dias (Rossmax AC701k meter)	Dias(osc)	Dias(aus)	Dias(fusion)
82	71.5	83	77.25
83	78.5	64	71.25
87	96	72	84
86	75.5	72	73.75
83	74	82	78
88	83	78	80.5
80	65.5	69	67.25
78	78	100	89
78	93.5	74	83.75
75	71.5	63	67.25

b) Threshold = 80% of average

Our designed system			
Sys(Rossmax AC701k meter)	Sys(osc)	Sys(aus)	Sys(fusion)
113	136	125	130.5
122	126	122	124
126	126	137	131.5
124	123	134	128.5
120	136	138	137
124	128	128	128
122	124	118	121
119	123	123	123

118	133	116	124.5
118	127	127	127

Our designed system			
	Dias(osc)	Dias(aus)	Dias(fusion)
Dias(Rossmax AC701k meter)			
82	71.5	83	77.25
83	78	64	71
87	95.5	72	83.75
86	72	72	72
83	73.5	82	77.75
88	78	83	80.5
80	65.5	69	67.25
78	72	100	86
78	86.5	74	80.25
75	71.5	63	67.25

c) **Threshold = 50% of average**

Our designed system			
	Sys(osc)	Sys(aus)	Sys(fusion)
Sys(Rossmax AC701k meter)			
113	134	136	135
122	127	128	127.5
126	137	137	137
124	134	134	134
120	139	138	138.5
124	128	128	128
122	124	119	121.5

119	131	131	131
118	133	133	133
118	127	127	127

	Our designed system		
Dias(Rossmax AC701k meter)	**Dias(osc)**	**Dias(aus)**	**Dias(fusion)**
82	71.5	83	77.25
83	77.5	64	70.75
87	89	72	80.5
86	66.5	72	69.25
83	73	82	77.5
88	83	78	80.5
80	65.5	69	67.25
78	68	100	84
78	86.5	74	80.25
75	71.5	63	67.25

Table 3.4: Average standard deviation of three subjects

For Threshold=100%			
	Subject 1	**Subject 2**	**Subject 3**	**Subject 4**
Std Dev (sys)	7.25	8.04	4.61	6.63
Std Dev (dias)	7.79	5.92	4.56	6.09
For Threshold=80%			

	Subject 1	Subject 2	Subject 3	Subject 4
Std Dev (sys)	6.05	8.20	2.69	5.65
Std Dev (dias)	6.86	5.93	4.59	5.79
For Threshold=50%				
	Subject 1	Subject 2	Subject 3	Subject 4
Std Dev (sys)	6.74	9.30	2.61	6.21
Std Dev (dias)	6.80	6.13	4.80	5.91

3.4.1.3 Experiment 3

In this section, we present the accuracy of our system for real subjects based on the optimized parameters (α = 0.5) from Experiment 1. We selected three categories of patients, one subject in each of the categories: Normal, Hypertension and Hypotension patient. The measurement is repeated for oscillometric and auscultatory measurement of 100 times.

Table 3.5:Data generated for Normal, Hypertension and Hypotension patient

No of subjects	Oscillometric		Auscultatory		No of measurements	Number of folds	Total samples
	Systolic	Diastolic	Systolic	Diastolic			
3	2		2		100	1	1200

The detail description of the database is shown in Table 3.5. The obtained results with our developed instrument are compared against the reference meter (RossmaxAC701k Upper Arm Blood Pressure Meter). The Rossmax meter is selected for the reference measurement since this meter uses the advance dual sensor cuff system, which senses both pressure and sound. The meter meets the AAMI accuracy standard requirements (AAMI/ANSI/ISO 81060-2).

Table 3.6 : Quadrant A, B, and D % values in Clarke Grid Chart.

Fusion Scheme		Quadrant values (%)			Regression r=A+B
		A	**B**	**D**	
Complementary Fusion at various α values	*α= 0.3*	41.16	50.16	8.60	91.32
	α= 0.4	41.50	49.16	9.33	90.66
	α= 0.5	41.67	49.17	9.17	90.82
	α= 0.6	42.50	48.67	8.83	91.16
	α= 0.7	42.50	48.67	8.83	91.16
MIN		49.33	45.50	5.17	94.83
MAX		38.00	49.50	12.50	87.50

Table 3.7 : Standard Deviation in systolic and diastolic pressure for complementary fusion method with $\alpha = 0.5$ for Normal, Hypertension, and Hypotension subject (Here, *'Std'* corresponds to standard deviation)

Subject	Pressure	Stdfor complementary fusion with alpha=0.5
Normal	**Systolic**	2.45
	Diastolic	1.75
Hypertension	**Systolic**	2.7
	Diastolic	2.9
Hypotension	**Systolic**	1.78
	Diastolic	2.5

Figure 3.11 and Figure 3.12 presents the waveform acquired in real time for auscultation and oscillometric sensor on the oscilloscope. Further, Table 3.7 represents the standard deviation at the parametrized α = 0.5 value for measuring systolic and diastolic pressure for Normal, Hypertension and Hypotension patients. Similarly, Figure 3.9 illustrates the graphical representation of results. The major observations of these experiments are as follows. We have successfully implemented the real-time data acquisition system for obtaining oscillometric and auscultation signal by fusion algorithm. The average measurement error for systolic and diastolic pressure with our approach shows the standard deviation approximately between 1.7 to 2.9 range, which is well within the acceptable limit.The designed low-cost pressure meter is not clinically validated for a large population size as per BHS and AAMI standards. The proposed system will give directions to the researcher community to employ sensor fusion methods to describe the completeness of the system under observation. Also, the said implementation has demonstrated data acquisition in real time for several sensors. The study can be extended for more number of fusion algorithms and large number of sensors.
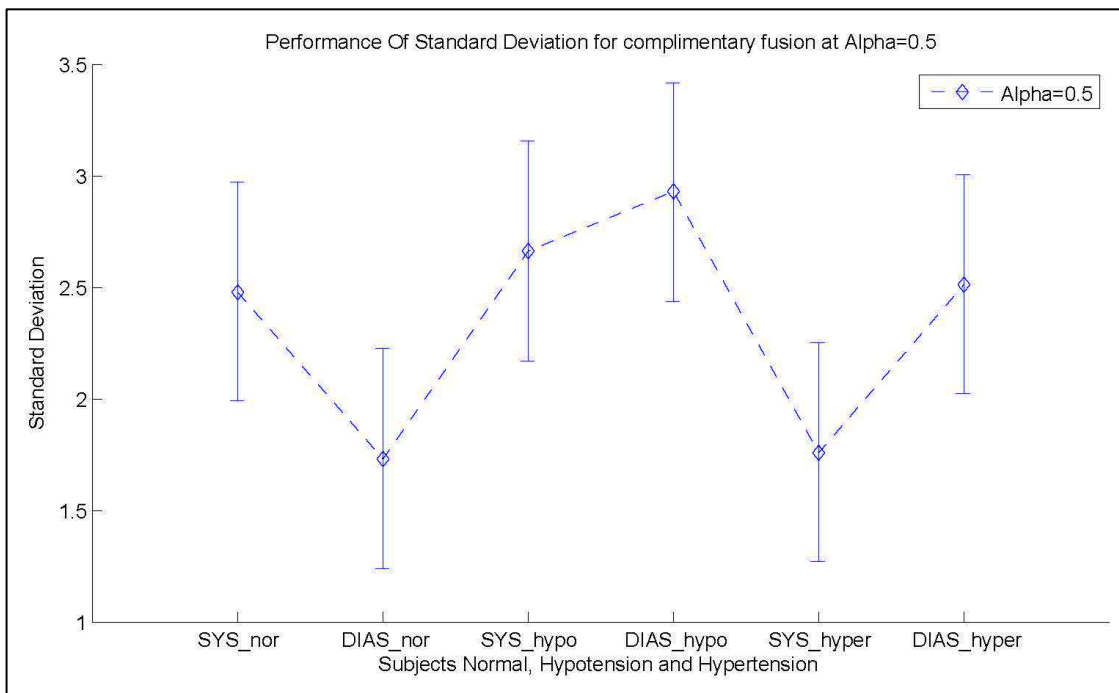
Figure 3.9: Performance measurement in terms of standard deviation for complementary fusion with $\alpha = 0.5$

This study describes the design of an integrated oscillometric and auscultatory based blood pressure meter to determine the systolic and diastolic blood pressure values of Normal, Hypertension and hypotension subjects. The oscillometric and auscultatory methods were

individually tested in a laboratory environment and fused for data using the complementary fusion method to improve the measurement accuracy with minimum error. The various stages of the develpoment of the human blood pressure meter are shown in Figures 3.13 to 3.15.The proposed method is quite efficient in the measurement of blood pressure for Hypertension and Hypotension subjects which is demonstrated through the simulation studies for 100 recordings in 20 fold. The error analysis and prediction error are presented using the standard deviation and Clarke Error Grid analysis. It is found that the fusion methods help in improvising the measurement error accuracy and prediction accuracy for the nearly non-biased fusion at. The interpretation of the Clarke Error Grid indicates that complementary rule can help in improvising the prediction and can also improvise the overall prediction accuracy around average 90. Although the system meets the basic requirements, it can further be enhanced with the combination of complex circuitry for motion artifacts, sensor data pre-processing and prediction algorithms.
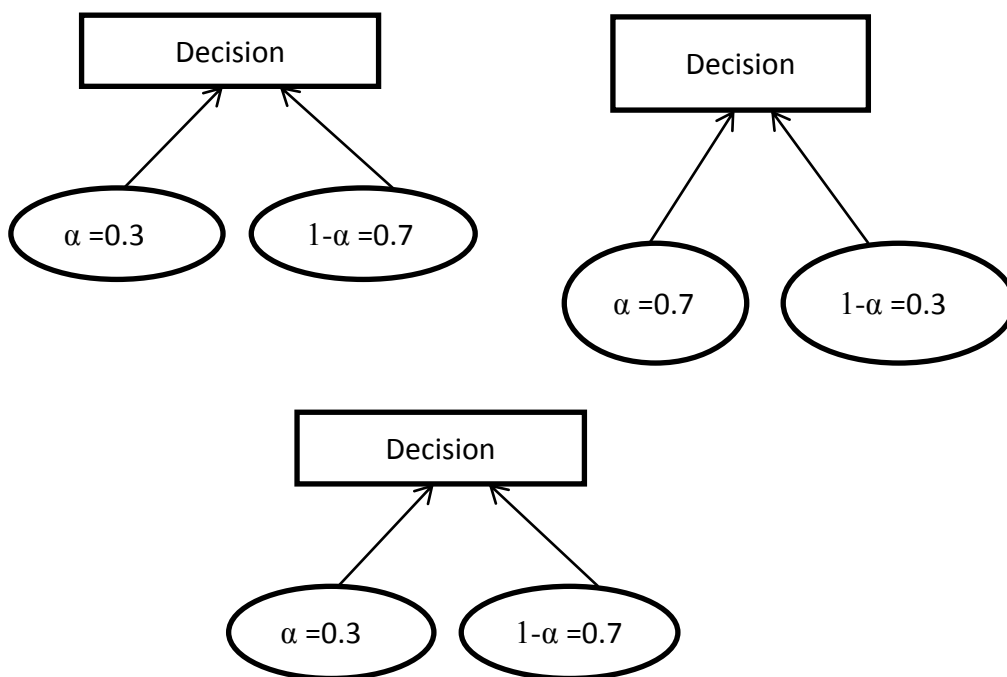
Figure 3.10 : Various complementary methods for values of α
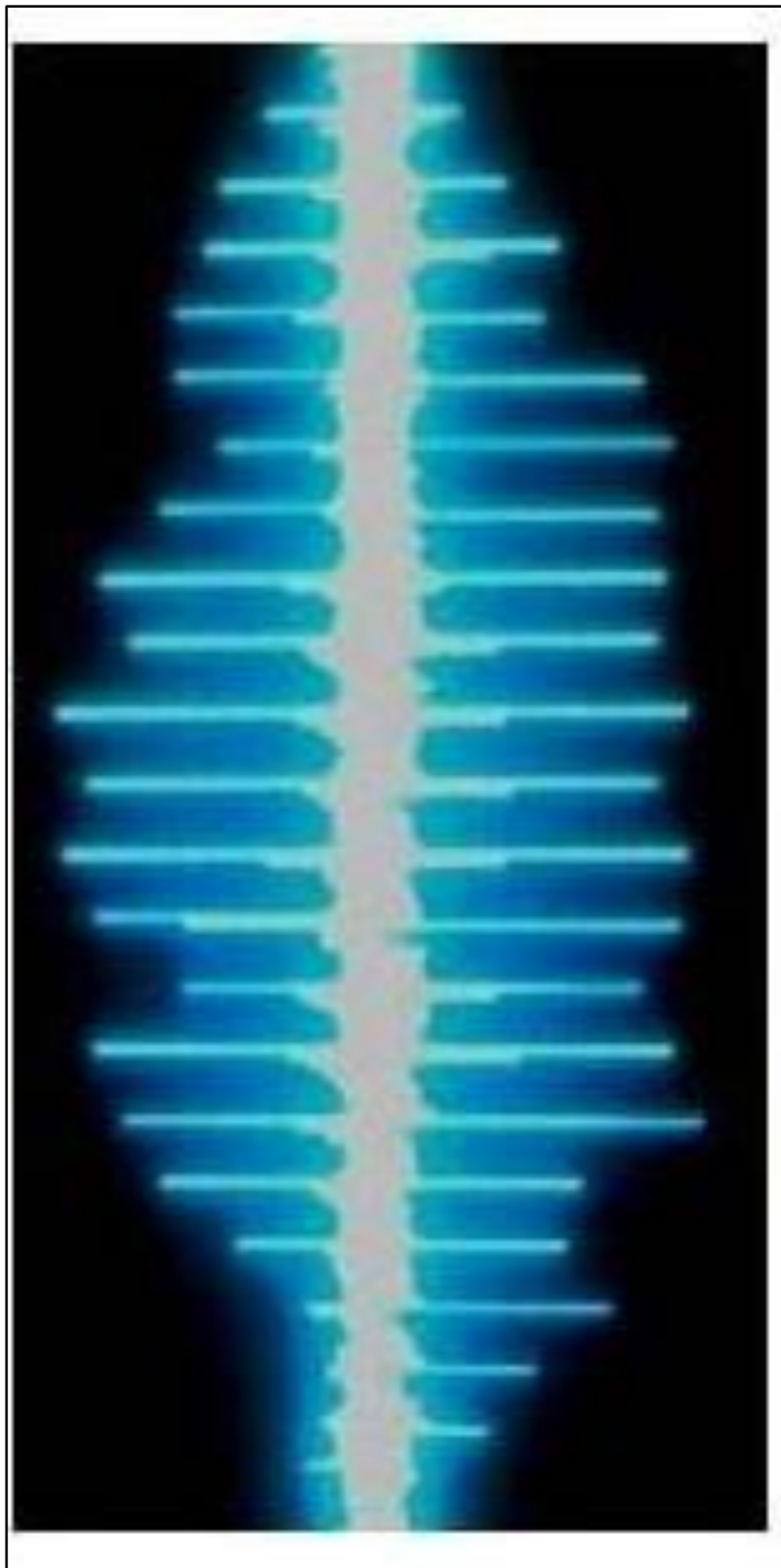
Figure3.11: Auscultation waveforms observed on oscilloscope

Figure3.12:Oscillometric waveform for piezo sensor observed over the oscilloscope

Figure3.13: The 2-sided Printed Circuit Board Design of the proposed system

Figure3.14:The meter assembled in custom design box using 3-D printing for various components
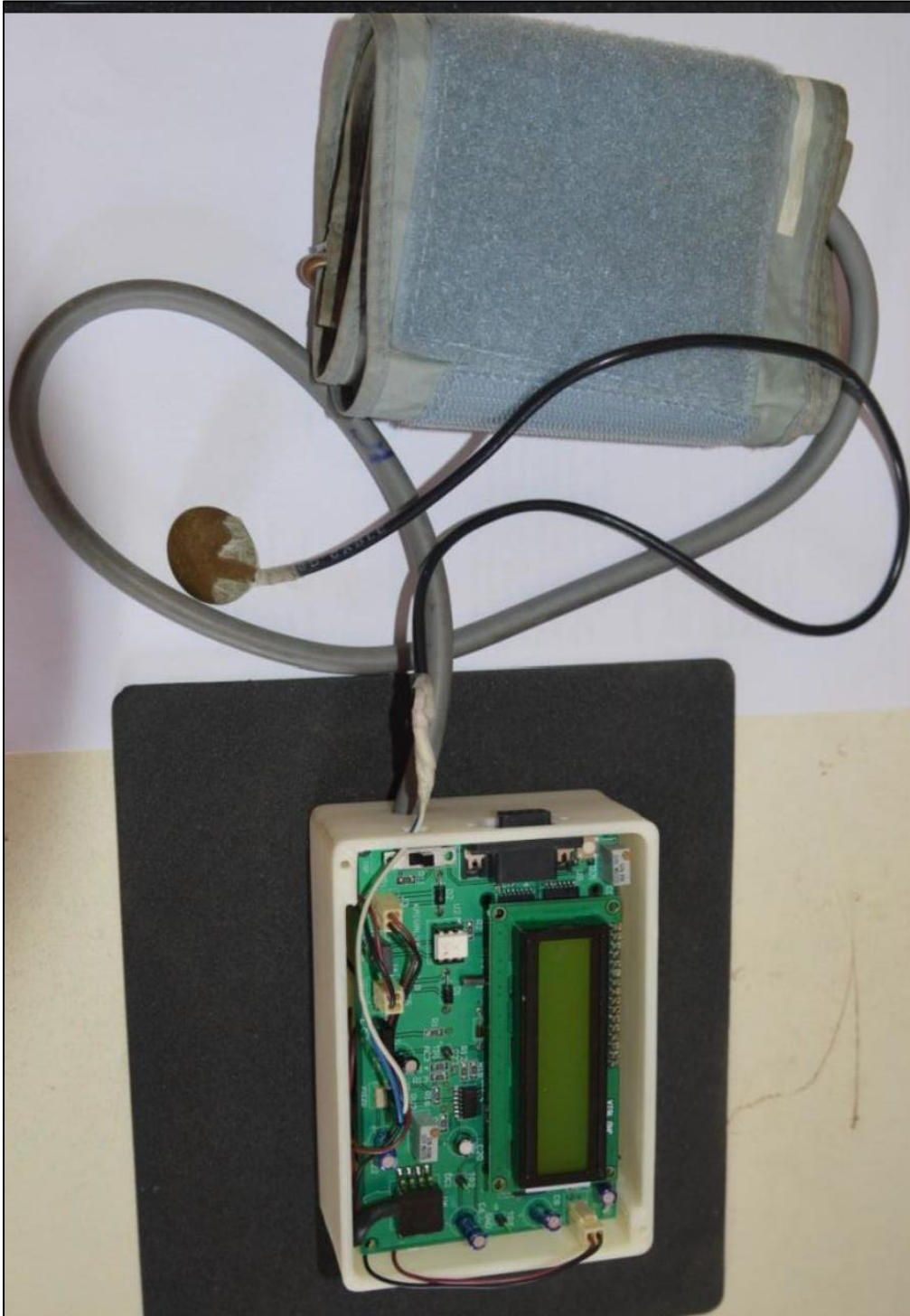
Figure3.15:The final integrated meter for both the sensors with cuff.

3.5 Human Electrocardiogram(ECG) System

3.5.1 Implementation of ECG Model by Sharrys

McSharry's has modeled an ECG signal with practical PQRST morphology and heart rate dynamics[154]. The model creates a standard practical EC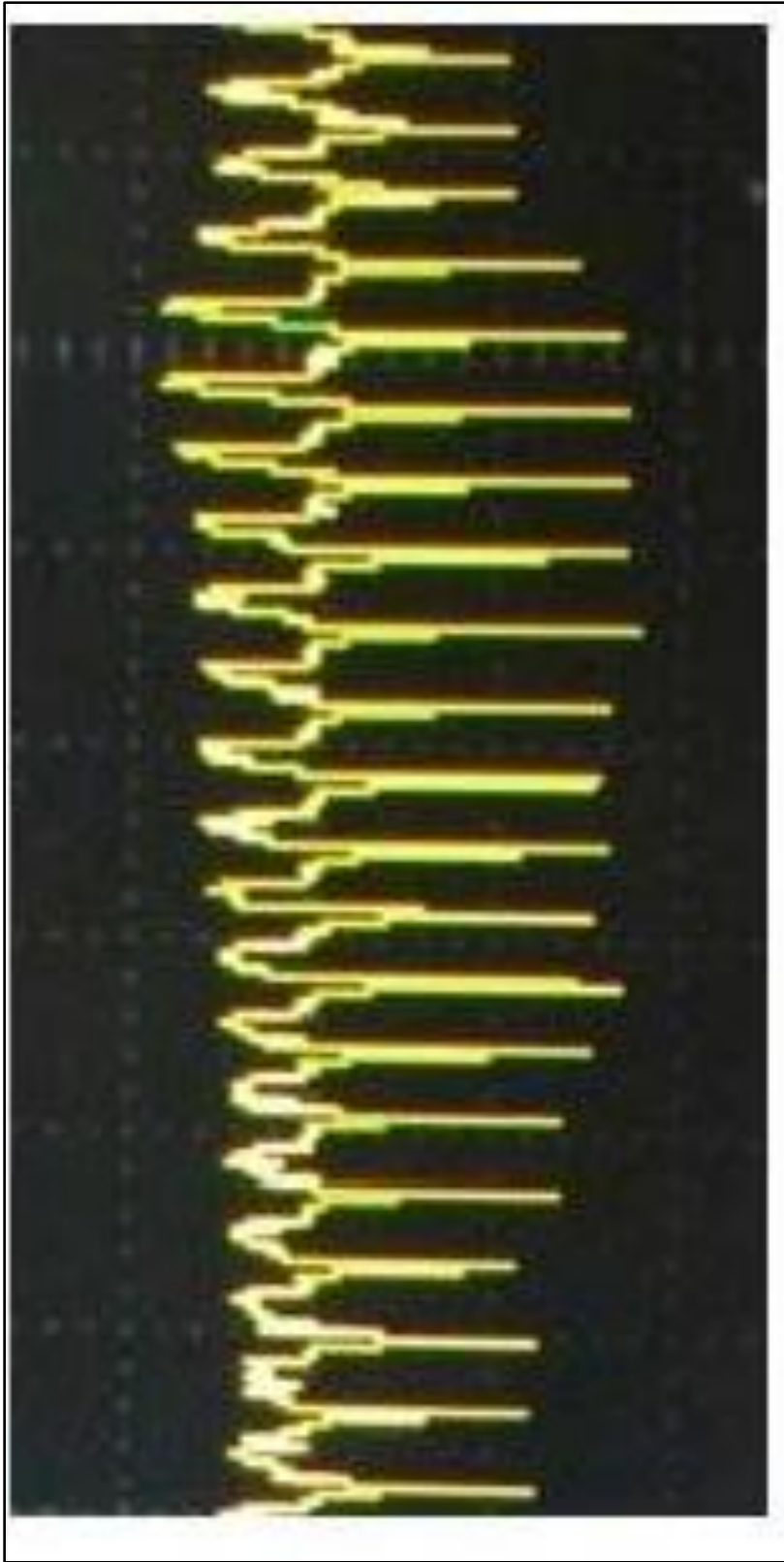G signal with features that can be generated with the mean and standard deviation of the heart rate and frequency-domain features of HRV. To extract useful pathological information from the real physiological signals (like ECG) effective signal processing techniques are needed [155,156,157]. Filtering is the most widely used signal processing technique because if the signal is corrupted by noise then no matter what signal processing or statistics is used it tends to become irrelevant. After filtering the next step is usually find the R peaks in the QT-interval detection [158,159,160], and then find the heart rate from the RR interval. The RR intervals are the time interval between two consecutive R peaks, the inverse this time interval gives us the current heart rate. The RR recordings over time give us a fair insight into the pathological state of a human being. A lot of signal processing is being developed by researchers [161,162,163]to get a better understanding of more fiducial and non-fiducial features of the heart. A live ECG signal such as those found in ECG databases like Physionet will be affected by certain noise parameters but certainly not all the possible noise sources. With the generation of synthetic ECG, it is possible to add different types of noise conditions. Then comparison studies can be done to find the best signal processing algorithm for the given noise.

The model creates a trajectory with coordinates (x, y, z) (in a three-dimensional (3-D) state-space. The ECG's quasi-periodicity is expressed in the trajectory's motion around an attracting unit radius limit cycle in the (x, y) plane. Each revolution corresponds to one RR-interval or heartbeat in this circle. The ECG's interbeat variation is performed using the trajectory movement.

The ECG reproduces interbeat variation by moving the path in the direction. Events corresponding to adverse and positive attractors / repellers in the direction describe distinct points on the ECG, such as the P, Q, R, S, and T.These events are positioned at set corners along the circle of the unit provided by Θ_P, Θ_Q, Θ_R, Θ_s, Θ_T. When the path approaches one of these occurrences, it is pushed up or down from the limit cycle and then pulled back to the limit cycle as it moves away.

The dynamic equations of motion are given by a set of three differential equations adapted from Mc Sharry's model[2] given below.

$$\dot{x} = ax - wy \qquad (3.8)$$

$$\dot{y} = ay + wx \qquad (3.9)$$

$$\dot{z} = -\sum_{i \in P,Q,R,S,T} a_i \Delta_i exp(-\Delta \frac{\theta_i^2}{2b_i^2}) - (z - z_0) \qquad (3.10)$$

where; $a = 1 - \sqrt{x^2 + y^2}$, $\Delta\theta_i = \theta - \theta_i (mod 2\Pi)$ $\theta = atan2(y,x)$ The times and angles (θ_P, θ_Q, θ_s, θ_T) are relative to the R peak. ai gives the positive or negative peaks of the PQRST wave and bi gives the width(duration) of each significant component (P, Q, R, S, T). The ECG wave varies as a function of heart rate as shown in Figure 3.16 (a, b, c). The model parameters of the system implemented is shown in Table 3.8.

Table 3.8:Model system parameters of ECG model

Index(i)	P	Q	R	S	T
Time(secs)	-0.2	-0.05	0	0.05	0.3
θ_i	-1/3 π	-1/12 π	0	1/12 π	1/2 π
a_i	1.2	-5	30	-7.5	0.75
b_i	0.25	0.1	0.1	0.1	0.4
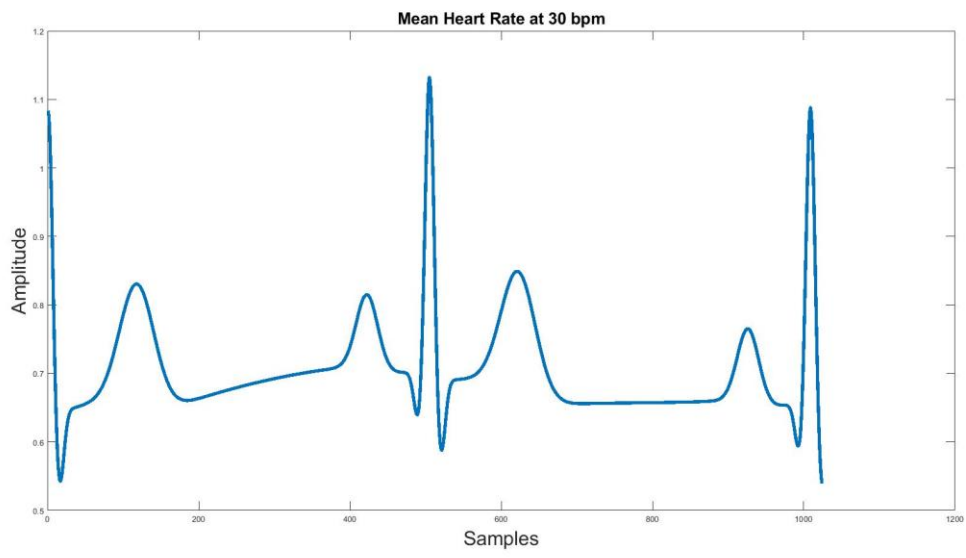
(a)
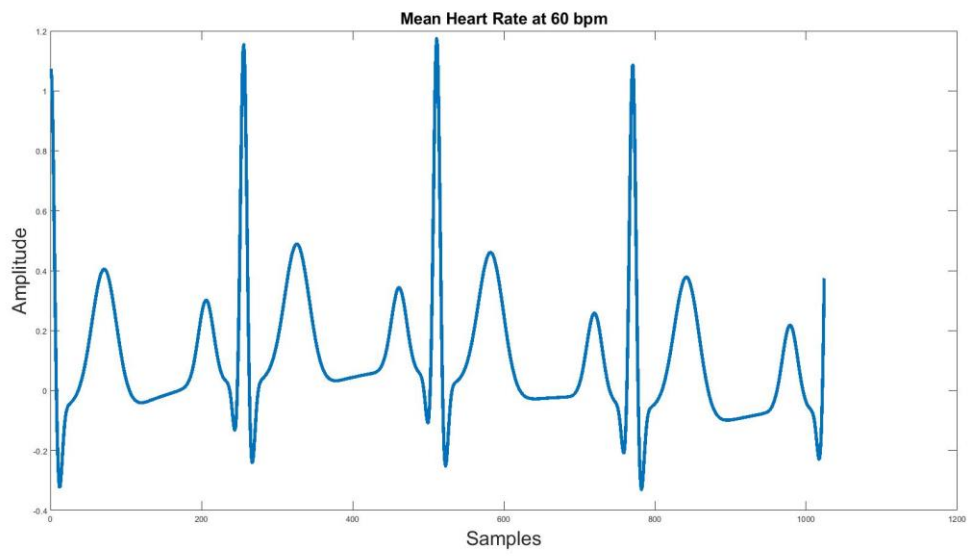
(b)
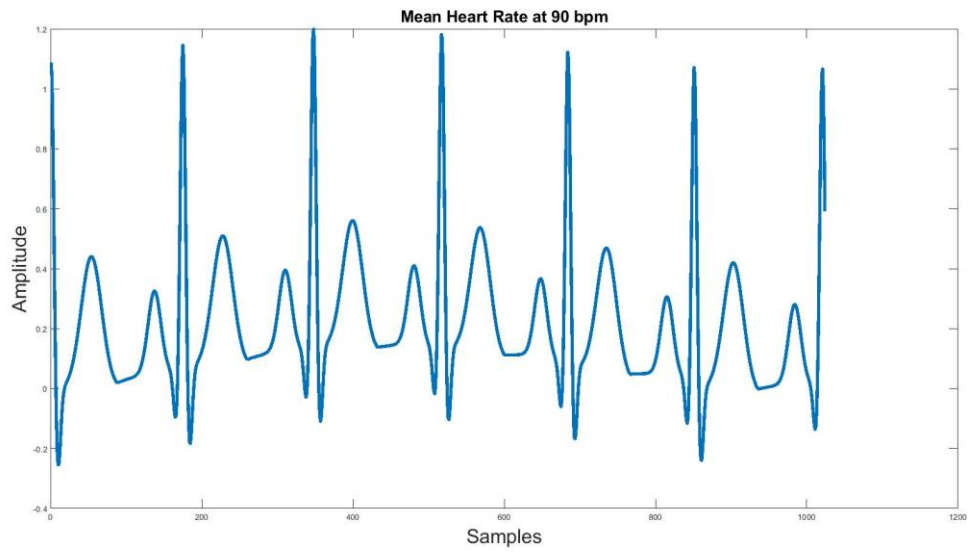
(c)

Figure 3.16: The ECG model to generate the (a) Mean Heart Rate 30bpm, (b) Mean Heart Rate 60bpm and (c)Mean Heart rate 90bpm

Chapter 4

Modelling of EEG System

4.1 Human Electroencephalogram (EEG) System

Decoding the neuronal activity of the human brain has been intriguing researchers for a long time [164,165,166,167].   But owing to the complexity of the human brain which consists of billions of neurons it becomes cumbersome to understand the various underlying neuronal processes [168,169,170]. One way of simplifying this is by using mathematical models that try to mimic the activity of the various levels of the human brain. The bases of these models are usually the differential equations associated with the state of the variable of the system describing it, which explains the dynamics of the brain. Physically it corresponds to membrane potentials of each neural mass of interest. In a macroscopic sense, the state variables are the variables that describe the neuron model state while at the abstract level it is the membrane potential. The differential equations describe the flow of state in the time domain between the interplay of the system equations. Such time flows form orbits, thus producing time series for all of the states. Modeling brain neural activities by mathematical models usually give simplification of the real brain activity with a useful insight into the processes that generate neural activity, if the variables under interest are properly chosen. One can also change the system's parameters to obtain different state variables indicating specific behaviors that might not be possible in real-world experiments. Understanding of neural activities is being done by macroscopic or microscopic models. Microscopic models describe the activity at the level of a single neuron. Microscopic neural mass models are based on the coupling of several single neurons as shown in Figure 4.1 and hence computational expensive, since it

involves large number of parameters. Macroscopic neural mass models have less detail and involve an average pattern of a large group of neurons similar to EEG(Electroencephalogram) signals. The single neuron models can be grouped for larger cortical columns but will need a powerful processor for processing these large number of neurons.
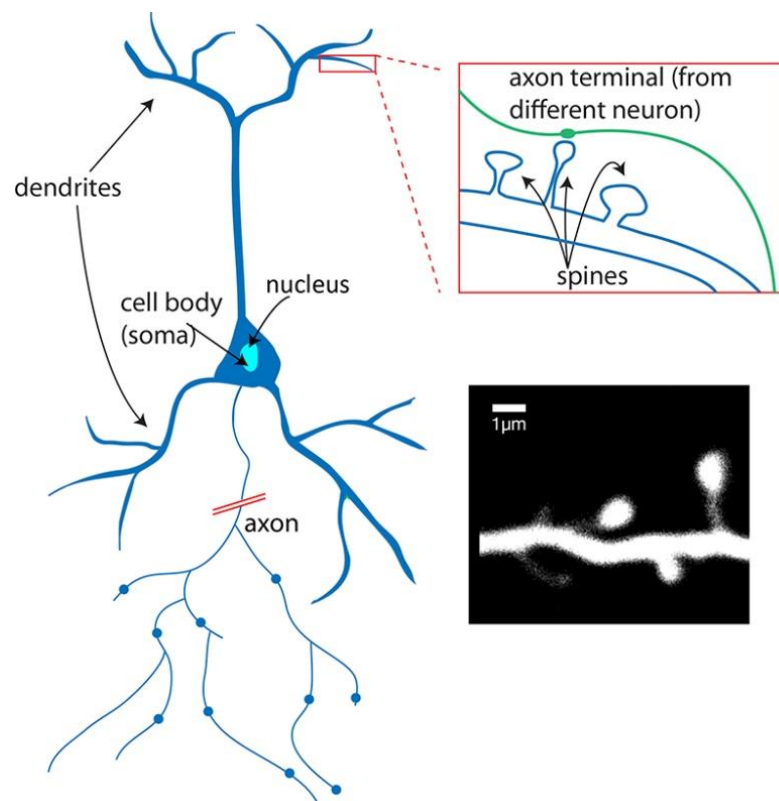
Figure 4.1: The neuron depicting nucleus, dendrites and axon terminal

The solution to this is the use of macroscopic models that depict the average activity of neuronal populations as few number of variables are involved with it. These orbits capture the features of the system like steady state, periodic, quasi-periodic, and chaotic. The main variable of interest of such ensembles describing the Neuronal Mass Model (NMM) is the mean and variance state of membrane potential for the set of an ensemble of neuron's synapses in space. The mean membrane potential increases and decreases in response towards the collective synaptic inputs and this increases or decreases depending on the variation of afferent inputs. Variance can be ignored or minimized if the ensemble activity is coherent; which therefore reduces the number of dimensions so that the interesting local

population can be modeled for excitatory and inhibitory neurons using small numbers of equations (as seen in Figure 4.3) representing the regions over said neural mass. This approach is usually used to describe neural mass models (NMM).

Coarse grained models in a sense simplify the complex models. Originally developed by Lopes Da Silva in 1970's [166] and further extended by Freeman [171,172,173], Wendling [174,175], Zavalgia (176) and so on. Dendrite's receive information/signals from the axons of other neurons. Pyramidal neurons account for 80% neurons in the cerebral cortex. Remaining are the excitatory and inhibitory interneurons (GABAa&GABAb). External input is all the activity from neighboring cortical column.

4.2 Modeling of EEG System

As shown in Figure 4.2 the developed neural mass model consists of four populations which generate the EEG activity. The pyramidal neurons, excitatory neurons, fast and slow inhibitory neurons represent the different populations neurons over the region of cortex. The alpha waves are generated by the interplay of the pyramidal and slow inhibitory interneurons. The fast inhibitory neurons have a self-loop which helps in mimicking the gamma activity of the brain. Single Neural mass where inputs are transformed to potentials using Post Synaptic Potentials(PSP) transforms.
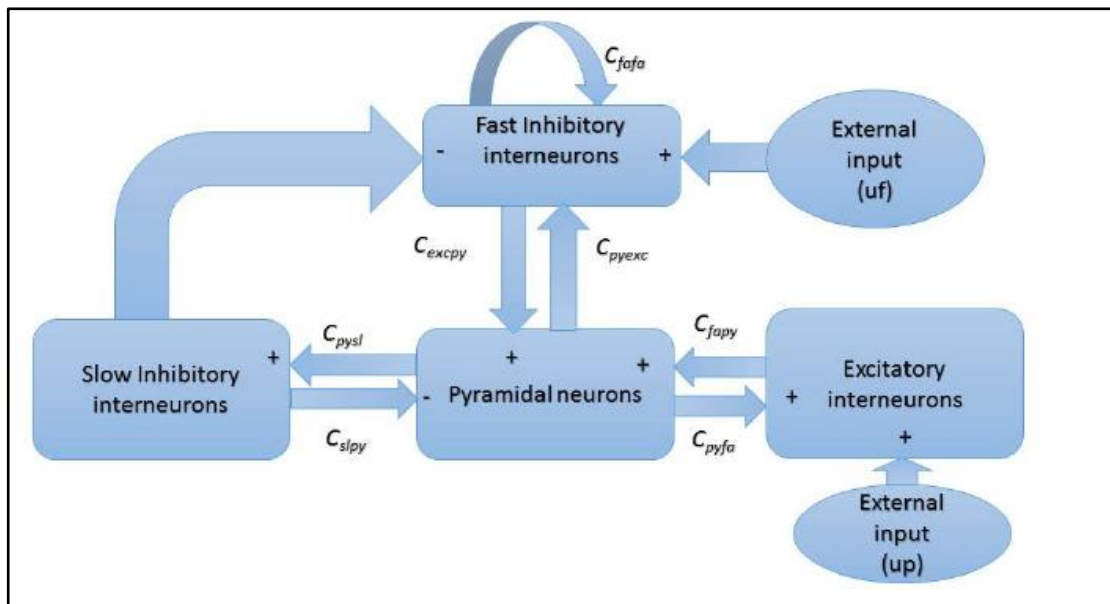
Figure 4.2: Schematic of neural mass model

The average number of synapses from this input to the population are multiplied by a constant. The addition and subtraction of the excitatory and inhibitory potentials produces u(t) over timethe mean membrane potential. Sigmoid function converts u(t) to generate the average pulse rate of the population. The described four neuronal populations i.e. the pyramidal neurons, excitatory interneurons, slow inhibitory interneurons, and fast inhibitory interneurons are derived by two variables the mean firing rate firing $z(t)$ as described in Equation which is a function of mean membrane potential u(t), and mean post synaptic potential $v(t)$. We obtain the mean membrane potential from the weighted summation of inputs. The mean firing rate is deduced by the membrane potential via a sigmoid function:

$$z\ (t) = \frac{2e_0}{1 + e^{-r(v_r - u)}} - e_0 \qquad\qquad (4.1)$$

The maximum firing rate v_{max} of the population of neurons, v_r is the value of the potential for which a 50% mean firing rate is achieved, and r is the slope of the sigmoid at v_r; where the parameter v_r will serve as mean firing threshold. The sigmoid function is parametrized equally for all populations in the model. The mean firing rate, $z(t)$, of one population is coupled to the unweighted mean post synaptic potential population, with help of the transfer function which represents dendrites.

4.2.1 Overview of a neural mass model

The pyramidic population unit of nerve cells excites and receives feedback from all 3 population units of the interneuron population. The slow inhibitory unit of the population of interneurons inhibits the rapidly inhibitory unit of the population of interneurons. For dynamic self-inhibition, the rapid inhibitory interneuron population has an additional state variable, C_{fafa}. The self-feedback loop in the rapidly inhibitory population are of first order and serve as a LPF with cut-off frequency f_c. The quick inhibitory interneuron and pyramidal neuron units are excited for each node by autonomous Gaussian noise. The noise reflects the mean firing rate of outer neural communities that are unmodeled.To transform it to mean post-synaptic potentials, the noise is carried through the dendritic transfer function of pyramidal neurons. In order to excite the pyramidal neurons and quick inhibitory interneurons respectively. The pyramidal population's mean membrane potential

is the primary output for each node. In earlier cortical neural mass models, the pyramid population unit was the primary output (and input) unit [167,177].
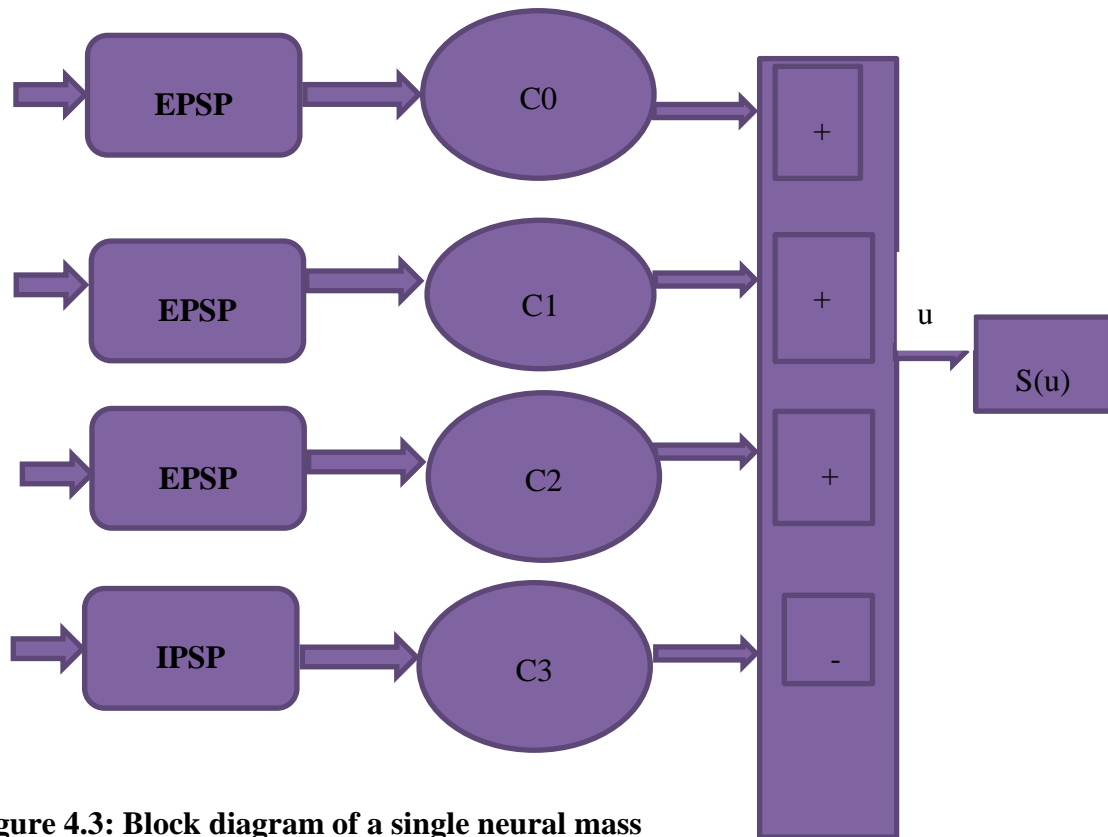
Figure 4.3: Block diagram of a single neural mass

The mean membrane potential of the neurons represents the node's population activity; this output is therefore similar to macroscopic electrophysiological brain signals such as LFP, ECoG, and EEG[113,114,178,179,180,181]. Here the Figure 4.2 illustrates the multiple interacting local populations, such as excitatory and inhibitory neurons in different layers of the cortex, to be modeled by a small number of equations. Here we present a macroscopic Wendling NMM which is developed from the original works of Lopes DaSilva and Freeman. The extended Wendling model [174] can be described by a set of differential equations given below (Equations 4.2 -4.19)).

4.2.1.1 Pyramidal neuronal population

$$\frac{dy_{py}(t)}{dt} = x_{py(t)} \tag{4.2}$$

$$\frac{dx_{py}(t)}{dt} = G_e w_e Sig(z_{py}(t)) - 2w_{exc} y_{py}(t) - w_{exc}^2 x_{py}(t) \tag{4.3}$$

$$\tag{4.4}$$

$$z_{py}(t) = \frac{2e_0}{1+e^{-rvpy}} - e_0 \tag{4.5}$$

$$v_{py}(t) = C_{pyexc} y_{exc}(t) - C_{pysl} y_{sl}(t) - C_{pyfa} y_{fa}(t)$$

4.2.1.2 Excitatory neuronal population

$$\frac{dy_{exc}(t)}{dt} = x_{exc}(t) \tag{4.6}$$

$$\frac{dx_{exc}(t)}{dt} = G_{exc} w_{exc}(z_{exc}(t) + \frac{u_p(t)}{C_{pyexc}}) - 2w_{exc} x_{exc}(t) - w_{exc}^2 y_{exc}(t) \tag{4.7}$$

$$z_{exc}(t) = \frac{2e_0}{1+e^{-rvexc}} - e_0 \tag{4.8}$$

$$v_{exc}(t) = C_{excpy} y_{py}(t) \tag{4.9}$$

4.2.1.3 Slow inhibitory neuronal population

$$\frac{dy_{sl}}{dt}(t) = x_{sl}(t) \tag{4.10}$$

$$\frac{dx_{sl}(t)}{dt} = G_{sl} w_{sl} z_{sl}(t) - 2w_{sl} x_{sl}(t) - w_{sl}^2 y_{sl}(t) \tag{4.11}$$

$$z_{sl}(t) = \frac{2e_0}{1+e^{-rvsl}} - e_0 \tag{4.12}$$

$$v_{sl}(t) = C_{slpy} y_{py}(t) \tag{4.13}$$

4.2.1.4 Excitatory neuronal population

$$\frac{dy_{fa}(t)}{dt} = x_{fa} \tag{4.14}$$

$$\frac{dx_{fa}(t)}{dt} = G_{fa}w_{fa}z_{fa}(t) - 2w_{fa}x_{fa}(t) - w_{fa}^2 y_{fa}(t) \tag{4.15}$$

$$\frac{dy_{lo}(t)}{dt} = x_{lo} \tag{4.16}$$

$$\frac{dx_{lo}(t)}{dt} = G_{exc}w_e u_{fa}(t) - 2w_{exc}x_{exc}(t) - w_{lo}^2 y_{lo}(t) \tag{4.17}$$

$$z_{fa}(t) = \frac{2e_0}{1+e^{-rvfa}} - e_0 \tag{4.18}$$

$$v_{fa}(t) = C_{fapy}y_{py}(t) - C_{fasl}y_{sl}(t) - C_{fafa}y_{fa}(t) + y_{lo}(t) \tag{4.19}$$

Table 4.1: Model system parameters of neural mass model

System parameters	Description	Value
A	Average excitatory synaptic gain	3.35mV
B	Average slow inhibitory synaptic gain	22mV
G	Average fast inhibitory synaptic gain	10mV
a	Reciprocal of excitatory time constant	100Hz

b	Reciprocal of slow inhibitory time constant	50Hz
g	Reciprocal of fast inhibitory time constant	500Hz
C	General connectivity constant	135
C_{pyexc}	Connectivity :pyramidal to excitatory cells	1
C_{exppy}	Connectivity : excitatory to pyramidal cells	0.8
C_{pysl}	Connectivity :pyramidal to slow inhibitory cells	0.25
C_{slpy}	Connectivity : slow inhibitory to pyramidal cells	0.25
C_{pyfa}	Connectivity :pyramidal to fast inhibitory cells	0.3
C_{slfa}	Connectivity : slow to fast inhibitory cells	0.1
C_{fapy}	Connectivity : fast inhibitory to pyramidal cells	0.8
v_0	Sigmoid function: potential at half of max firing rate	6mV
e_0	Sigmoid function: half of maximum firing rate	2.5Hz
r	Sigmoid function: Steepness parameter	$0.56mV^{-1}$

4.2.2 Implementation of Human Neural Mass Model

The neural mass model developed is based on extended Wendling's neural mass model as shown in Figure 4.4 has been designed in MATLAB 2016) to generate the alpha, beta and gamma brain waves as shown in Figure 4.5 (a, b, c) respectively using Runge-Kutta (RK4) method. The input u_{fa} and u_p are given as Gaussian white noise with standard deviation SD=3 and mean as m=90.The mean strength and time series are denoted by G and w. Different units of the population are characterized by their time constant T= 1/w and the low frequency gain from the G / w dendritic transmission feature. Each population unit's

dendritic transfer function is referred to as $H_{lx}(S)$, {p stands for pyramidal neuron population, q refers to exciting interneuron population, f refers to quick inhibitory interneuron population, s represents slow inhibitory interneuron population}. The model parameters are shown in Table 4.1.
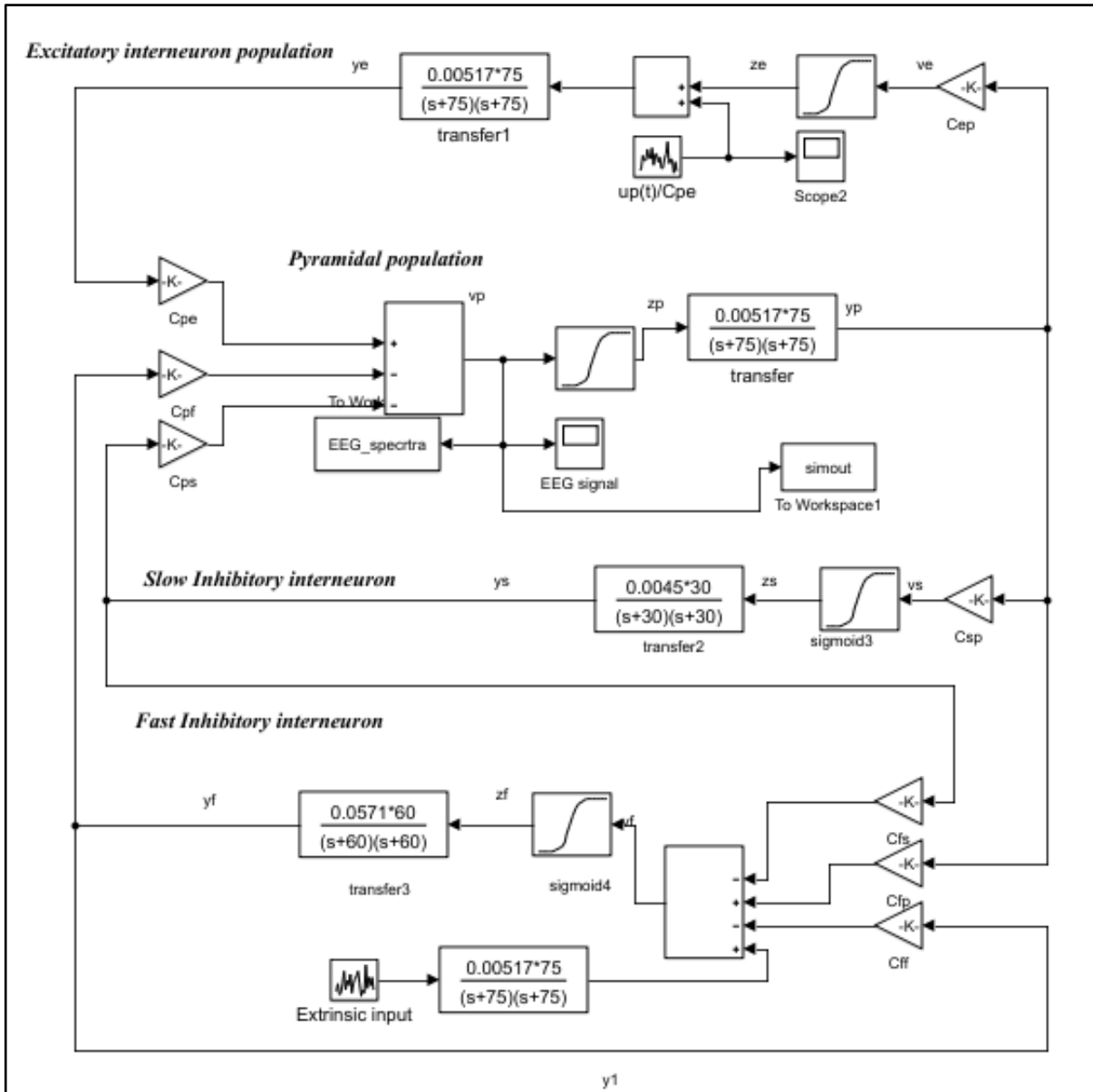
Figure 4.4: Implemented Neural Mass model

A single node is constituted by four interconnected population units. The weighted outputs from the other units are inputs to each population unit, reflecting the mean exciting or inhibitory post-synaptic potential of an exciting or inhibitory population (EPSP or IPSP). Here the Constant connectivity strengths that are called synaptic gains,

weigh the input synaptic potentials. The $C_{\alpha\beta}$ represents a synaptic gain among populations where α, β;refers respectively to the target and source population; e.g. the steady C_{pysl} is the gain from the synaptic association between the slow inhibitory population and the pyramidal neuron population.
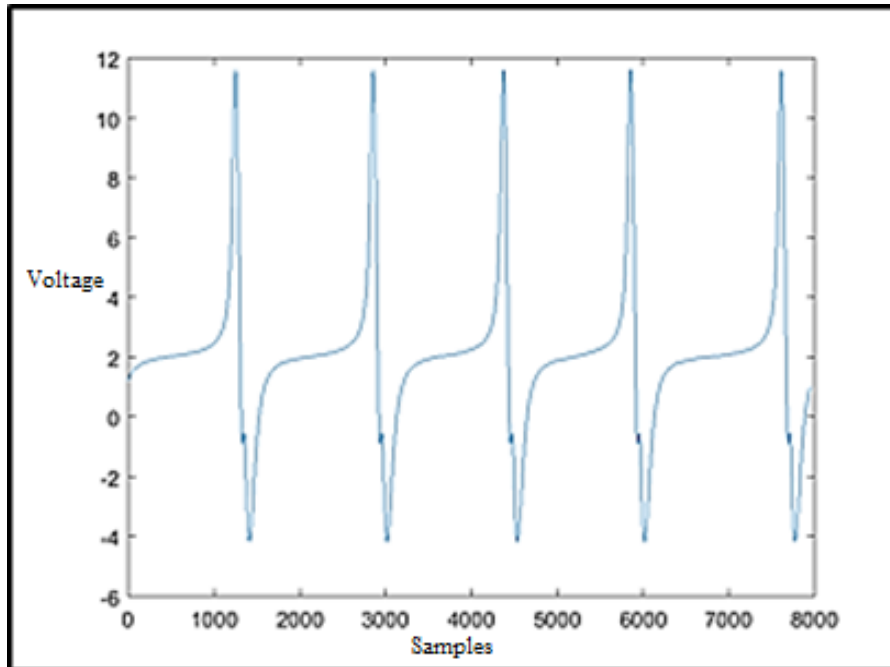
(a)
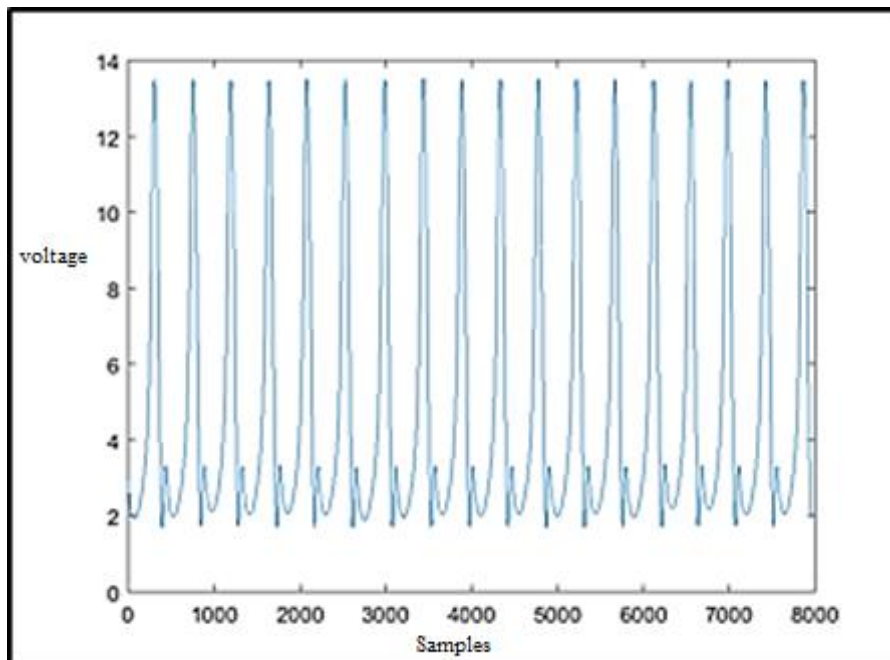
(b)
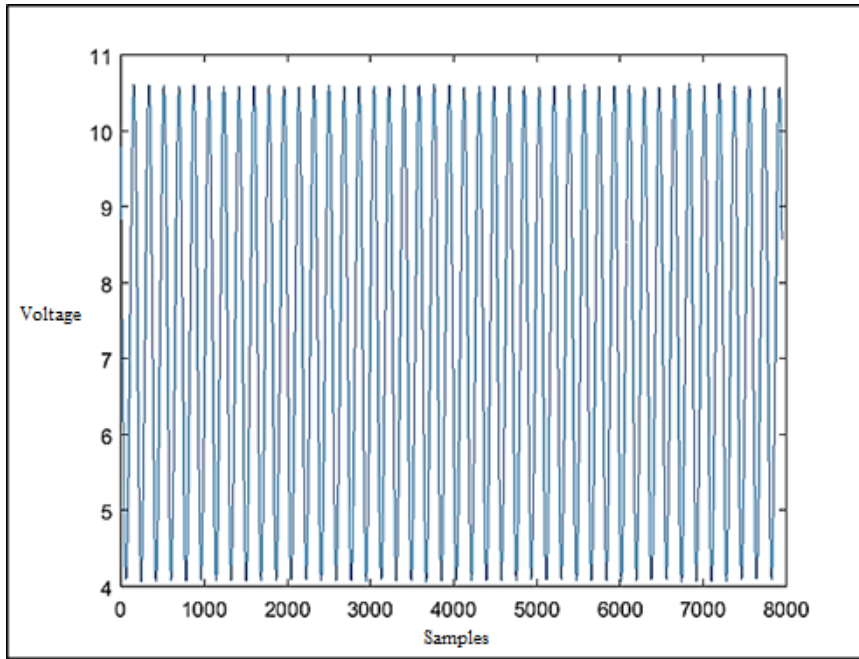
(c)

Figure 4.5: The NMM to generate the (a) alpha, (b) beta and (c) gamma brain waves

Chapter 5

Symphathetics and Para-Symphathetics in Human Body

5.1 Sympathetic Neurons Activities

In the stellate ganglion are the sympathetic neurons that control cardiac function. It gets pre-ganglionic sympathy feedback from the intermediate column (and other spinal neurons) and coordinates effective neural reactions to the center cervical ganglia to the core either directly or through the ansasubclavia [182,183,184,185]. Efferent post-ganglionic fibers travel alongside the coronary vasculature to enter the epicardial areas to the endocardium. Stellate ganglion stimulation results in increased dromotropy, chronotropy, lusitropy, and inotropy [186]. Mechanosensory, chemosensory, or multimodal in nature are cardiac afferent neurons [187]. They transduce a range of chemicals, including different neuropeptides, such as gene-related peptide P, bradykinin, and calcitonin.

These cardiac afferents are also engaged in initiating local vascular and inflammatory responses that can play a significant part in cardiac remodeling [188]. In the atria and ventricles are the sympathetic nerve fibers. There is a regional reaction to the correct sympathetic paravertebral ganglia versus the left sympathetic paravertebral ganglia, with predominant impacts respectively on the anterior and later ventricular walls [189]. In

relation to increasing the firing of the sinoatrial node and enhancing atrioventricular nodal conduction, sympathetic output results in shortening of the prospective length of ventricular action [190].
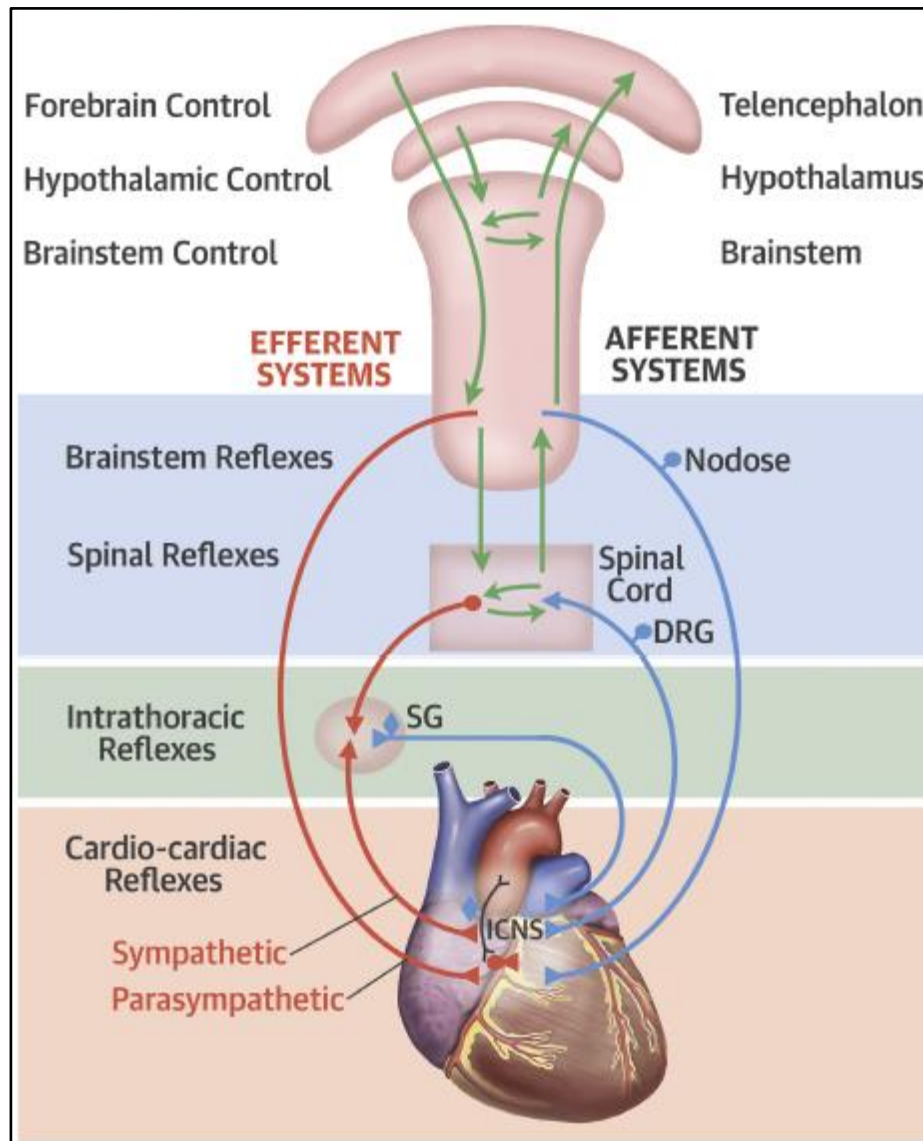
Figure 5.1: Afferent and efferent elements in the parasympathetic nervous system

5.2 Parasympathetic Neurons Activities

There are also significant afferent and efferent elements in the parasympathetic nervous system (Figure5.1 and Figure 5.2). This system's cardio motor feature enables slow heart rate, lower blood pressure, and balances the system to guarantee

sympathovagalexcitation is counterbalanced. The parasympathetic impacts are coordinated through the cervical vagus nerve, which splits into the upper and lower cardiac nerves to finally enter through the cardiac plexus into the core. The parasympathetic nerve fibers are much more heterogeneously distributed, with the sinoatrial node, atrioventricular node [191], and ventricles [192] being significantly inward.

Neurons in the ICNS coordinate the parasympathetic reaction of the cardiomotor that receive pre-ganglionic parasympathetic feedback from the cervical vagus and provide a homogeneous or coordinated reaction to the atria and ventricles [193,194].

Depending on what aspect of the neuroaxis is involved, cervical vagus stimulation can generate distinct responses. Stimulation in the intact state can lead in immediate and reactive or reflex responses on the inherent cardiac nervous system as a consequence of core and peripheral interactions initiated throughout the cardiac neuronal hierarchy.

Low-level stimulation given to the cervical vagus may lead in tachycardia, likely as a consequence of involving cardiac afferent fibers, whereas higher-level stimulation in bradycardia may result in results [195].

The cardiac ANS is a complex equilibrium between sympathetic and parasympathetic inputs in the resting state. After transecting the cervical vagus from the central nervous system, a significant rise in heart rate indicates that the central neuronal cholinergic drive plays a considerable role in regulating the basal heart rate [195].

5.3 Modeling of Central Nervous System(CNS) for Human Body

The autonomic nerves regulate cardiac and vascular function. Parasympathetic and sympathetic efferent nerves control heart and vasculature which are found in the cell bodies of the medulla oblongata. The central nervous system receives input from baroreceptors and chemoreceptors which are responsible to maintain blood pressure and chemistry respectively. There are billions of neurons in the brain which receive and transport neurotransmitters in the brain. Each of these neurons is classified as sensory, motor, or interneurons. Sensory neurons are neurons that detect changes in the external environment and generate impulses that are sent to the brain. Motor neurons activate muscle cells and control motor activity like walking, speaking, etc. Various cardiovascular models have been described in the literature to have a better understanding of the underlying mechanisms of the heart and vasculature. Cardiovascular systems are proposed

in the literature in the form of empirical and functional models. Extended models are also available which include the respiratory system interaction through an autonomic neural controller [196]. The various components of the cardiovascular system help in regulating cardiac output (see Fig. 6). The cardiac output is a function of Heart Rate and stroke volume. Heart Rate is a complex parameter obtained through sympathetic (f_{tbs}) and parasympathetic (f_{tp}) peripheral nerve response. The f_{tbs}, f_{tp} and α-sympathetic(f_{tas}) nerve responses are generated through central autonomic control from the complex integration of central respiratory control (N_t), chemoreflexes (F_{chem}), lung stretch receptors reflexes (f_{ls}), baroreflexes (f_{cs}) and CNS responses [197, 198]. The f_{tas} signal which signifies the α-sympathetic nerve response regulates the total peripheral resistance (TPR) to produce arterial blood pressure (ABP) which further generates stroke volume via a change in venous return and cardiac contractibility.

Short-term rhythmic activity in HRV calculations is a result of the interplay between autonomic neural system, blood pressure and respiratory activities [199]. A heart rate tachogram is commonly used to notice these short term changes between consecutive RR intervals over time. HRV is considered thus as a function of heart and brain which reflect the changes in the ANS dynamics. HRV can be measured in the frequency domain by using FFT of other power spectral density algorithms. The RR interval of the ECG is transformed into specific frequency components. Power spectral analysis plots of HR oscillations reveal specific frequency components wherein heart rate cycles are classified as HF (0.15–0.40 Hz); LF (0.04–0.15 Hz); VLF (0.0033–0.04 Hz); and ULF (below 0.0033–0.2 Hz).

5.3.1   Integration of the ECG, ABP and NMM models

Human body physiology is regulated through the central neural control (CNS) which takes signal from the respiratory system and ambiance which signifies atmospheric pressure, temperature and various gases in the environment. The central nervous system then controls the metabolic control of various organs through the afferent nerves and the efferent nerves reflecting the various reflex of the organs back to the CNS, which regulates the cardiovascular system(CVS) for the stroke volume(SV) of the blood and heart rate(HR). The SV and HR collectively synthesizes the cardiac output of the heart balancing the body for the coherence or non-coherence states. We have defined and

simulated here in this work the Neural Mass Model(NMM), which is one of the component which feeds the CNS and controls the cardiovascular system for the human blood pressure (ABP) and heart rate. We have defined and simulated arterial blood pressure model i.e. Windkessel model; describing the arterial blood pressure for the particular input volume of the blood and ECG model for the computing heart rate and heart rate variability(HRV) as shown in Fig 1.4.1. The model has open for the researcher communities for discussion and experimentation for further improvisation

5.3.2 ANS for Coherence

The well-being of an organism is determined by the healthy functioning of the regulatory systems. For this to happen there should be optimal variability in the functioning of the regulatory systems. Too much variability is harmful to effective physiological processes, too little variation means deterioration or diseases. Evidence shows the age of a patient reflects the relationship between regulatory capacity and reduced HRV.As a person gets older the HRV decreases due to loss of neurons in the spinal cord which reduces signal transmission [197] and reduces regulatory capacity. Functional gastrointestinal disorders, inflammation, and hypertension are caused due to lower HRV. While patients with functional gastrointestinal disorders often have reduced HRV [200], HRV has increased vagal tone and improved symptom ratings in these patients [201].
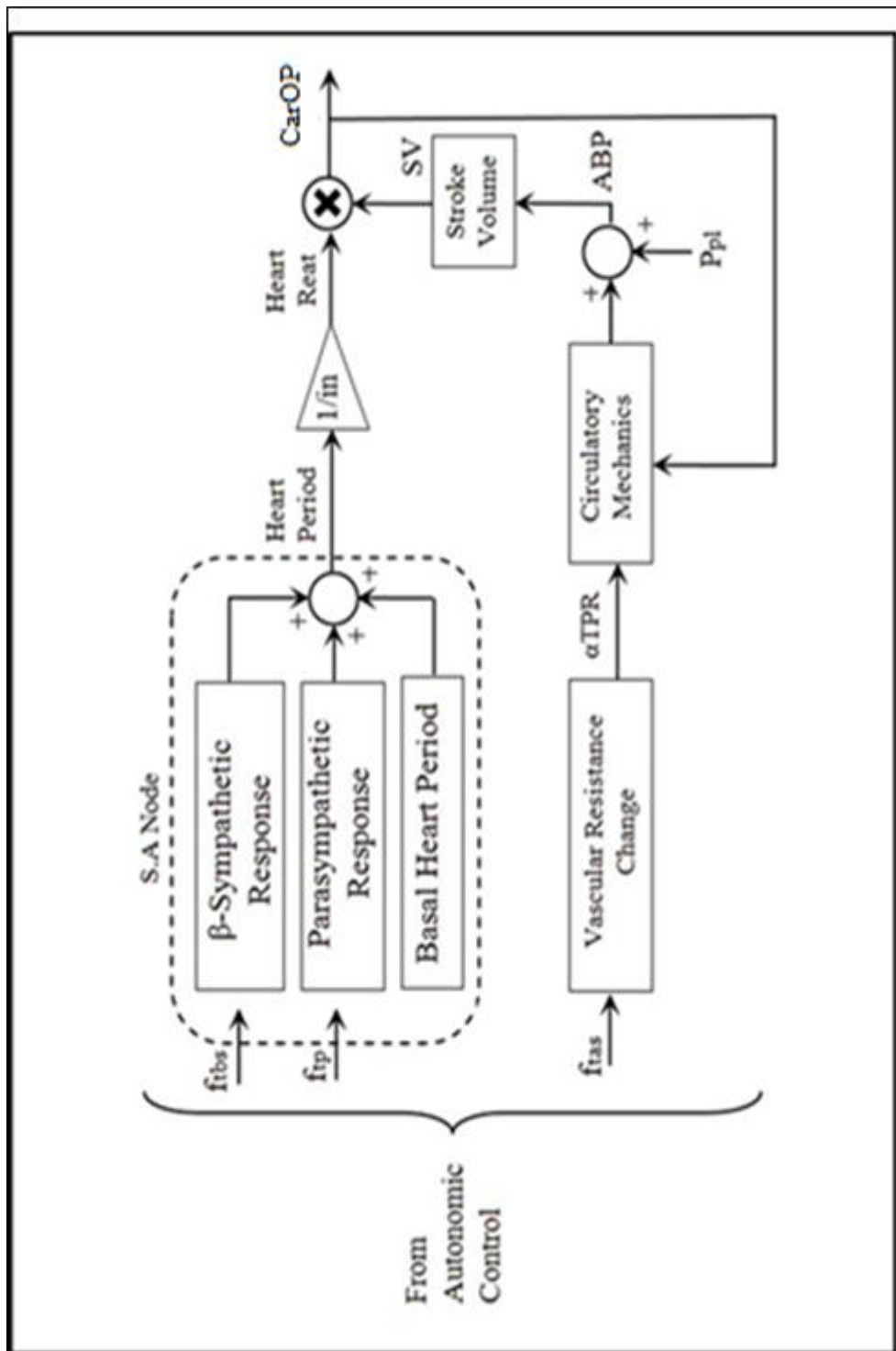
Figure 5.2: Illustrates the nervous system link between the heart and brain. The Sympathetic branch increases the heart flow while the parasympathetic slows the rate.

5.3.2.1 High-Frequency Band

The power in HF varies over 0.15–0.4 Hz band of frequencies. This band is known as the respiratory band due to HR perturbations related to the respiratory cycle. It reflects the vagal or parasympathetic activity of the ANS. Parasympathetic activity is often lowered in patients under stress or if diagnosed with stress. Also as a person ages, the parasympathetic activity reduces thereby reducing HRV [202]. Normally the parasympathetic activity increases at night and decreases during daytime for a healthy individual [203].

5.3.2.2 Low-Frequency Band

The power in the LF varies over 0.04–0.15 Hz band of frequencies. This band is called the baroreceptor range since it reflects the baroreceptor activity at rest [204]. The afferent signals from the heart and other visceral organs along with baroreceptor signals are passed onto the brain via the vagus nerves. Located in the chambers of the heart and vena cava, carotid sinuses (which contain the most fragile mechanoreceptors), and the aortic arch are baroreceptors which are stretch fragile mechanoreceptors. The baroreflex reduces blood pressure when the blood pressure is observed too high by inhibiting sympathetic activation along with parasympathetic activation. Peripheral resistance is lowered by sympathetic inhibition, whereas activation of the parasympathetic branch reduces heart rate and contractility. Cycle to cycle differences in heart rate per unit change in blood pressure is calculated as the baroreflex gain. Aging and weakened regulatory ability cause a decrease in baroreflex gain.

5.3.2.3 Autonomic Balance and the LF/HF Ratio

One can accept that the SNS and PNS are the two branches of ANS. These branches can be simultaneously active to regulate the SA node firing, i.e., where an increase in SNS activity is coupled with a decrease in PNS activity. Certain orthostatic challenges sometimes disturbed the SNS activities and vagal withdrawal. Also, psychological stresses induced changes in SNS and PNS activity [205].

Hence, the relation of SNS and PNS in LF power spectral density is complex nonlinear and solely depends on the experimental paradigm employed to the subject [206, 207]. The LF/HF is a ratio of LF and HF power is used to reflect sympathetic and parasympathetic activities. The low ratio gives the idea of energy conservation and engaging in tend-and-befriend behaviors [208]. The high value of ratio indicates high sympathetic activities than parasympathetic which is seen when subjects are meeting challenges which demand high SNS activities. But due to the above-cited reasons in LF power, the said ratio has to be used with caution.

5.4   Discussion and conclusion

Researchers are keen on understanding the interaction between CVS and ANS which are predictors of adverse cardiovascular events. The source of such events has to be diagnosed to pinpoint abnormality of ANS or a pathological organ response. Also, other factors like age, lipid profile, smoking status, and family history will also play a role in the prediction of CV events. The coherence model of the psycho-physiological system proposed by the Institute of Hearth-math focuses on increasing the self-regulatory capacity of an individual, which reflects in maintaining the heart rhythms. These rhythmic activities reflect the perception over cognitive, biological, social and ecological networks in living systems. Here afferent pathways that collect basal regulatory information from the cardiovascular system are given more relevance in this model. They claim that to have improved performance better self-regulation and well-being of living systems, the system should go through positive emotion which induces coherence and harmonious physiological mode. This is very often known as physiological coherence which describes the orderly and stable system rhythm generated by living beings which is quantified by the maximum peak of 0.04–0.26 Hz of the HRV power spectrum.

Chapter 6

Some Applications of EEG

6.1 Brain Computer Interface

In current years, extraordinary improvements have been made in knowing the functioning of the human mind. Technological developments consisting of functional magnetic resonance imaging (fMRI), positron emission tomography (PET), and magnetoencephalography (MEG) have made feasible the mapping of the cerebral images from hemodynamic, metabolic or electromagnetic measurements. Among these brain imaging techniques, electroencephalography (EEG) is of great significance due to its simplicity, accessibility, and temporal resolution, and has been regarded with renewed interest in recent years, due to superior techniques of analysis and interpretation of its data. These techniques can improve the spatial decision of traditional EEG, making it possible to address the analysis of activities of the brain in a noninvasive way by using the temporal resolution of EEG signals (of the order of milliseconds). With high-resolution EEG, it's now viable to acquire cortical activation maps describing the activity of the mind at the cortical stage all through the execution of a given experimental project.Human beings communicate with the external world through the motor and sensory pathways. But the damage to these pathways makes it difficult to communicate with the external world. Humans who suffer from neuromuscular diseases like quadriplegic patients, amyotrophic lateral sclerosis cannot move their limbs due to damage to the spinal cord. Brain-computer interface-based systems can be of great help to such type of patients for communication [209]. BCI's have also been used in selective attention based studies, speller systems, and

prosthetics. There are normally two types, i.e., invasive and non-invasive BCI's as shown in Figure 6.1. Invasive BCI's include ECoG, neural implants, single-cell recording, etc.; whereas non-invasive BCI's include EEG, MEG, fMRI, etc. Invasive BCI's are more accurate compared to non-invasive BCI, but since it requires surgery it is only used on animals or more recently on patients suffering from severe disabilities or diseases[210,211,212].

6.1.1 Various signal acquisition methods to measure brain activities
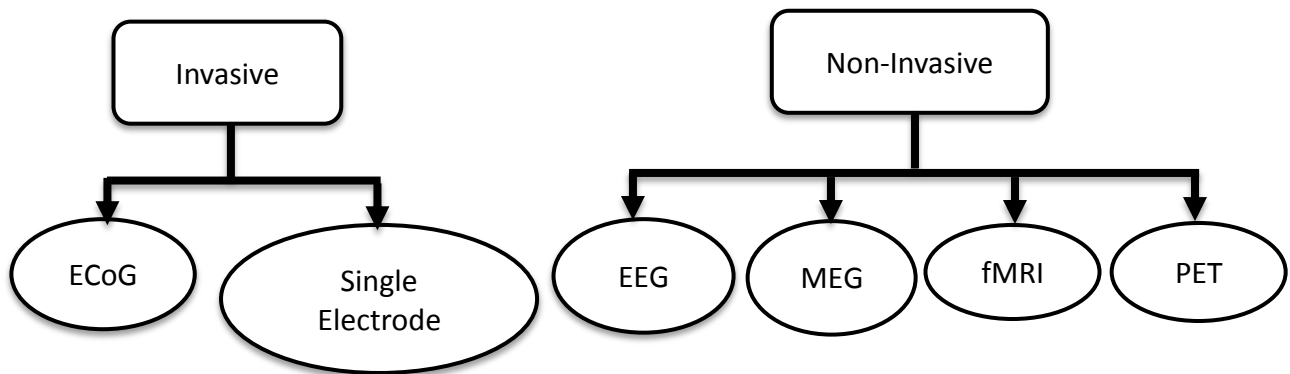
Figure 6.1: Methods used to measure brain activities

EEG has a high time resolution and can capture the physiological changes underlying the cognitive processes much better than other brain imaging techniques (such as Magnetic Resonance Imaging or Positron Emission Tomography scanners). EEG recordings do have limitations such as low spatial resolution and low signal to noise ratio since they are affected by various artefact's like muscle activity, power line interference, motion etc. and difficulty in source localization. But it's low cost, portability and ease to the user under observation make it a potent option. Electroencephalography records electrical activity and brain waves using electrodes placed on the scalp.EEG recordings are widely used for non-invasive BCI as it has a good temporal resolution. An EEG recording is done by placing an electrode strip or cap on the scalp. There are various non-invasive EEG-based BCI interfaces such as evoked potentials, P300 signals [210], Slow Cortical Potentials [211], Motor imagery [212], etc. The evoked potentials occur due to an external stimulus that can be based on vision, sound, or touch (somatosensory) [213, 214] or a combination of them [215]. In P300-based BCI's a positive peak is elicited at a delay of

about 300 milliseconds', when an irregular stimulus occurs after a pattern of regular stimuli. Mu rhythm arises due to imagined motor activity in Motor imagery based BCI.
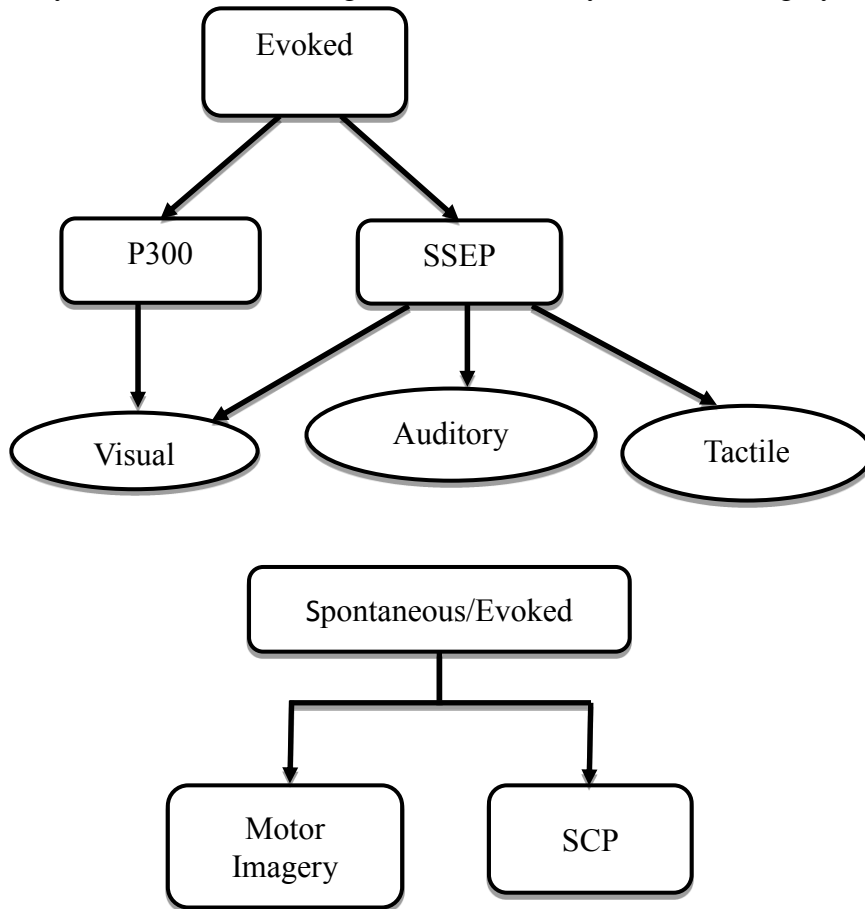
Figure 6.2: Evoked stimulus based BCI paradigms and Spontaneous stimulus based BCI paradigms

6.1.2   Application of EEG as SSVEP based Brain Computer Interface

Evoked potentials are the activities or responses generated either by an external stimulus or an internally driven cognitive process. Externally evoked potentials are called as exogenously generated evoked potentials whereas the internal cognitive potentials are called as endogenously evoked potential's. These are named as auditory, visual or tactile evoked potentials depending on the external stimulus which can take the form of audio, visual or touch. Visually evoked potentials are further classified as transient or steady state evoked potentials as shown in Figure 6.2. In Transient VEP's the rate of stimulation is usually less than 2 Hz as compared to Steady State visually evoked potentials where the rate of stimulating frequencies ranges from 5-100Hz [216]. Generally, it has been seen that

the SSVEP has a higher amplitude response at low and medium frequency stimulating frequencies compared to higher frequencies. But higher frequencies have the advantage of causing less fatigue to the subject and reduction as well in risk of photosensitive epileptic seizures. SSVEP have been widely used in Brain Computer Interface systems like moving a mouse cursor [230], speller [219], controlling wheelchairs [231], electrical prosthesis [215], biometrics and attentional based studies [217,218]. The use of SSVEPS in spatial attention based studies has garnered a lot of interest over the years. In one such work SSVEP responses were captured when the subject attended a visual display in one field while he ignored the another similar visual in an opposite field. The 20.8 Hz and 27.8Hz were the stimulating frequencies in the left and right field respectively [217]. The amplitude response of the SSVEP corresponding to the attended frequency increased. Variable Resolution Electromagnetic Tomography is usually used to estimate the current source densities and it is found out that the SSVEP had a focal origin in the contralateral parieto-occipital cortex. In another study by Jian Ding et al changes in attention also can occur in the just a single field of display [218]. They have presented random disc in two concentric annuli. One concentric circle has a fixed stimulation frequency while the other has a random broadband flicker. Occipital frontal lobes are phase locked to the stimulating frequency when the subject attends it at delta and lower alpha band frequencies. When attention is shifted towards the other engaging unattended flicker the parietal lobe and posterior frontal cortex, responds preferentially to the unattended flicker. It is widely used due to its high signal to noise ratio which is key to any system. High SNR in turn causes an increase in accuracy.

In VEP's a stimulus such as flash is used to elicit activity in the occipital lobe which is the visual processing unit of the brain. SSVEP reflect the changes in the cortical activity due to recurrent stimulus presentation. This cortical activity generates an electrical signal at the frequency of stimulation and its harmonics. These electrical activitiesare captured by the EEG system which is more prominent in the occipital lobe. The advantage of SSVEP over other BCI's is that the subject requires little or no training, its information transfer rate is high. SSVEP has also been explored for selective attention [219]. Many researchers are exploring research in the area of cognitive neuroscience. In one such work, a BCI-based speller paradigm has been designed by Movahedi et al. [220]. Chen et al. [221] have built a high information transfer rate speller paradigm with 45 commands. Here

in our work, we proposed steady-state visual evoked potential-based BCI for smart appliance control. We use non-invasive EEG techniques to read the raw electrical signals using a single channel (a single electrode) system. A stimulus of flickering LED's help produce the steady-state visual evoked potentials, only the potentials are taken up from the occipital lobe are amplified and transmitted over a Bluetooth module to a computing system which performs feature extraction (using Fast Fourier Transform (FFT) algorithm) and classification (using multiclass SVM algorithm) to classify the incoming signal for determined automation control in smart appliances.

6.1.2.1 Signal Acquisition and Features Extraction
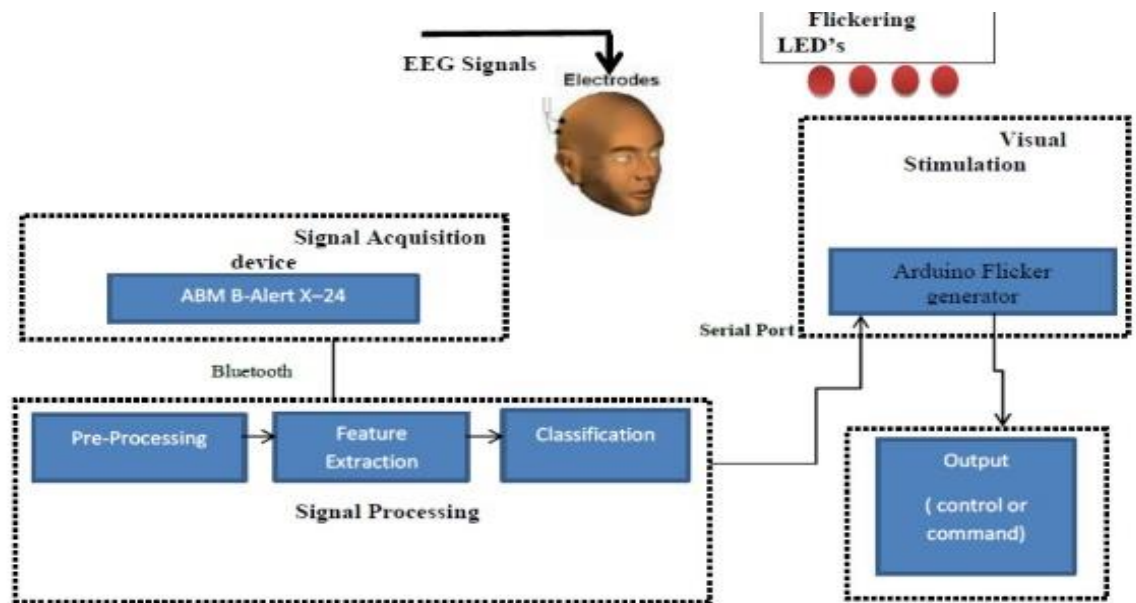
Figure 6.3. BCI system build on SSVEP using B-Alert X-24 device

We proposed a BCI system build on SSVEP using B-Alert X-24 device via a Bluetooth interface for controlling home appliances as shown in Figure 6.3. The design includes a stimulating platform, EEG signal acquisition unit, signal processing unit, and MATLAB for feature extraction and classification. The stimulating platform as shown in Figure 6.4 generates the frequency based paradigm with the help of four light emitting diodes (LEDs) [222].
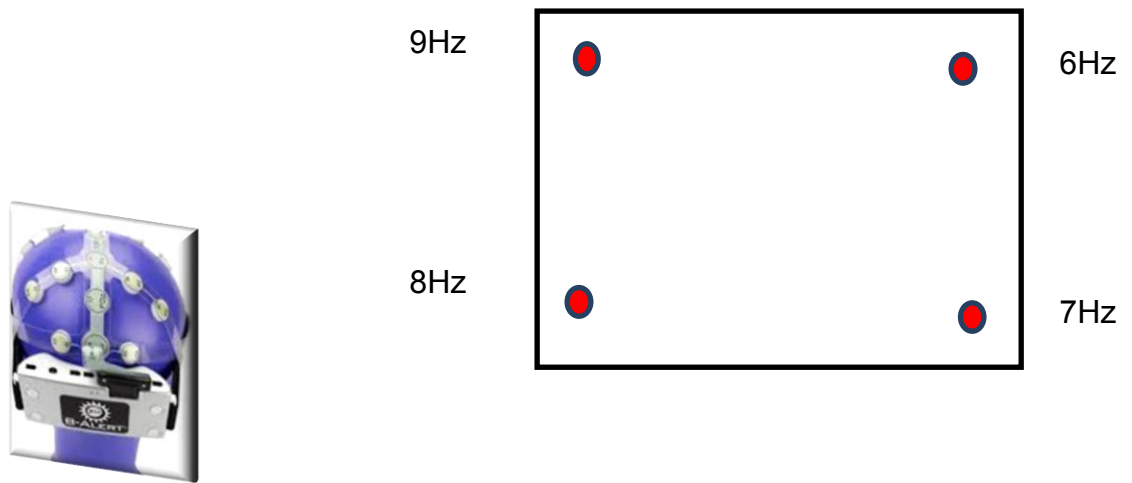
Figure 6.4: Subject gazing at the SSVEP based flickering LED of interest.

6.1.2.1.1 Signal Acquisition

Here, the B-Alert X-24 series mobile EEG system as shown in Figure 6.7 is used which has 20 EEG channels that acquire high-quality signals. The brain response can be recorded with system like B-Alert X series mobile EEG system following 10/20 EEG standard with a 256 Hz sampling frequency [223]. The reference sensor is usually placed on the right temple and the right ear lobe served as the ground via an ear clip. In case of B-Alert X-24 system one has 20 channels as shown in Figure 6.5 for high quality EEG and four optional signals like for ECG (2 channels), EMG and EOG (1 channel each). Automated impedance check is possible in most of such system for confirming the connectivity of channels. The Bluetooth based module (Figure 6.8) are usually used for data acquisition over 20 meters. On-board accelerometer sensor is inbuilt in system to quantify head movement and position. In the 10-20 system, electrode names begin with one or two letters indicating the general brain region or lobes where the electrode is placed (Fp = frontopolar; F = frontal; C = central; P = parietal; O = occipital; T = temporal). The cortical areas of the brain as shown in Figure 6.6 are covered by the EEG strip.
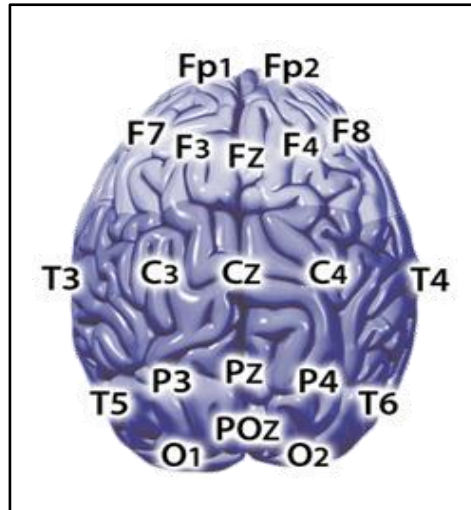
Figure 6.5. B-Alert 10/20 sensor location
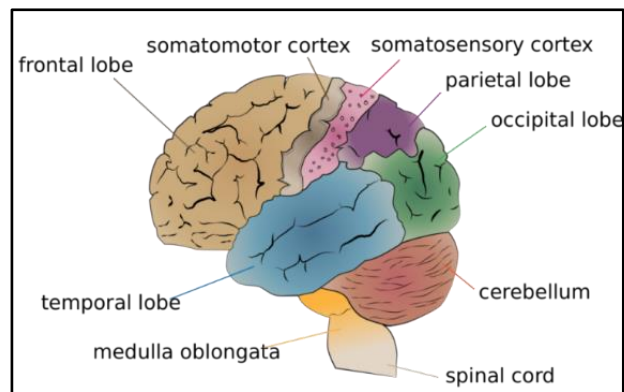
Figure 6.6: Different cortical areas of the brain

Figure6.7. B-Alert headset with 20 EEG sensor strip mounted on a scalp model

Figure 6.8: Bluetooth module

6.1.2.1.2 Stimulus Presentation

The stimulus can be presented by light emitting diodes(LED), liquid crystal display or LED monitors. The stimulus can be of any shape of color. The intensity or luminance should be good enough to elicit SSVEP responses. At the same time, it should not be too bright so as to cause discomfort to the subjects. Different patterns have been used such as checkerboards [224], moving shapes of varying contrast and color. LED's based stimulus have the advantage of portability and are cheaper compared to LED or LCD monitors. One can generate flickering frequencies from the SSVEP range of 2-100Hz. LCD's on the other hand are dependent on the refresh rate and can generate frequencies in the entire range. But their limitation is that they can generate only a limited number of different patterns with it.

6.1.2.1.3 Experimental paradigm

Individual's seizures occur in brain mass in response to the external stimuli like sound, vision or tactile stimuli, rather than spontaneous occurring seizures [225]. We have chosen our stimulus such that it does not affect a photosensitive subject. We chose four LED's that flicker at 6, 7, 8, and 9 Hz. Here, lower frequencies are chosen as these frequency regions have a stronger amplitude response and higher accuracy. Secondly, we have avoided the lower delta range of brain frequency as it may cause dizziness. The

microcontroller board is programmed to flicker the LED at the frequencies discussed above.

6.1.2.1.4 Database creation

Total ten subjects (all male with a mean age of 22 years) participated in the experiment. All the subjects had normal visual acuity. They were comfortably seated in a chair in front of four blinking LEDs. The subjects sat at a distance of around 40 cm from the target stimuli. Their brain waves were recorded with described EEG system at a 256 Hz sampling frequency in a low decibel dark room. The reference sensor was placed on the right ear lobe and the left ear lobe served as the ground via electrodes. Impedance checking in established to ensure proper contact of the electrodes with the scalp. The subjects had to focus on the flickering LED's over 2 min as shown in Figure 6.9. The procedure was repeated six times over a frequency. A total of 24 trials, 2 minutes were performed on every subject. The raw EEG signals are stored in the EDF file format. Preprocessing, feature extraction and classification are established in MATLAB 2017.

6.1.2.1.5 Feature Extraction

The raw EEG signal is passed through a Finite Impulse Response filter having a lower cut-off at 4 Hz and a higher cut-off at 18 Hz. This range removes all the dc components as well as high frequency and power line noise. The transition width of the filter has been set to 0.2 Hz and the filter order is selected to be 30. The filter is tapered to avoid ringing or edge artifacts. The noisy and filtered raw EEG signal from channel O1 is shown in Figure 6.10. The next step is to extract features from the signal. Canonical Correspondence Analysis (CCA) [226, 227] and Fast Fourier Transform (FFT) have been extensively used by researchers [228]. We chose FFT in our work to extract the peak frequencies. The FFT and its inverse are defined as Equations 6.1 and 6.2, in which the signals are transformed between time domain and frequency domain.

$$X(K) = \sum_{n=0}^{N-1} x(n) e^{j2n\pi k/N} \qquad\qquad (6.1)$$

$$x(n) = \sum_{k=0}^{N-1} X(K) e^{-j2n\pi k/N} \qquad\qquad (6.2)$$

FFT is a digital signal processing method to compute the discrete Fourier Transform (DFT) of a signal. This is used to transform a time domain signal to its

frequency domain. The computational complexity of the DFT which is $2*N^2$ is reduced to $2*N*\log(2*N)$ in FFT. The sampling frequency for FFT computation was set at 256 Hz to match the EEG sampling frequency. The maximum peak valuess detected by the FFT algorithm are the features fed to the classifcation algorithm.

6.1.2.1.6 Signal Classification using multiclass SVM

Figure 6.9: Subject under test

Support vector machine (SVM) created by Cores and Vapnik is a controlled learning computer based on the hypothesis of statistical learning or Vapnik-Chervonenkis (VC)[229]. It is possible to view the SVM as a binary classifier. It abstracts a border of choice from the information and utilizes it to classify patterns that belong to both classes. The 1/w margin, a distance between the optimum hyperplane separation and the instances on either side of it, is an important notation in the SVM. The vectors on these margins are called vectors of assistance. The solution is depicted as a linear combination of only support vectors that ignore the other information in a linear separable situation. The complexity of the SVM model is therefore generally not affected by the number of features selected. The essence of the SVM lies in the projection to a high-dimensional feature space

of linearly non-separable input data and finding an optimal hyperplane in the feature space with the maximum possible margin.

For a workout set labeled as {Xi, yi}, I = 1, 2, L and l are the amount of training samples, the issue of finding ideal hyper plane over bias, b and vector w weight.Where x is the class label input vector y { −1, 1}. The first portion of the issue is intended to maximize the margin between the two classes. The second term aims to reduce the training errors by penalizing the solutions of a large slack variable ξi with the cost of penalty, C. Larger C value makes constraints hard to ignore and hence, minimize the margin.

Using the Lagrangian multiplier technique and formulating its dual problem with kernel tricks, this restricted quadratic programming issue can be solved more easily.Where, there, there's a Lagrangian multiplier. A straightforward sequential minimal optimization algorithm can solve this dual issue with linear quality limitations.

The rise in the dimensionality of the information through nonlinear function mapping may help with a linear hyperplane to separate classes. Using the kernel feature K(xi, xj) mapping is obtained and the most frequently used kernels are polynomial, Gaussian. The other technique, OAA solves the k-class issue by solving k amount of two classification assignments, requiring only k binary models, each devoted to detecting a specific class. In this technique, each binary SVM model is trained only for the present class and adverse label for all other classes with full information with the positive label. Both of these techniques are regarded appropriate for issues with multi-class classification [245]. SVM, which was initially created for binary classification, is successfully used by adopting a group of binary SVMs for multi-class classification problems. The most commonly used ways for multiclass classification are one-against-all (OAA), one-against-one (OAO) and a directed acyclic graph SVM (DAGSVM)[245]. The OAO method performs pairwise

classification by constructing k (k − 1) / 2 binary models. We have used the OAA method for our study and it has been implemented in MATLAB.
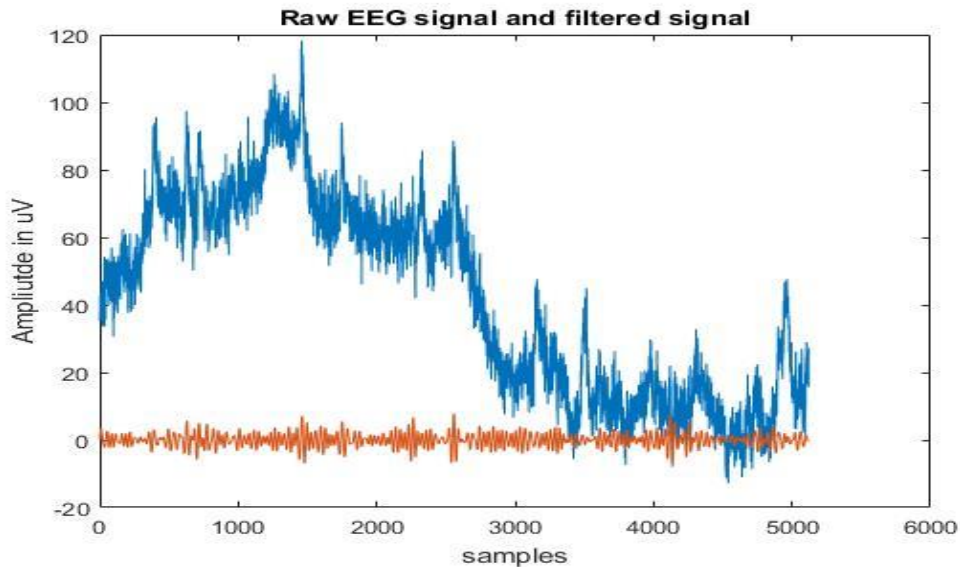
Figure 6.10: Noisy and Filtered waveform at occipital lobe O1 location

6.2   Steady State Evoked Potentials BCI results

In SSVEP the main work is to find out the most dominant frequency which corresponds to the frequency of the stimulus from the recorded EEG signals. When we run FFT analysis over the raw EEG signal acquired from the O1 location, we can differentiate between the SSVEP frequencies. Each fundamental frequency has corresponding harmonics at 2f and 3f. These harmonics can also be used to decrease misclassification errors. We have chosen the fundamental frequency in such a manner that it does not overlap with the harmonics of other frequencies. Figure 6.11 a–d depicts the frequency domain representation of an SSVEP signal for stimulus frequencies of 6, 7, 8, and 9 Hz respectively. The FFT output produces dominant frequencies at 6, 7, 8, and 9 Hz which can be used for specific applications. Also one can use the multiclass SVM feature classification method to classify the input signals to discriminate the SSVEP signals perceived by the subject.
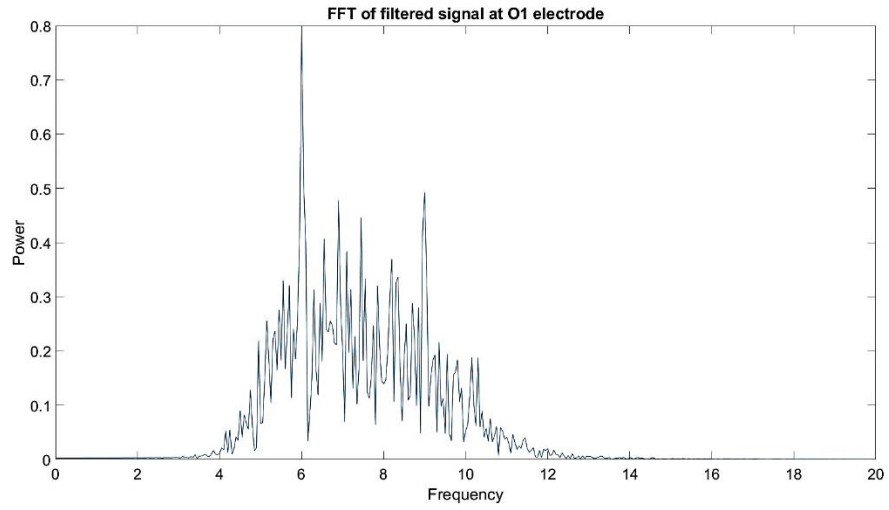
(a)
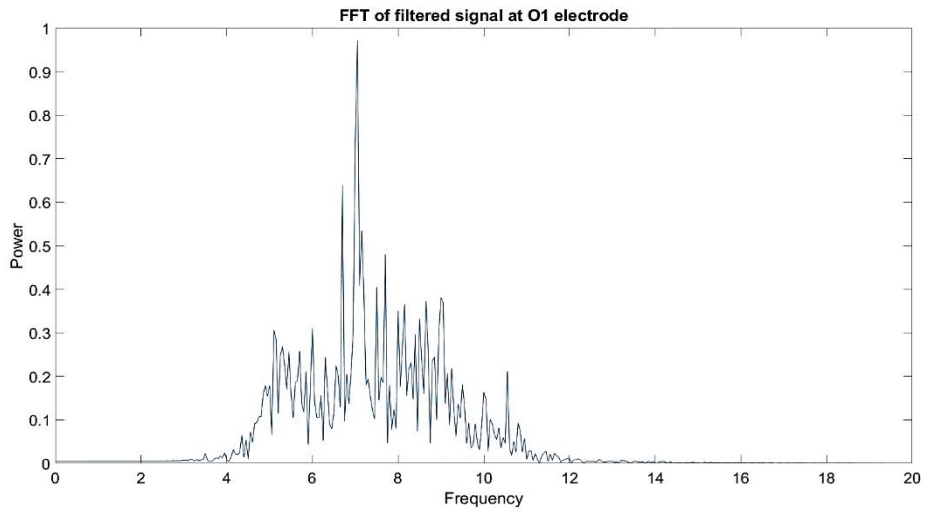
(b)
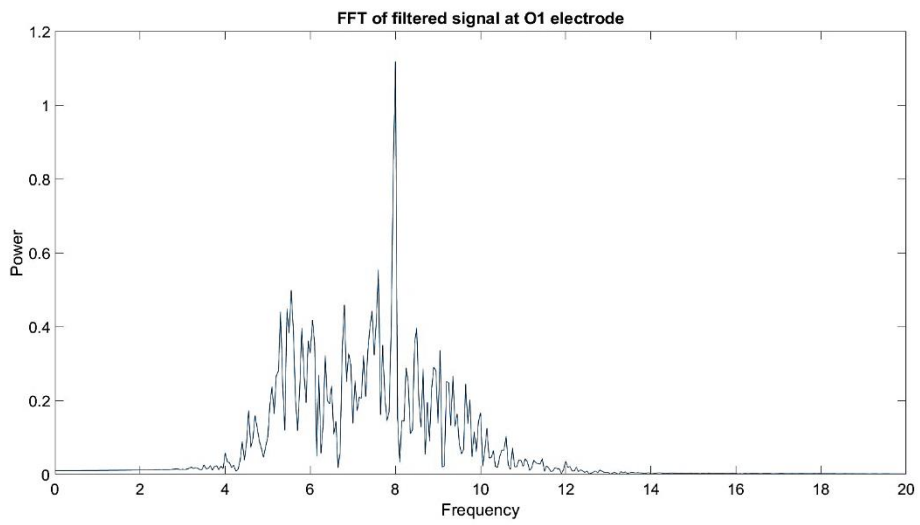
(c)
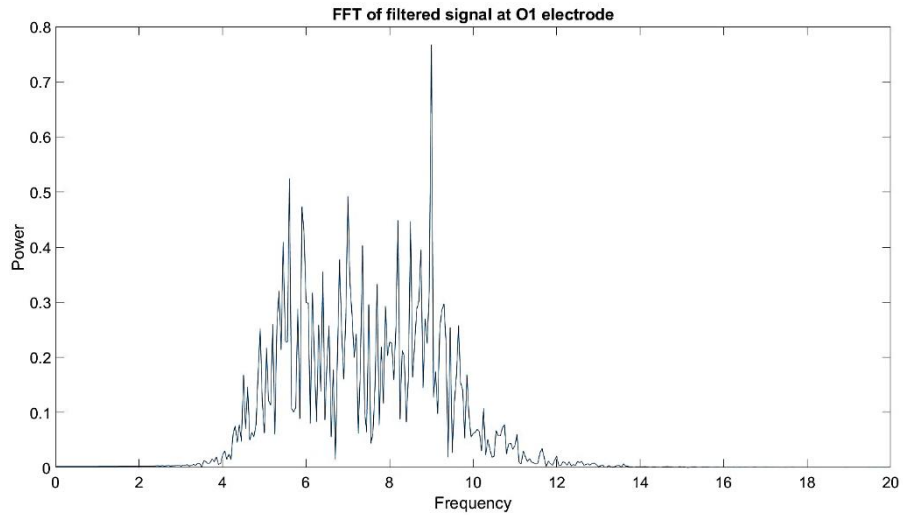
(d)

Figure 6.11: Power spectrum at a) 6 Hz b) 7Hz c) 8Hz and d) 9Hz
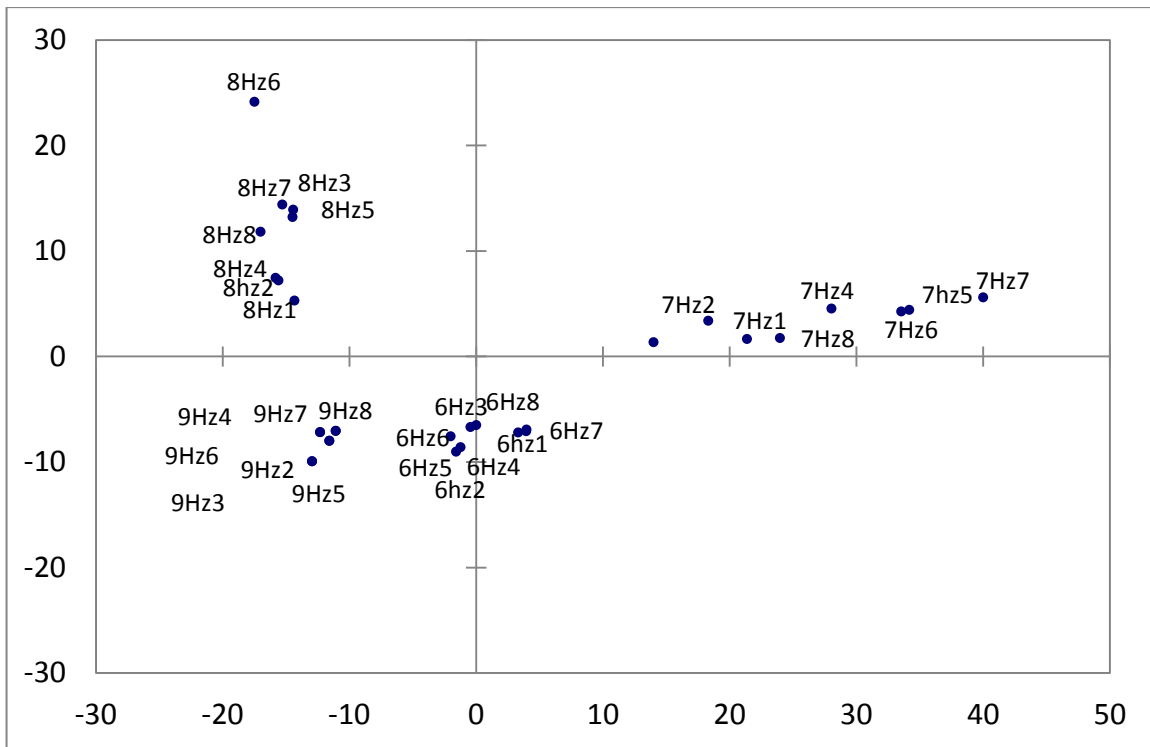
Figure6.12: Scatter plot of SSVEP frequencies under interest

6.3 Summary

In this work, we proposed a BCI-based on SSVEP for home automation with wireless technology.We have successfully tested the preliminary design of BCI system for

both online and offline analyses. In the proposed system, a subject just gazes an independent flickering target having low frequencies to turn on/off-normal day to days' electrical gadgets like a bulb or fan. We also discovered that when the flickering frequencies were kept above the delta brain (above 4 Hz) and below the beta brain (below 12 Hz) one obtained pretty good detection of frequencies. We also noticed that the subject's eyes are tired after some trials. This can be reduced by adjusting the distance of the stimulus LED box for each subject rather than keeping a fixed distance since each user will have different eye sensitivity. In this study, instead of producing the stimulus on an LCD screen the LED's are used which is portable for the user, thus allowing better flexibility to the user. Another advantage of using LED's is that one has the flexibility to decide on various frequencies as compared to an LCD screen where the frequencies are a multiple of the monitor refresh frequency rate. One can use a phase-based SSVEP system instead of the current frequency based system to reduce the fatigue caused to the eye retina and to improve performance. At present, the frequencies we have selected have 1 Hz spatial separation between them. Also one can reduce the separation to 0.2 or 0.5 Hz so that we can accommodate more commands within the 4–12 Hz range. The length of each trial can be reduced from 120 seconds to check how it performs with a shorter trial length to increase the information transfer rate. Classification algorithms based on ensemble, discriminant or neural networks can be used to reduce misclassification error.

Chapter 7

Conclusion and Scope for Future Work

7.1 Future Scope

There is good potential for the SSVEP based study and one can design diverse applications in this area. We propose application of SSVEP in biometrics.

7.1.1 Application of EEG in biometrics

Subject identification and verification are two different processes together, wherein for identification the subject need not be physically present, example if photo of the person is available, then one can check whether he or she exists in a certain criminal database. Verification requires the presence or direct involvement of the person as it mostly deals with authorizing a person or allowing to access security systems.Traditional authentication methods use "what you know "(i.e. authenticator based on knowledge) or "what you have "(i.e. authenticator based on objects) to identify users. These can be unintentionally disclosed or simply lost or stolen. "what you are "(i.e., ID-based authenticator) gives an edge, as people are "who they are "regardless of "what they know "or "what they have".

Also, EEG devices are undergoing significant development, which leads to an increasing number of users accepting them as brain-computer interfaces (BCI). This creates an opportunity to advantage of a person's unique "inner self" for authentication. Several literary studies attempt to explore the potential biometric use of EEG. Biometric systems based on EEG can be based on the use of exogenous or endogenous brain activity. Endogenous activity is when the subject is asked to relax and not perform any particular task. The problem is that EEG activity varies from person to person. Exogenous activity is when the subject is asked to perform some tasks, such as looking at flickering LEDs, counting mentally, imagining, etc. [212]. Biometrics such as fingerprint and face have become ubiquitous in all walks of life and there is continuous work being done for subject identification and verification. But there are certain problems with fingerprint biometrics as a person's biometric can easily be picked from smooth surfaces to spoof and in the process compromising with the authenticity of the system. A lot of research has been done to showcase the vulnerability of finger-based biometric systems. Facial images can again be spoofed or masks can be used to bypass the identification system. There has been tremendous effort being put in to overcome the liability of these biometric systems, hence there is no harm in considering another biometric or biometrics in the offing. More recently physiological signals like pulse pressure, electrocardiogram, electromyography, electroencephalography, functional magnetic resonance imaging has garnered interest as a potential biometric. EEG has been used extensively for medical prognosis and diagnosis from its inception, and more recently in BCI to help people with severe motor disabilities to communicate with people or control devices. The ECG signal like it's counterpart ECG has been used for a long time to determine the pathologic condition of human beings. ECG has distinctive features inherently present in them which helps in identifying individuals. Both of them come under the category of hidden biometrics, since it is not visible to the human naked eye and to access it requires a certain amount of expertise. For any trait to be considered as a biometric it must fulfill the certain criterion; a) Universality: The biometric trait should be present in all the subjects, b) Unique: It should have discriminative features that will vary from person to person, c) Repeatable: It should not vary over time. d) Accessible: We should access to the biometric trait, d) Robust: The trait should be good enough to avoid imposters and frauds.

EEG and ECG both possess all the above features, hence making a potent emerging biometric candidate. Apart from this EEG and ECG assure us of the liveliness of the person which is missing in other biometrics and also it is impossible to steal and forge them. There are certain issues with EEG biometric a) Cost: At present the cost of EEG systems is quite high. b) The setup time is quite long compared to other biometric traits. c) Repeatability studies need to be carried out. d)The acquisition process can be a bit taxing with current EEG systems but a lot of effort is being put by researchers to make it easier and faster. Most of the research done in EEG biometrics or BCI's is task dependent. The aim is to understand which areas of the brain called the Broadmann areas to respond to the given tasks whether it is audible, visual, tactile form and also to understand the functional connectivity amongst them. But more recently there have been studies that have reported that neural signature[126,127] is independent of task-related activity. EEG and ECG have been studied individually as unimodal biometric, but there has no study according to our knowledge after extensive literature survey which suggests or utilizes the combination of both. It is a well-known fact that multimodal biometrics have been useful to overcome the shortcomings present in unimodal biometric systems. There has been fusion done on ECG and other modalities like EMG and EEG and handwritten signature and so on[126,127,128,129,130].There are hardly any databases that have recorded EEG and ECG in unison. In this work, we propose a novel approach to the fusion of EEG and ECG biometrics for person identification and verification. Both the physiological traits are interlinked to each other hence garnering more interest to see how fusing such traits will improve the performance of the biometric system.

7.2   Stimulus design and presentation

The stimulus here presented is based on visually evoked stable potential (SSVEP) based on visual stimulus. The block diagram in Figure 7.1, which shows the biometric system based on EEG. It's split into five sub-blocks. It consists of three rows and three columns, each flickering at a given frequency. The frequency range selected is in the theta band. The reason for choosing this design is to present alphanumeric characters ' L," T' and ' 7.' At the intersection of the flickering lines that made up the letter or number, the subjects were asked to focus. The experiment is attended by fifteen subjects(all males). None of the subjects had an epilepsy history. The subject sat comfortably on a chair about

60 cm from the stimulus. The stimulus is based on top-down cognitive processing in the brain [238]. At the beginning of each stimulus, an auditory cue was given (Refer Figure 7.2). There were two trials per subject and each trial lasted 180 sec. There were a total of 30 segments on each trail. Of the 30 segments, 10 segments each corresponding to the letter "L, "T "and "7. " Each segment lasted six seconds, i.e. one second for the auditory cue and the other five for the stimulus flickering. Since the total number of studies per subject was two, there were 20 segments of' L," T' and' 7.' The stimulus presentation was carried out on a 24-inch LCD using the Psychtoolbox toolbox in MATLAB 2017a.
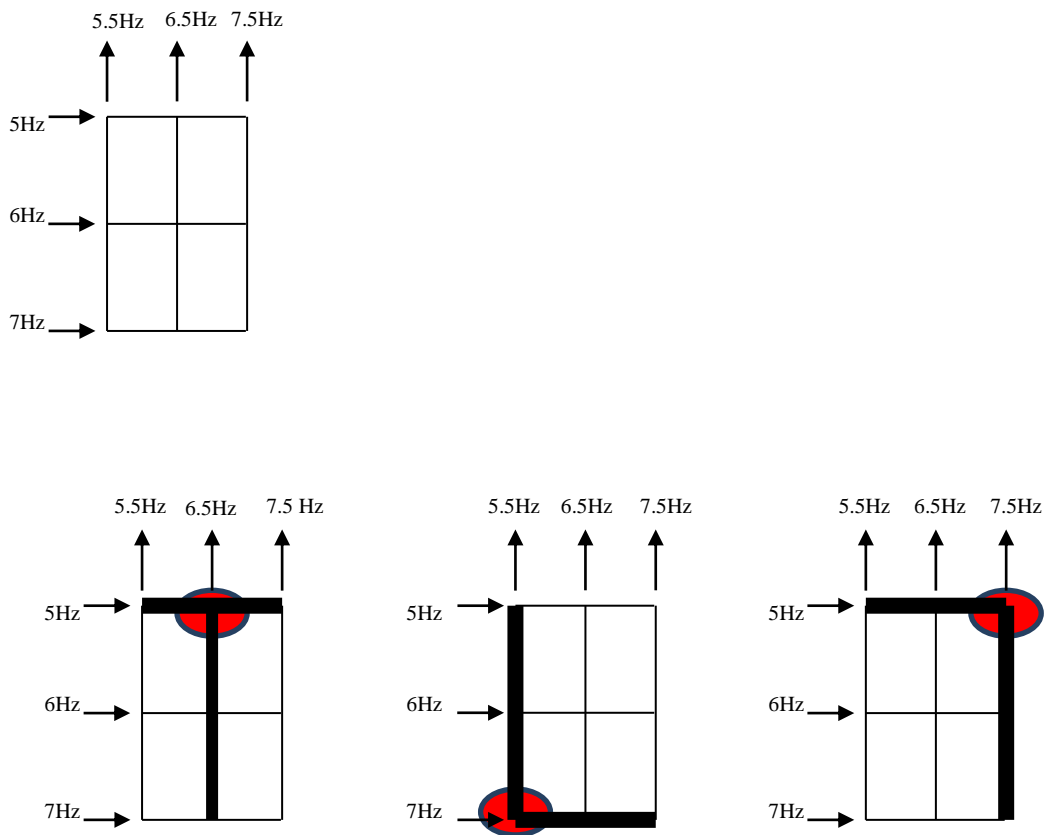
Figure 7.1: SSVEP evoked using grid shaped line array. (Adapted for Min et al. (SSVEP top down paradigm, Nature 2016)).

7.3 Preliminary Database acquisition
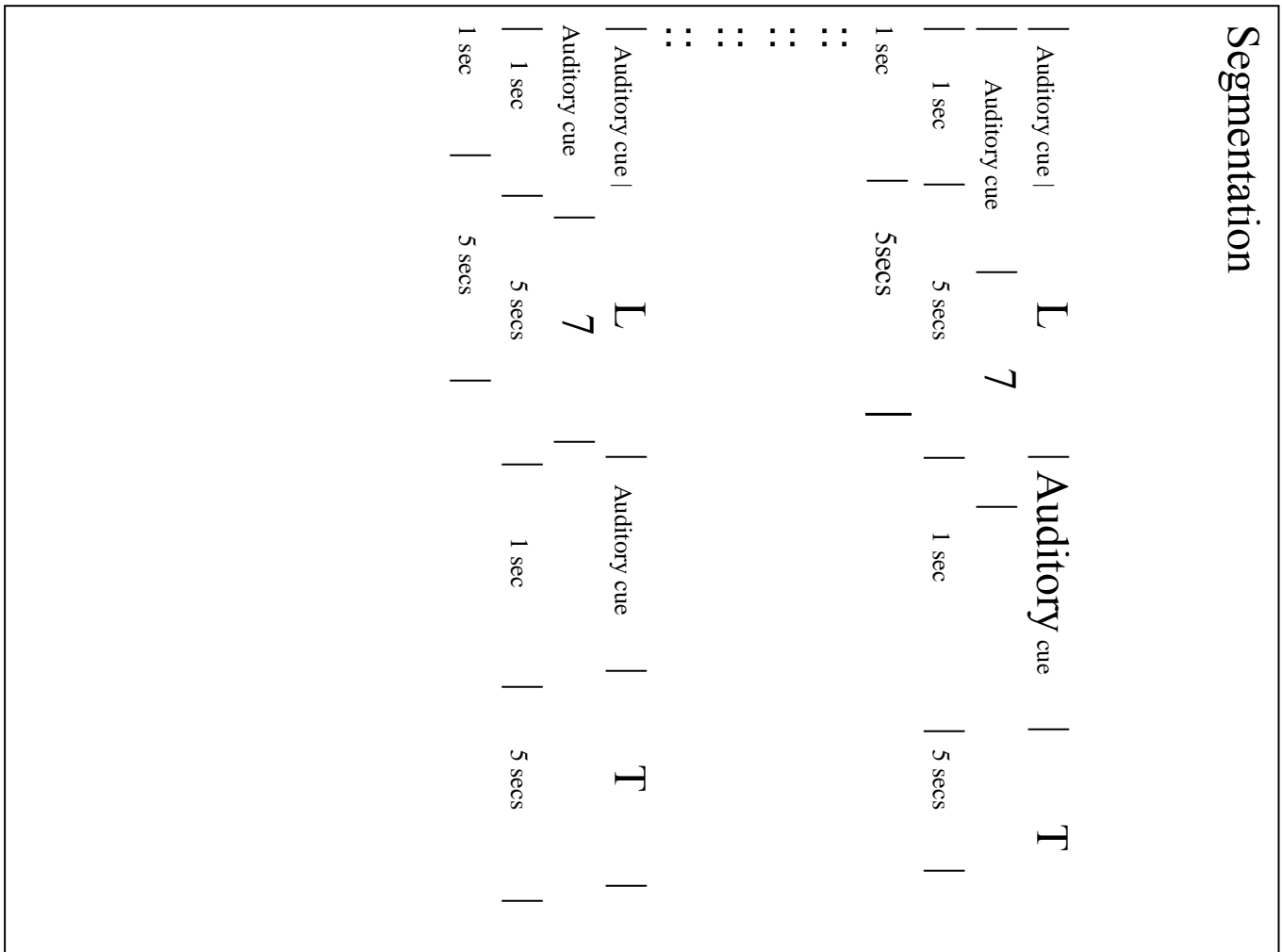
Figure 7.2: Stimulus time line for SSVEP Signal.

The EEG data were obtained from ABM using the B-Alert system 24 channelsEEG system. The computer receives data via Bluetooth. Before recording, the impedance matching is done to ensure proper contact at electrode sites to obtain good quality signals. The EEG strip is based on the international 10-20 system [223]. Set up time varies between 5-15 minutes per subject.

7.4 Feature Extraction

Evaluating spectral maps alone is not enough. To understand how information is processed in the brain, how different brain regions communicate with each other and the

direction of the information flow is important. Spatiotemporal distribution of brain activity and network conduct provides significant psychophysiological data and understanding brain function is essential to picture functional connectivity [232, 233,234,235,236]. As such, the assessment of Granger causality was used to identify vital neurodynamic networks for the top-down grid-shaped SSVEP paradigm. Analysis of the causality of Granger is frequently used to predict the causal directional relationships between electrophysiological signals [236,237]. Directed Transfer Function (DTF), in specific, is a computing technique for measuring causality between an arbitrary amount of signals [239, 240].DTF is suggested as a technique for extracting directional information flow between brain structures to overcome possible inaccurate measures (e.g., coherence analysis) when applied to multivariate systems [241]. DTF can be considered as one type of multivariate causality of Granger and can be used to handle multichannel signals derived from the coefficients of a multivariate autoregressive model (MVAR) that fits the data [242]. For estimating MVAR models, the ARfit package [243] can be used to calculate DTF. The eConnectome software allowed cortical source imaging assessment and subsequent cortical source activity connectivity analysis. The Directed Transfer Function (DTF) as shown in Fig 7.3 is a method used to obtain this information. The causality relationship between two regions of interest is found using Auto Regressive models. Node 1 's current value can be predicted by Node 2 's previous values and so on. In MATLAB 2017a, DTF analysis was carried out using the eConnectome toolbox. The 26 Region of Interests (ROIs) has been selected. Information flow graphics give similar information on how areas of the brain communicate with each other but in the spatial domain as shown in Figure 7.3.
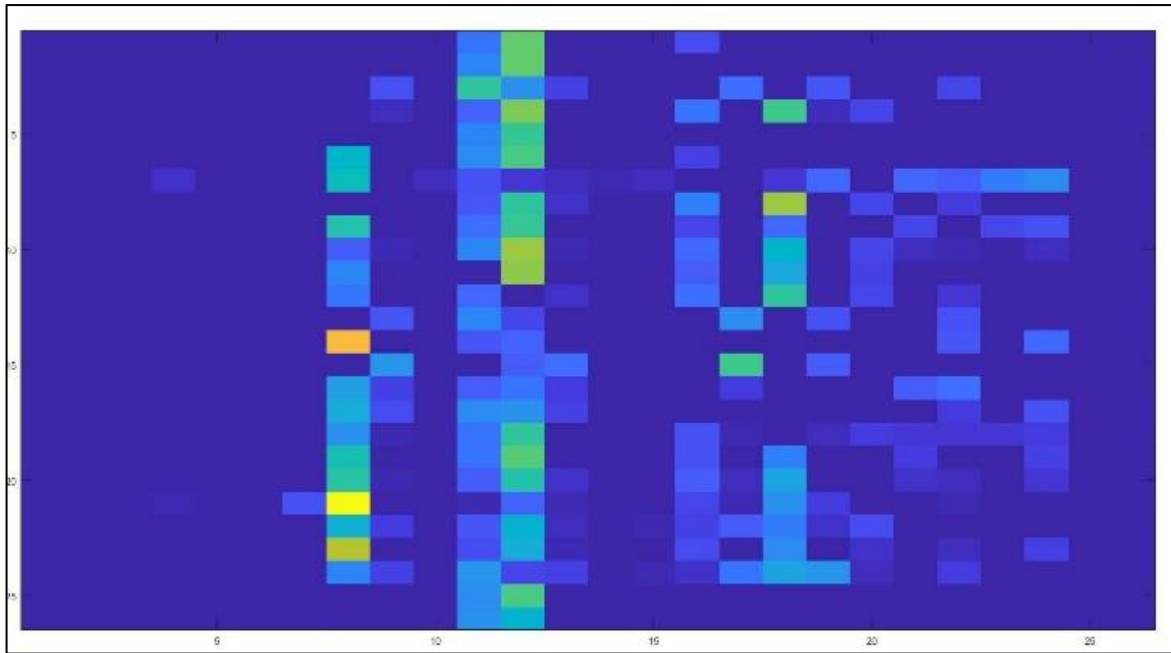
Figure 7.3: DTF matrix of one segment at one particular frequency (26 X 26)

The EEG signals were used for extraction of the function in the frequency range from 5 Hz to 14 Hz. This frequency range involves the flickering frequencies of the stimulus along with the amount of the combination frequencies corresponding to the letter. Source waveforms were estimated at all chosen ROIs and directional information flow (Refer Figure 7.4) across sources was shown by DTF assessment. The DTF feature produces arbitrary values representing functional connectivity that are still subject to statistical evaluations of their meaning [235].
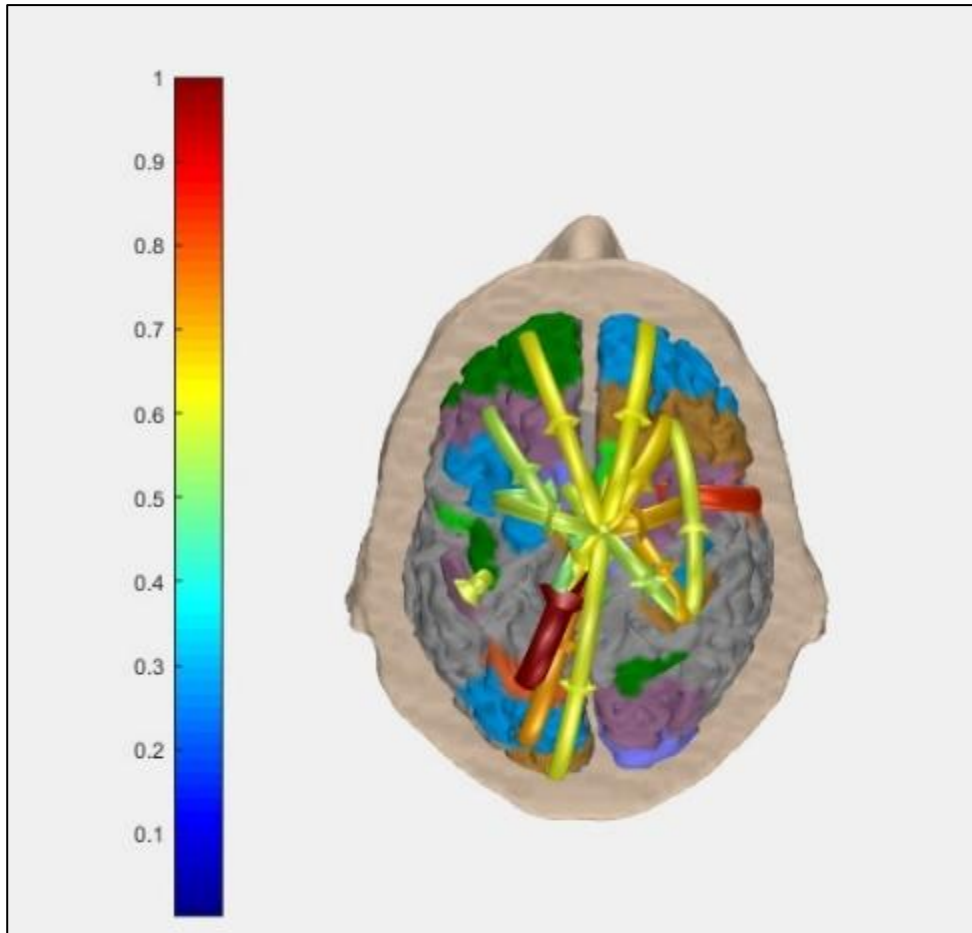
Figure 7.4: Information Flow Graphics
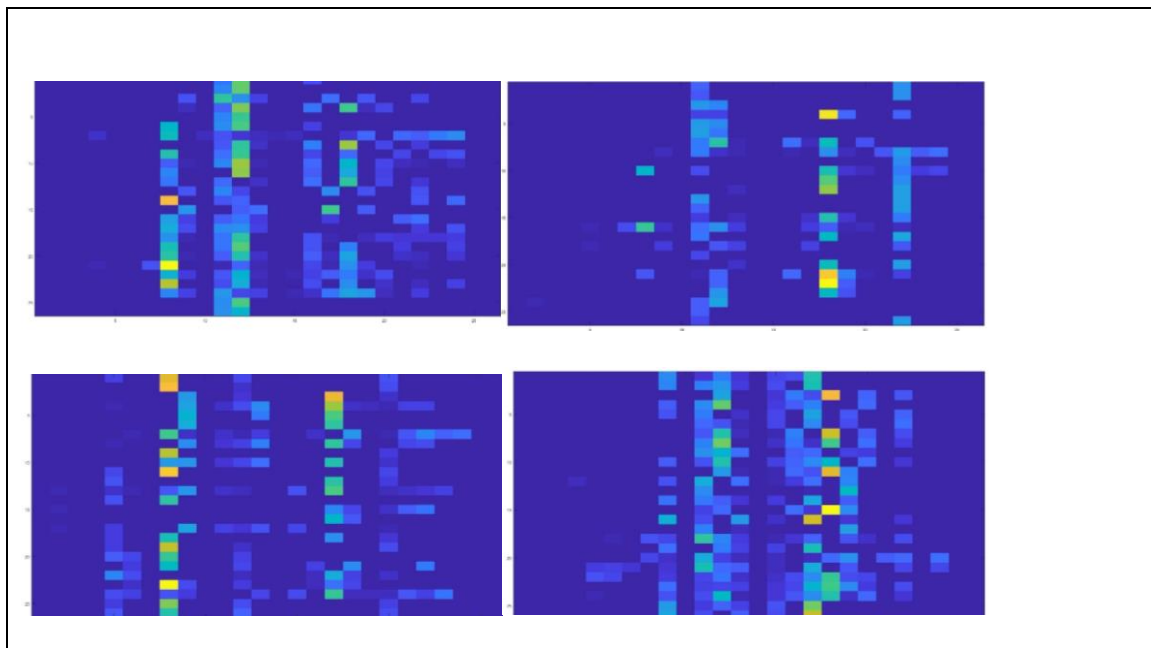
Figure 7.5: DTF matrices of Subject 1, Subject 2, Subject 3 and Subject 4
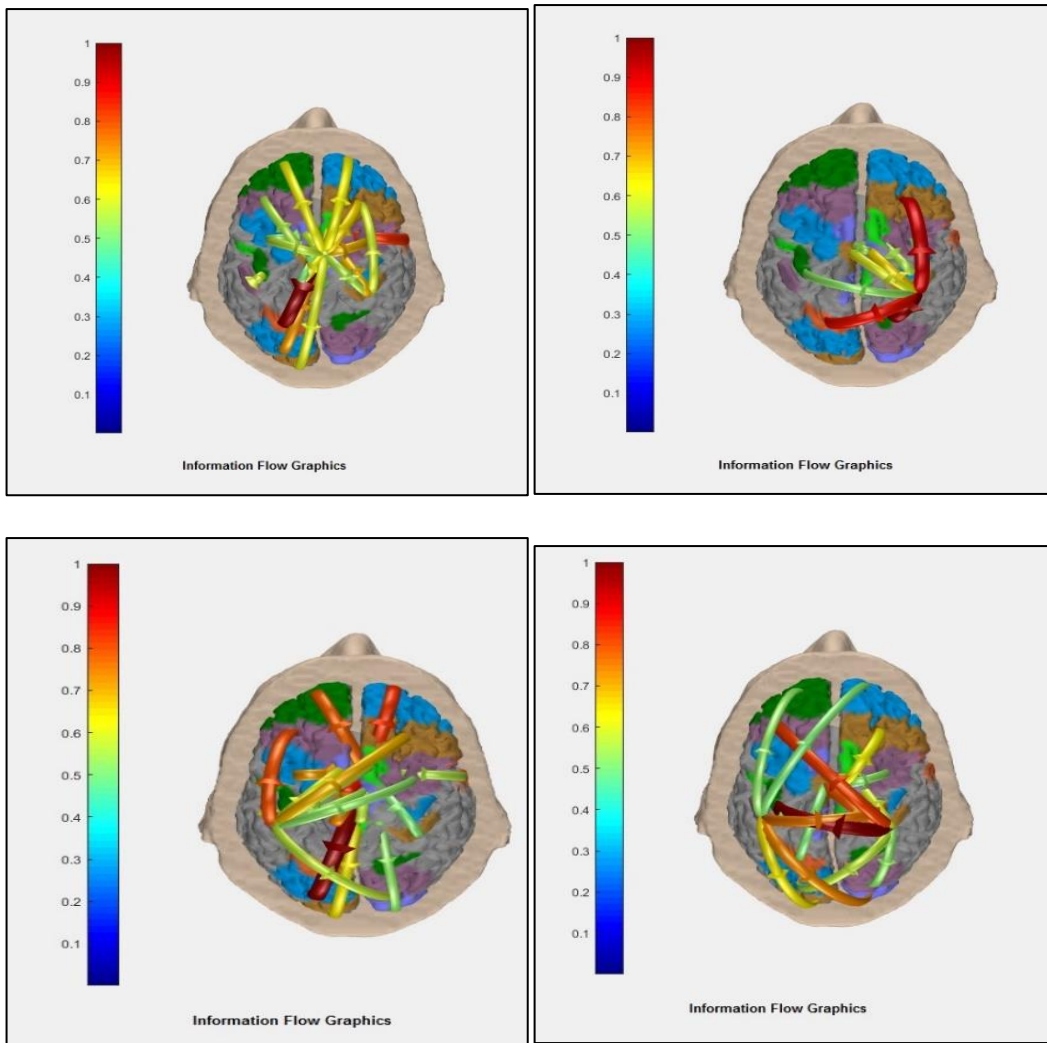
Figure 7.6: Information Flow Graphics of Subject 1, Subject 2, Subject 3 and Subject 4

Due to the extremely nonlinear relationship between the DTF function and the time series data from which it is obtained, a non-parametric statistical test technique based on surrogate data is used to assess the information. In this method, one transforms the original time series into Fourier space, maintaining unchanged the magnitudes of the Fourier coefficients, but shuffling the Fourier coefficients phases randomly and independently. The surrogate data was then converted back to the time domain in the Fourier space. This stage shuffling method maintains the time series spectral structure that is suitable for DTF assessment as DTF measures frequency-specific causal relationships. The estimation of connectivity was introduced to the surrogate data after shuffling. For each set of source time series, we repeated the shuffling and connectivity estimation procedures 1000 times,

creating an empirical distribution of the DTF values under the null hypothesis that there is no causal connectivity (p<0.05) [244].

7.5 Classification

A DTF matrix was calculated for 10 different frequencies (5-14 Hz). Each DTF matrix is of size 26 X 26 X 10 for one stimulus. Four such DTF matrix is shown in Fig 7.4. One can see the directional flow of the signal in the brain neural mass (Refer Figure 7.6), which depict the uniqueness for the stimuli subjected to various subjects. Hence for each subject there a total of 60 X (26 X 26 X10) = 600 matrices. These matrices are then saved as images to input them to deep learning based protocol i.e. CNN. For four subjects a total of 2400 images each of size 26 X 26. For support vector machine (SVM) based classification, the matrices are reshaped from 26 X 26 X 10 to 676 X10 row vectors. For each subject total 60 X (676 X10) = 600 row vectors of length 676.Total for say four subjects there are 2400 row vectors of length 676. For the Convolutional neural network(CNN) classification out of the 600 images, 400 images were used for training and the remaining 200 images for testing. For Support Vector Machines (5-fold cross validation) classification, 400-row vectors were used for training and 200 for testing. A 100% classification was obtained for both the methods. This preliminary studies state that there is potential for the biometrics authentications.

7.6 Database acquisition

The database is created for the video paradigm suggested above. In session 1 there were 28 subjects (18 males and 10 females). Here, each subject is asked to perform the tasks given below over alphanumeric paradigm (4 trials) and continuous authentication (4 trials) as shown in Table 7.1. In session 2 there were 18 subjects (14 males and 4 females). Session two was done after 15 days to perform analysis for repeatability. Care is ensuring to ensure that none of the subjects had any history of epilepsy. The subject is seated comfortably on a chair at a distance of around 60 cms from the stimulus. The subject was asked to focus at the intersection of the rectangular boxes which made up a letter. Each of the horizontal or vertical lines. An auditory cue (refer Figure 7.2) is given at the start of each stimulus. Stimulus presentation was implemented using the Psychtoolbox toolbox in MATLAB

2017 a. The setup time to mount the EEG cap over each subject varied from 20-30 minutes.

Table 7.1: Created a database of 28 subjects (18 males and 10 females) Session 1 and Session 2 (14 males and 4 females).

Session I and II - 05 Second for three letter 10 times + 1 sec auditorycue							
LCD				Continuous Authentication			
Instance 1	Instance 2	Instance 3	Instance 4	Instance 1	Instance 2	Instance 3	Instance 4

7.7 Conclusion

DFT is very computing power intensive and required good computing machines. One may note that on i3 processor the DTF computing takes 30 minutes. Hence, the study will be extended for biometrics application in near future. Hence, the thesis can be concluded with following.

- Blood pressure meter was developed based on auscultation and oscillometric principles and validated for subjects.
- Windkessel simulation studies performed to generate the data for the best fusion strategies to combine the blood pressure systolic and diastolic values for auscultation and oscillometric principles.
- Successfully implemented and studied independency the Neural Mass Model, ECG(HRV) model and Windkessel Arterial Blood Pressure model.
- The above three model integrated to implement the Autonomous Neural System (ANS) Model to understand the complexity in the Coherence of the Physiological system.
- Studied and implemented brain computer interface system as an application of EEG signals. The Study is extended for various paradigm for SSVEP signals analysis.

- Proposed implemented EEG biometric system with a preliminary database of ten subjects and demonstrated classification accuracy of 100% using Support Vector Machines and Convolutional Neural Networks. Also proposed paradigm for Continuous Authentication.

7.8 Future Work

- Validation with standard protocols(British Hypertension Society or Advancement of Medical Instrumentation)

- One can explore a cheaper system such as Neurosky Think gear for the acquisition of signals. Neurosky Think Gear ASIC Module is a single channel (EEG electrode, the reference electrode and ground electrode) EEG amplifier with a sampling rate of 512 Hz. The exciting features of this are that, it directly connects to a dry EEG electrode and provides extremely low-level signal detection in the range of 3–100 Hz bandwidth.

- In BCI paradigm that can generate more number of commands by using the following grid structure where the resolution between each frequency is 0.5Hz.
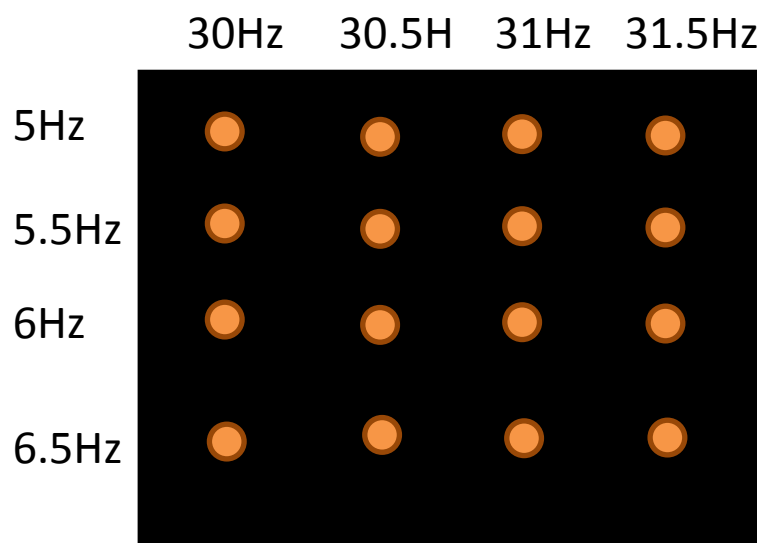
Figure 7.7: Grid structure with better frequency resolution

- Increase the size of the existing database for the EEG and ECG biometric system for two Paradigms and for two sessions for 50 subjects across both the sessions.

- Compare different state of the art machine learning algorithms for better biometric recognition.

- Implement the proposed multimodal approach with ECG and EEG for better recognition rates

REFERENCES

[1] Kaplan, R. and Kaplan, S. "The Experience of Nature: A Psychological Perspective." Cambridge University Press, Cambridge, New York, (1989).

[2] Hamilton-Smith, E. and Mercer, D. "Urban Parks and Their Visitors." The Parks Division, Melbourne and Metropolitan Board of Works, Melbourne, pp.1–79 (1991).

[3] Rohde, C. L. E. and Kendle, A. D. "Nature for people." Kendle, A.D.and Forbes, S.(eds)Urban Nature Conservation—Landscape Management in the Urban Countryside. E. and F. N. Spon, London, pp. 319–335 (1997).

[4] Parsons, R. (1991). "The potential influences of environmental perception on human health." Journal of Environmental Psychology, 11, pp. 1–23 (1991).

[5] Ulrich, R. S. "Biophilia, biophobia, and natural landscapes." Kellert, S. R. and Wilson, E. O. (eds), The Biophilia Hypothesis. Shearwater Books/Island Press, Washington D.C., pp.73–137 (1993).

[6] Leather, P., Pyrgas, M., Beale, D., & Lawrence, C. "Windows in the workplace." Environment and Behavior, 30(6), pp. 739–762 (1998).

[7] Kaplan, R. "The nature of the view from home." Environment and Behavior,33(4), pp. 507–542 (2001).

[8] Taylor,A.F., Kuo, F.E.,& Sullivan, W.C. "Views of nature and self-discipline: Evidence from inner city children." Journal of Environmental Psychology,22(1–2), pp. 49–63 (2002).

[9] Armour, J. A. "Anatomy and function of the intrathoracic neurons regulating themammalian heart." I. H. Zucker & J. P. Gilmore (Eds.), Reflex control of the circulation Boca Raton, FL: CRC Press, pp.1-37 (1991).

[10] Armour, J. A. "Neurocardiology—Anatomical and functional principles" (Publication No. 03-011). Boulder Creek, CA: Heart Math Research Center, Institute of Heart Math. (2003).

[11] Armour, J., A., &Kember, G. C. "Cardiac sensory neurons." J. A. Armour& J. L.Ardell (Eds.), Basic and clinical neurocardiology , New York, NY: Oxford University Press, pp. 79-117 (2004).

[12] Armour, J. A. "Peripheral autonomic neuronal interactions in cardiac regulation." In J. A. Armour& J. L. Ardell (Eds.), NeurocardiologyNew York, NY: Oxford University Press, pp. 219-244 (1994).

[13] Chernigovskiy, V. N. "Interoceptors." Washington, DC: American Psychological Association (1967).

[14] Grossman, P., Janssen, K. H. L., &Vaitl, D. (Eds.). "Cardiorespiratory and cardiosomatic psychophysiology." New York, NY: Plenum Press (1986).

[15] Randich, A., &Gebhart, G. F. "Vagal afferent modulation of nociception." Brain Research Reviews, 17, pp. 77-99 (1992).

[16] Drinkhill, M. J., & Mary, D. A. "The effect of stimulation of the atrial receptors on plasma cortisol level in the dog." Journal of Physiology, 413, pp. 299-313 (1989).

[17] Coleridge, H. M., Coleridge, J. C., & Rosenthal, F. "Prolonged inactivation of cortical pyramidal tract neurons in cats by distention of the carotid sinus." Journal of Physiology, 256, pp.635-649 (1976).

[18] Svensson, T. H, &Thoren, P. "Brain noradrenergic neurons in the locus coeruleus: Inhibition by blood volume load through vagal afferents." Brain Research, 72 (1), pp.174-178 (1979).

[19] Foster, A., & Stone, T. W. "Evidence for a cardiovascular modulation of central neuronal activity in man." Experimental Neurology, 51, pp.141-149 (1976).

[20] Lader, M., & Mathews, A. "Physiological changes during spontaneous panic Attacks." Journal of Psychosomatic Research, 14 (4), pp.377-382 (1970).

[21] Montoya, P., Schandry, R., & Muller, A. "Heartbeat evoked potentials (HEP), Topography and influence of cardiac awareness and focus of attention" Electroencephalography and Clinical Neurophysiology, 88, pp.163-172 (1993).

[22] Schandry, R., & Montoya, P. "Event-related brain potentials and the processing of cardiac activity." Biological Psychology, 42, pp.75-85 (1996).

[23] Schandry, R., Sparrer, B., &Weitkunat, R. (1986). From the heart to the brain: A study of heartbeat contingent scalp potentials. International Journal of Neuroscience, 30, pp.261-275 (1986).

[24] Lane, R. D, Reiman, E. M., Ahern, G. L., & Thayer, J. F. "Activity in medial prefrontal cortex correlates with vagal component of heart rate variability during emotion." Brain and Cognition, 47, pp. 97-100 (2001).

[25] Wake, E., &Brack, K. (2016). Characterization of the intrinsic cardiac nervous system. Autonomic Neuroscience, 199, pp. 3–16 (2016).

[26] Barbara Kukanova and Boris Mravec. "Complex intracardiac nervous system." Bratislavskelekarskelisty,volume 107(3)pp.45-51(2006).

[27] Wölk, C., & Velden, M. (1989). Revision of the baroreceptor hypothesis on the basis of the new cardiac cycle effect. In N. W. Bond & D. A. T. Siddle (Eds.), Psychobiology: Issues and applications (pp. 371-379). North-Holland: Elsevier Science Publishers.

[28] Wölk, C., Velden, M., Zimmerman, U., & Krug, S. (1989). The interrelation between phasic blood pressure and heart rate changes in the context of the "baroreceptor hypothesis." Journal of Psychophysiology, 3, 397-402.

[29] McCraty, R., Atkinson, M., & Bradley, R. T. (2004b). Electrophysiological evidence of intuition: Part 2. A system-wide process? Journal of Alternative and Complementary Medicine, 10 (2),325-336.

[30] Lehrer,P.M,Vaschillo,E.,Vaschillo,B.,Lu,S.E.,Eckberg,D.L.,Edelberg,R. Hamer, R.M. "Heartrate variability biofeedback increases baroreflex gain and peak expiratory flow." Psychosomatic Medicine, 65 (5), pp.796-805 (2003).

[31] Mauskop, A. "Vagus nerve stimulation relieves chronic refractory migraine and cluster headaches." Cephalalgia, 25 (2), pp. 82-86 (2005).

[32] Adair, J., R., & Manning, J. W. "Hypothalamic modulation of baroreceptor afferent unit activity". American Journal of Physiology, 229, pp.1357-1364(1975).

[33] Cameron, O. G. "Visceral sensory neuroscience: Interoception." New York, NY: Oxford University Press (2002).

[34] Foreman, R. "Organization of visceral input." In T. L. Yaksh, Lynch, C. III, W.M. Zapol, M. Maze, J. F. Biebuyck, & L. J. Saidman (Eds.), Anesthesia: Biologic Foundations, Philadelphia: Lippincott-Raven Publishers, pp. 663-683 (1997).

[35] Frysinger, R. C, & Harper, R. M. "Cardiac and respiratory correlations with unit discharge in epileptic human temporal lobe." Epilepsia, 31 (2), 162-171 (1990).

[36] Oppenheimer, S., & Hopkins, D. "Suprabulbar neuronal regulation of the heart." In J. A. Armour& J. L. Ardell (Eds.), Neurocardiology New York, NY: Oxford University Press, pp. 309-341 (1994).

[37] Zhang, J. X., Harper, R. M., &Frysinger, R. C. "Respiratory modulation of neuronal discharge in the central nucleus of the amygdala during sleep and waking states." Experimental Neurology, 91, pp. 193-207 (1986).

[38] Ulrich,R. S. "Natural versus urban scenes: Some psychophysiological effects. Environment and Behavior, 13(5), pp. 523–556 (1981).

[39] Ulrich, R., Simons, R., Losito, B., Fiorito, E., Miles, M., &Zelson, M. "Stress recovery during exposure to natural and urban environments.",Journal of Environmental Psychology, 11(3),pp.201–230 (1991).

[40] Gladwell,V.F.,Brown,D.K.,Barton,J.L.,Tarvainen,M.P.,Kuoppa,P.,Pretty,J, et al. "The effects of views of nature on autonomic control." European Journal of Applied Physiology, 112(9),pp. 3379–3386 (2012).

[41] Laumann, K., Gärling, T., &Stormark, K. M. "Selective attention and heart rate responses to natural and urban environments." Journal of Environmental Psychology, 23(2),pp. 125–134 (2003).

[42] Park, B. J., T sunetsugu, Y., Kasetani, T., Kagawa,T.,& Miyazaki, Y. "The physiological effects of Shinrinyoku (taking in the forest atmosphere or forest bathing): Evidence from field experiments in 24 forests across Japan." Environmental Health and Preventive Medicine, 15(1),pp. 18–26 (2009).

[43] Tyrväinen, L., Ojala, A., Korpela, K., Lanki, T., Tsunetsugu, Y., & Kagawa, T. The influence of urban green environments on stress relief measures: A field experiment." Journal of Environmental Psychology, 38, pp.1–9 (2014).

[44] Berman, M. G., Jonides, J., & Kaplan, S. "The cognitive benefits of interacting with nature." Psychological Science, 19(12),pp.1207–1212 (2008).

[45] Berman, M. G., Kross, E., Krpan, K. M., Askren, M. K., Burson, A., Deldin, P. J., et al. "Interacting with nature improves cognition and affect for individuals with depression." Journal of Affective Disorders, 140(3).

[46] Hartig, T., Evans, G., Jamner, L., Davis, D., &Garling, T. "Tracking restoration in natural and urban field settings." Journal of Environmental Psychology, 23(2), pp. 109–123 (2003).

[47] Ward Thompson, C., Roe, J., Aspinall, P., Mitchell, R., Clow, A., & Miller, D."More green space is linked to less stress in deprived communities: evidence from salivary cortisol patterns." Landscape and Urban Planning,105(3), pp. 221–229 (2012).

[48] Wells,N.M. "At home with nature: Effects of greenness on children' s cognitive functioning." Environment and Behavior, 32(6),pp. 775–795 (2000).

[49] White, M. P., Alcock, I., Wheeler, B. W., &Depledge, M. H. "Would you be happier living in a greener urban area? A fixed-effects analysis of panel data", Psychological Science, 24(6), pp.920–928 (2013).

[50] Tennessen,C.M.,&Cimprich,B."Views to nature: Effects on attention", Journal of Environmental Psychology, 15(1),pp. 77–85 (1995).

[51] Berto, R. "Exposure to restorative environment s helps restore attentional capacity", Journal of Environmental Psychology, 25(3), pp. 249–259 (2005).

[52] MaheshkumarKuppusamy, Dilara Kamaldeen, Ravishankar Pitani, Julius Amaldas, Poonguzhali Shanmugam. "Effects of Bhramari Pranayama on health e A systematic review." Journal of Traditional and Complementary Medicine 8 ,11e16 (2018).

[53] Büssing, Arndt et al. "Effects of yoga on mental and physical health: a short summary of reviews." Evidence-based complementary and alternative medicine: eCAM vol. 2012 -165410 (2012).

[54] Chong CS, Tsunaka M, Tsang HW, Chan EP, Cheung WM. "Effects of yoga on stress management in healthy adults: a systematic review." Alternative Therapies in Health and Medicine,17(1):32–38 (2011).

[55] Martens R, Vealey RS, Burton D. "Competitive anxiety in sport." Human Kinetics; 1990.

[56] Brown RP, Gerbarg PL. "Sudarshan Kriya yogic breathing in the treatment of stress, anxiety, and depression: part I-neurophysiologic model." J Altern Complement Med, 11(1):189e201 (2005).

[57] Miguel-Humara MA. "The relationship between anxiety and performance: a cognitive-behavioral perspective." Online J Sport Psychol, 1(2) (1999).

[58] Hardy L, Jones G, Gould D. "Understanding psychological preparation for sport: theory and practice of elite performers." Chichester, UK: Wiley, 1996.

[59] Orlick T, Partington J. Mental links to excellence. Sport Psychol ,2: 105e30 (1988).

[60] WHO https://www.who.int/gho/ncd/risk_factors/blood_pressure_prevalence_text/en/

[61] Jubran A. Pulse oximetry. Crit Care. 2015;19(1):272. Published 2015 Jul 16

[62] D. A. Birrenkott, M. A. F. Pimentel, P. J. Watkinson and D. A. Clifton. "A Robust Fusion Model for Estimating Respiratory Rate from Photoplethysmography and Electrocardiography." in IEEE Transactions on Biomedical Engineering, vol. 65, no. 9, pp.2033-2041, Sept. 2018.

[63] W. Karlen, A. Garde, D. Myers, C. Scheffer, J. M. Ansermino and G. A. Dumont. "Estimation of Respiratory Rate from Photoplethysmographic Imaging Videos Compared to Pulse Oximetry." in IEEE Journal of Biomedical and Health Informatics, vol.19, no.4, pp.1331-1338 (July-2015).

[64] R. Sitaram, N. Weiskopf, A. Caria, R. Veit, M. Erb and N. Birbaumer. "fMRI Brain-Computer Interfaces." in IEEE Signal Processing Magazine, vol. 25, no. 1, pp. 95-106, 2008.

[65] Alexander N.Pisarchik, ParthChholak, Alexander E. Hramov. "Brain noise estimation from MEG response to flickering visual stimulation." Chaos, Solitons & Fractals: X, Volume 1, 100005 (March 2019).

[66] S. Ueno, K. Iramina and H. Yoshida. "Source Analysis and Measurement of MEG Activity During Sleep." in IEEE Translation Journal on Magnetics in Japan, vol. 8, no.10, Oct. 1993, pp 680-684.

[67] G. Zhao, Y. Ge, B. Shen, X. Wei and H. Wang. "Emotion Analysis for Personality Inference from EEG Signals." in IEEE Transactions on Affective Computing, vol. 9, no. 3, pp. 362-371, 1 July-Sept. 2018.

[68] M. Thulasidas, Cuntai Guan and Jiankang Wu. "Robust classification of EEG signal for brain-computer interface." in IEEE Transactions on Neural Systems and Rehabilitation Engineering, vol. 14, no. 1, pp. 24-29, March 2006.

[69] Yoo SY, Ahn JE, Cserey G, Lee HY, Seo JM. "Reliability and Validity of Non-invasive Blood Pressure Measurement System Using Three-Axis Tactile Force Sensor." Sensors (Basel), 2019;19(7):1744 (April 2019).

[70] Meidert AS, Saugel B. "Techniques for Non-Invasive Monitoring of Arterial Blood Pressure." Front Med (Lausanne), 4:231 Jan 2018.

[71] Sahu, Dinesh, and M Bhaskaran. "Palpatory method of measuring diastolic blood pressure." Journal of anaesthesiology, clinical pharmacology vol. 26,4, pp. 528-530 (2010)

[72] Vaidya JS, Vaidya SJ. "Diastolic Blood Pressure Can Be Reliably Recorded by Palpation." Arch Intern Med.,156(14):1586 (1996).

[73] KOROTKOFF NC. "On methods of studying blood pressure." Bull Imperial Acad Med (St. Petersburg) 4:365-367, 1905.

[74] O'Sullivan, John & Allen, John & Murray, Alan. "A clinical study of the Korotkoff phases of blood pressure in children." Journal of human hypertension. 15. pp. 197-201 (2001).

[75] Babbs, Charles F. "The origin of Korotkoff sounds and the accuracy of auscultatory blood pressure measurements" Journal of the American Society of Hypertension, Volume 9, Issue 12, 935 - 950.e3 (2015).

[76] Zhi Zhang MD, Weichun Xi MD, Bingjiang Wang MD, Guang Chu MD, Fang Wang MD "A convenient method to verify the accuracy of oscillometric blood pressure monitors by the auscultatory method: A smartphone-based app" J Clin Hypertens (Greenwich) Volume21, Issue2 pp. 173-180 (Feb 2019).

[77] Ramakrishnan D., "Using Korotkoff Sounds to Detect the Degree of Vascular Compliance in Different Age Groups", J Clin Diagn Res,10(2): pp.CC04–CC7 (2016).

[78] Fan Pan, Peiyu He, Chengyu Liu, Taiyong Li, Alan Murray, Dingchang Zheng. "Variation of the Korotkoff stethoscope sounds during blood pressure measurement Analysis using a convolutional neural network". IEEE Journal of Biomedical and Health Informatics, volume 6, pp. 1593-1598 (Nov 2017).

[79] Fan Pan, Fei Chen, Chen Liu, Zhipeng Yang, Zhihong Liu, and Dingchang Zheng. "Quantitative Comparison of Korotkoff Sound Waveform Characteristics: Effects of Static Cuff Pressures and Stethoscope Positions." Ann Biomed Eng46(11), pp.1736-1744 (2018).

[80] Yuqi Wang, Jin She, Haiyan Xiang, Yinhua Li, Juan Liu, Deyu Li, Mengsun Yu. "Improving Auscultatory Blood Pressure Measurement with Electronic and Computer

Technology: The Visual Auscultation Method" American Journal of Hypertension, Volume 22, Issue 6, pp 624–629 (2009)

[81] Babbs CF. "Oscillometric measurement of systolic and diastolic blood pressure validated in a physiologic mathematical model." Biomed Eng Online. 2012; 11:56.(2012)

[82] Lim PK, Ng SC, Jassim WA, et al. "Improved Measurement of Blood Pressure by Extraction of Characteristic Features from the Cuff Oscillometric Waveform." Sensors (Basel), 15(6): pp.14142–14161 (2015).

[83] Mohamad Forouzanfar,HilmiR. Dajani, VoicuZ. Groza, MiodragBolic, SreeramanRajan, IzmailBatkin Bayesian fusion algorithm for improved oscillometric blood pressure estimation Published Medical Engineering and Physics 000: pp.1-5 (2016).

[84] Soojeong Lee, Joon-Hyuk Chang. "Deep learning ensemble with asymptotic techniques foroscillometric blood pressure estimation." Computer Methods and Programs in Biomedicine 151: pp.1-13 (2017).

[85] Kurt Barbé, YuriyKurylyak, Francesco Lamonaca. "Logistic ordinal regression for the calibration of oscillometric blood pressure monitors" Biomedical Signal Processing and Control 11 pp. 89–96 (2014).

[86] Wang, Ruiping et al. "Cuff-Free Blood Pressure Estimation Using Pulse Transit Time and Heart Rate." International Conference on Signal Processing vol. 2014: pp. 115- 118 (2014).

[87] Lee, Joonnyong et al. "Novel blood pressure and pulse pressure estimation based on pulse transit time and stroke volume approximation." Biomedical engineering online vol. 17,1 81. 18 Jun. 2018.

[88] Bennis FC, van Pul C, van den Bogaart JJL, Andriessen P, Kramer BW, Delhaas T. "Artifacts in pulse transit time measurements using standard patient monitoring equipment." 14(6): e0218784 (PLoS ONE 2019).

[89] Foo, J.Y.A., Wilson, S.J., Williams, G.R. et al. "Motion artefact reduction of the photoplethysmographic signal in pulse transit time measurement" Australas Phys Eng Sci Med 27: 165 (2004).

[90] S. Magder, "The meaning of blood pressure", Magder Critical Care,22:257 (2018).

[91] SeyedehSomayyehMousavia, Mohammad Firouzmandb, Mostafa Charmi, Mohammad Hemmatia, Maryam Moghadamc, YadollahGhorbanid. "Blood pressure estimation from appropriate and inappropriate PPG signals using A whole-based method."Biomedical Signal Processing and Control 47 pp.196–206 (2019).

[92] Xing, Xiaoman, and Mingshan Sun. "Optical blood pressure estimation with photoplethysmography and FFT-based neural networks." Biomedical optics express vol. 7,8 3007-20. (2016).

[93] Hemant Sharma. "Heart rate extraction from PPG signals using variational mode decomposition" Biocybertics and biomedical engineering 39, pp. 75-86 (Elsevier 2019).

[94] G. Drzewiecki. "Noninvasive arterial blood pressure and mechanics." The Biomedical Engineering HandBook, 3rd ed., J. D. Bronzino, Ed. Boca Raton, FL:CRC Press, 2006.

[95] G. L. Pressman and P. M. Newgard. "A transducer for the continuous external measurement of arterial blood pressure." IEEE Trans. Biomed.Eng., vol. 10, pp. 73–81, 1963.

[96] K. Yamakoshi, H. Shimazu, and T. Togawa. "Indirect measurement of instantaneous arterial blood pressure in the human finger by the vascular unloading technique." IEEE Trans. Biomed. Eng., vol. 27, pp.150–155, 1980.

[97] W. W. Nichols, M. F. O'Rourke, and C. Vlachopoulos. "McDonald's Blood Flow in Arteries: Theoretical, Experimental and Clinical Principles" 6th ed. London, UK: Hodder Arnold Publishers, 2011.

[98] H. F. Stegall, M. B. Kardon, and W. T. Kemmerer. "Indirect measurement of arterial blood pressure by doppler ultrasound sphygmomanometry" J. Appl. Physiol., vol. 25, pp. 793–798, 1968.

[99] M. Ramsey. "Noninvasive automatic determination of mean arterial pressure" Med. Biol. Eng. Comput., vol. 17, pp. 11–18, 1979.

[100]L. A. Geddes, M. Voelz, C. Combs, D. Reiner, and C. F. Babbs. "Characterization of the oscillometric method for measuring indirect blood pressure" Ann. Biomed. Eng., vol. 10, pp. 271–280, 1982.

[101]M. Nitzan. "Automatic noninvasive measurement of arterial blood pressure." IEEE Instrum. Meas. Mag., vol. 14, pp. 1094–6969, 2011.

[102] J. Landgraf, S. H. Wishner, and R. A. Kloner. "Comparison of automated oscillometric versus auscultatory blood pressure measurement." The American Journal of Cardiology 106, 386 (2010).

[103] M. Heinemann, K. Sellick, C. Rickard, P. Reynolds, and M. Mc-Grail, "Automated versus manual blood pressure measurement: a randomized crossover trial International Journal of Nursing Practice 14, 296 (2008).

[104] Bhaskar Shahbabu, Aparajita Dasgupta, and Sanjaya Kumar Sahoo. "Which is More Accurate in Measuring the Blood Pressure? A Digital or an Aneroid Sphygmomanometer." Journal of Clinical and Diagnostic Research : JCDR, Vol-10(3): LC11-LC14 (2016).

[105] Turner, Jeffrey M. et al."Blood pressure targets for hemodialysis patients Kidney International, Volume 92, Issue 4, 816 – 823.

[106] D. K. Park, H. S. Oh, J. H. Kang, I. Y. Kim, Y. J. Chee, and J. S. Lee. "Novel method of automatic auscultation for blood pressure measurement using pulses in cuff pressure and korotkoff sound" Computers in Cardiology pp. 181-184 (2008).

[107] J. Jilek and T. Fukushima, "Oscillometric blood pressure measurement: the methodology, some observations, and suggestions." Biomedical Instrumentation & Technology 39, 237 (2005).

[108] Hemanth Kapu, Kavisha Saraswat, Yusuf Ozturk, A. Enis Cetin. "Resting heart rate estimation using PIR sensors." Infrared Physics & Technology, 85, pp. 56–61 (Elsevier 2017).

[109] Parham Nooralishahi, Chu Kiong Loo, Liew Wei Shiung. "Robust remote heart rate estimation from multiple asynchronous noisy channels using autoregressive model with Kalman filter." Biomedical Signal Processing and Control, 47, pp.366–379 (Elsevier 2019).

[110] Arunkumar KR, Bhaskar M. "Heart rate estimation from photoplethysmography signal forwearable health monitoring devices." Biomedical Signal Processing and Control, Volume 50, pp.1–9 (Elsevier 2019).

[111] Erick Javier Argüello Prada & Rafael Daniel Serna Maldonado. "A novel and low-complexity peak detection algorithm for heart rate estimation from low-amplitude photoplethysmographic (PPG) signals." Journal of Medical Engineering & Technology, Volume 42, Issue 8 (2018).

[112] Norihiro Sugita, Narumi Matsuoka, Makoto Yoshizawa, MakotoAbe, Noriyasu Homma, HideharuOtake, Junghyun Kim, Yukio Ohtaki. "Estimation of heart rate variability using a compact radiofrequency motion sensor, Medical Engineering and Physics 37, pp. 1146–1151 (Elsevier 2015).

[113] Kun-Peng Gao, Han-Jia Yang, Xiao-Lin Wang, Bin Yang, Jing-Quan Liu. "Soft pin-shaped dry electrode with bristles for EEG signal measurements." Sensors and Actuators A 283, pp. 348–361 (2018).

[114] Guger C, Krausz G, Allison BZ, Edlinger G. "Comparison of dry and gel based electrodes for p300 brain-computer interfaces." Front Neurosci., 6:60 (2012).

[115] P. Kidmose, D. Looney, M. Ungstrup, M. L. Rank and D. P. Mandic. "A Study of Evoked Potentials from Ear-EEG." in IEEE Transactions on Biomedical Engineering, vol. 60, no. 10, pp.2824-2830, (Oct.2013).

[116] Simon L. Kappel, Mike L. Rank, Hans Olaf Toft, Mikael Andersen, and PrebenKidmose. "Dry-Contact Electrode Ear-EEG." IEEE Transactions on Biomedical Engineering, vol. 66, no. 1, (January 2019).

[117] Xing X, Wang Y, Pei W, et al. "A High-Speed SSVEP-Based BCI Using Dry EEG Electrodes." Sci Rep. 2018;8(1):14708 (2018).

[118] Chi-Chun Lo , Tsung-Yi Chien , Jeng-Shyang Pan , Bor-Shyh Lin. "Novel Non-Contact Control System for Medical Healthcare of Disabled Patients." in IEEE Access, vol. 4, pp. 5687-5694 (2016).

[119] Xing Zhao,Xia Wang and Xiaorong Hou. "A SSVEP Stimuli Encoding Method Using Trinary Frequency-Shift Keying Encoded SSVEP (TFSK-SSVEP)." Front. Hum. Neurosci., Volume 11 Article 278 (2017).

[120] A. Zhigalov, J.D. Herring, J. Herpers, T.O. Bergmann, O. Jensen. "Probing cortical excitability using rapid frequency tagging." NeuroImage 195, pp.59–66 (Elsevier2019)

[121] Alexander M. Dreyer, Christoph S. Herrmann. "Frequency-modulated steady-state visual evoked potentials: A new stimulation method for brain–computer interfaces." Journal of Neuroscience Methods 241, pp.1-9 (Elsevier 2015).

[122] Laura Acqualagna, Sebastian Bosse, Anne K Porbadnigk, Gabriel Curio, Klaus-Robert Müller, Thomas Wiegand, and Benjamin Blankertz. "EEG-based classification of video quality perception using steady state visual evoked potentials (SSVEPs)." J. Neural Eng. 12(IOP) 026012 (16pp) (2015).

[123] Emmanuel K. Kalunga, Sylvain Chevallier, Quentin Barthélemy, Karim DjouaniEricMonacelli, YskandarHamam. "Online SSVEP-based BCI using Riemannian geometry." Neurocomputing 191, pp. 55–68 (Elsevier 2016).

[124] Ajami S, Mahnam A, Behtaj S, Abootalebi V. "An Efficient Asynchronous High-Frequency Steady-State Visual Evoked Potential-Based Brain-Computer Interface speller: The Problem of Individual Differences." J Med Signals Sens, 8(4):pp. 215-224 (2018).

[125] Christopher Gundlach, Matthias M. Müller. "Perception of illusory contours forms intermodulation responses of steady state visual evoked potentials as a neural signature of spatial integration." Biological Psychology 94, pp. 55–60 (Elsevier 2013).

[126] Yogendra Narain Singh, Sanjay Kumar Singh, Phalguni Gupta. "Fusion of electrocardiogram with unobtrusive biometrics: An efficient individual authentication system."Pattern Recognition Letters 33, pp.1932–1941 (Elsevier 2012).

[127] Marcin D. Bugdol, Andrzej W. Mitas. "Multimodal biometric system combining ECG and sound signals." Pattern Recognition Letters 38, pp.107–112 (2014).

[128] Noureddine Belgacem, Régis Fournier, Amine Nait-Ali &FethiBereksi-Reguig. "A novel biometric authentication approach using ECG and EMG Signals." Journal of Medical Engineering & Technology, 39:4, pp. 226-238 (2015).

[129] M. Hammad, Y. Liu and K. Wang. "Multimodal Biometric Authentication Systems Using Convolution Neural Network Based on Different Level Fusion of ECG and Fingerprint." IEEE Access, vol. 7, pp. 26527-26542, 2019.

[130] Su, Kun& Yang, Gongping& Wu, Bo & Yang, Lu & Li, Dunfeng&Su, Peng & Yin, Yilong. "Human Identification using Finger Vein and ECG signals." Neurocomputing 332 (2018).

[131] Su F, Xia L, Cai A, Wu Y, Ma J. "EEG-based personal identification: from proof-of-concept to a practical system." Proceedings twentieth international conference pattern recognition, pp 3728 – 3731(2004).

[132] Lee HJ, Kim HS, Park KS. "A study on the reproducibility of biometric authentication based on electroencephalogram(EEG)." Proceedings of sixth international conference neural engineering (NER), pp 13–16(2013).

[133] La Rocca D, Campisi P, Vegso B, Cserti P, Kozmann G, Babiloni F, Fallani FDV. "Human brain distinctiveness based on EEG spectral coherence connectivity." IEEE Trans Biomed Eng 9294:1–7 (2014).

[134] Singhal GK, Ram Kumar P. "Person identification using evoked potentials and peak Matching." Proceedings of conference biometrics symposium, pp 1–6 (2007).

[135] Yearn SK, Suk HI, Lee SW. "EEG-based person authentication using face stimuli." International winter workshop brain computer interface (BCI), pp 58–61 (2013).

[136] Ramaswamy Palaniappan, Danilo P. Mandic. "Biometrics from Brain Electrical Activity: A Machine Learning Approach" IEEE Transactions on Pattern Analysis and Machine Intelligence, VOL. 29, NO.4 (2007).

[137] Ramaswamy Palaniappan, Danilo P. Mandic. "EEG Based Biometric Framework for Automatic Identity Verification." Journal of VLSI signal processing systems for signal, image and video quality49, 243–250 (2007).

[138] S. Marcel and J. D. R. Millan. "Person authentication using brainwaves (EEG) and maximum a posteriori model adaptation." IEEE Trans. Pattern Anal. Mach. Intell., vol. 29, no. 4, pp. 743–52, Apr. 2007.

[139] Byoung-Kyong Min, Sven Dähne, Min-HeeAhn, Yung-Kyun Noh & Klaus-Robert Müller."Decoding of top-down cognitive processing for SSVEP-controlled BMI." Scientific Reports, Nature (2016).

[140] Steinhubl SR, Wineinger NE, Patel S, et al. "Cardiovascular and nervous system changes during meditation." Front Hum Neurosci., 9:145(2015).

[141] Sze JA, Gyurak A, Yuan JW, Levenson RW. "Coherence between emotional experience and physiology: does body awareness training have an impact?" Emotion, 10(6), pp.803–814 (2010).

[142] Tiantian Jia1, Yoshiko Ogawa1, Misa Miura, Osamu Ito, Masahiro Kohzuki. "Music Attenuated a Decrease in Parasympathetic Nervous System Activity after Exercise." PLOS ONE, February 3, 2016.

[143] Otto, F.: Die Grundform des arteriellen Pulses. Zeitung fürBiologie 37, pp. 483–586 (1899).

[144] N. Westerhof, M.I.M. Noble, N. Stergiopulos. "Arterial WindkesselSnapshots of Hemodynamics:an Aid for Clinical Research and Graduate Education" (1st ed.), Springer Verlag, New York (2005).

[145] E.R. Rietzchel, E. Boeykens, M.L.D. Buyzere, D.A. Duprez, D.L. Clement. "A comparison between systolic and diastolic pulse contour analysis in the evaluation of arterial stiffness" Hypertension, 37 (6), pp. 15-22 (2001).

[146] R. M. Goldwyn and T. B. Watt. "Arterial Pressure Pulse Contour Analysis Via a Mathematical Model for the Clinical Quantification of Human Vascular Properties" IEEE Transactions on Biomedical Engineering, vol. BME-14, no. 1, pp. 11-17, Jan. 1967.

[147] N. Stergiopulos, B. E. Westerhof, J. -. Meister and N. Westerhof. "The four-element Windkessel model." Proceedings of 18th Annual International Conference of the IEEE Engineering in Medicine and Biology Society, Amsterdam, pp. 1715-1716 vol.4. (1996).

[148] Aubuchon, V. Blood Pressure Chart - Normal Blood Pressure Range – Vaughn's Summaries. [online] Vaughns-1-pagers.com. Available at:http://www.vaughns-1-pagers.com/medicine/blood-pressure.htm#bp-range-chart(2017).

[149] Meir Nitzan, ItzchakSlotki and Linda Shavit,"More accurate systolic blood pressure measurement is required for improved hypertension management: a perspective" Medical Devices: Evidence and Research, Volume 10, pp. 157-163(2017).

[150] Paolo Palatini. "Blood pressure measurement in the obese: still a challenging problem." Vol. 16, No 21 (2018).

[151] Osadciw L., Veeramachaneni K. "Fusion, Decision-Level." Li S.Z., Jain A. (eds) Encyclopedia of Biometrics. Springer, Boston, MA (2009).

[152] Shukla A., Tiwari R., Kala R. "Fusion Methods in Biometrics." Towards Hybrid and Adaptive Computing. Studies in Computational Intelligence, vol 307. Springer 2010).

[153] Meva, Dr. Divyakant&Kumbharana, Chandresh&, Associate. "Comparative Study of Different Fusion Techniques in Multimodal Biometric Authentication." International Journal of Computer Applications (2013).

[154] McSharry, P.E., Clifford, G.D., Tarassenko, L., Smith, L.A. "A dynamical model for generating synthetic electrocardiogram signals." IEEE Trans. Biomed. Eng. 50(3) (2003).

[155] Lyon, Aurore et al. "Computational techniques for ECG analysis and interpretation in light of their contribution to medical advances." Journal of the Royal Society, Interface vol. 15,138: 20170821 (2018)

[156] S. Mitra, M. Mitra and B. B. Chaudhuri. "Frequency-plane analysis of normal and pathological ECG signals for disease identification." Journal of Medical Engineering & Technology, Vol. 29, No. 5, pp. 219 – 226 (2005).

[157] Daluwatte, C et al. "Assessing ECG signal quality indices to discriminate ECGs with artefacts from pathologically different arrhythmic ECGs." Physiological measurement vol. 37,8: 1370-82 (2016).

[158] Qin Qin, Jianqing Li, Yinggao Yue, and Chengyu Liu. "An Adaptive and Time-Efficient ECG R-Peak Detection Algorithm." Journal of Healthcare Engineering, vol. 2017, Article ID 5980541, 14 pages, 2017.

[159] Rabbani, Hossein et al. "R peak detection in electrocardiogram signal based on an optimal combination of wavelet transform, hilbert transform, and adaptive thresholding." Journal of medical signals and sensors vol. 1,2: 91-8 (2011).

[160] Park, Jeong-Seon et al. "R Peak Detection Method Using Wavelet Transform and Modified Shannon Energy Envelope." Journal of healthcare engineering vol. 4901017 (2017).

[161] Lee, Seungmin et al. "Efficient Fiducial Point Detection of ECG QRS Complex Based on Polygonal Approximation." Sensors (Basel, Switzerland) vol. 18,12 4502 (2018).

[162] MahsaAkhbari, Mohammad B. Shamsollahi, Omid Sayadi, Antonis A. Armoundas, Christian Jutten. "ECG segmentation and fiducial point extraction using multi hidden Markov model." Computers in Biology and Medicine 79, pp. 21–29 (2016).

[163] E. Plesnik, O. Malgina, J.F. Tasič, M. Zajc. "Detection of the electrocardiogram fiducial points in the phase space using the euclidian distance measure"Medical Engineering & Physics 34 524–529 (Elsevier 2012).

[164] PL Nunez. "Electric Fields of the brain" Oxford University Press, New York,1981.

[165] A. van Rotterdam, F. H. Lopes da Silva, J. van den Ende, M. A. Viergever, and A. J.Hermans. "A model of the spatial-temporal characteristics of the alpha rhythm." Bulletin of mathematical biology, 44(2):283-305, (1982).

[166] F. H. Lopes da Silva, A. Hoeks, H. Smits, and L. H. Zetterberg. "Model of brain rhythmic activity. the alpha rhythm of the thalamus." Kybernetik, 15(1): pp.27-37 (1974).

[167] B. H. Jansen, G. Zouridakis, and M. E. Brandt. "A neurophysiologically-based Mathematical model of ash visual evoked potentials." Biological cybernetics, 68(3): pp. 275-283, 1993.

[168] Spiegler A, Knösche TR, Schwab K, Haueisen J, Atay FM. "Modeling Brain Resonance Phenomena Using a Neural Mass Model." PLoSComput Biol 7(12): e1002298 (2011).

[169] Dimitris Pinotsis, Peter Robinson, Peter beim Graben and Karl Friston. "Neural masses and fields: modeling the dynamics of brain activity." Front. Comput. Neurosci., 17 November 2014.

[170] Fasoli, Diego et al. "The Complexity of Dynamics in Small Neural Circuits." PLoS computational biology vol. 12,8 e1004992. 5 Aug. 2016.

[171] Freeman W.J. "Origin, structure, and role of background EEG activity. Part 1. Analytic amplitude." Clin Neurophysiol 115: pp. 2077-2088 (2004a).

[172] Freeman W.J. "Origin, structure, and role of background EEG activity. Part 2. Analytic phase." Clin Neurophysiol 115: pp. 2089-2107 (2004b).

[173] Freeman W.J. "Origin, structure, and role of background EEG activity. Part 3. Neural frame classification." Clin Neurophysiol 116(5): pp. 1118-1129 (2005).

[174] Wendling, F., Bartolomei, F., Mina, F., Huneau, C., Benquet, P. "Interictal spikes, fast ripples and seizures in partial epilepsies combining multi-level computational models with experimental data." Eur. J. Neurosci. 36(2), 21642177 (2012).

[175] Wendling, F., Bartolomei, F., Bellanger, J.J., Chauvel, P. "Epileptic fast activity can be explained by a model of impaired gabaergic dendritic inhibition." Eur. J. Neurosci. 15(9),14991508 (2002).

[176] Zavalgia, M., Cona, F., Ursino, M. "A neural mass model to simulate different rhythms in a cortical region." Comput. Intell. Neurosci. Hindawi 10 (2010).

[177] David O, Kiebel SJ, Harrison LM, Mattout J, Kilner JM, Friston KJ. "Dynamic causal modeling of evoked responses in EEG and MEG." NeuroImage,30: pp. 1255–1272 (2006).

[178] Herreras, Oscar. "Local Field Potentials: Myths and Misunderstandings." Frontiers in neural circuits vol. 10 101. 15 Dec. 2016.

[179] Jackson, Andrew, and Thomas M Hall. "Decoding Local Field Potentials for Neural Interfaces." IEEE transactions on neural systems and rehabilitation engineering: a publication of the IEEE Engineering in Medicine and Biology Society vol. 25,10 1705-1714 (2017).

[180] Hill, N Jeremy et al. "Recording human electrocorticographic (ECoG) signals for neuroscientific research and real-time functional cortical mapping." Journal of visualized experiments: JoVE ,64 3993. 26 Jun. 2012.

[181] Li, Yue et al. "Gesture Decoding Using ECoG Signals from Human Sensorimotor Cortex: A Pilot Study." Behavioural neurology vol. 2017 (2017): 3435686.

[182] Irie T, Yamakawa K, Hamon D, Nakamura K, Shivkumar K, Vaseghi M. "Cardiac sympathetic innervation via middle cervical and stellate ganglia and antiarrhythmic mechanism of bilateral stellectomy." Am J Physiol Heart Circ Physiol , 312: H392–405 (2017).

[183] Buckley U, Yamakawa K, Takamiya T, Andrew Armour J, Shivkumar K, Ardell JL. "Targeted stellate decentralization: implications for sympathetic control of ventricular Electrophysiology." Heart Rhythm, 13:282–8 (2016).

[184] Ellison JP, Williams TH. "Sympathetic nerve pathways to the human heart, and their Variations." Am J Anat ,124: pp. 149–162 (1969).

[185] Mizeres NJ. "The cardiac plexus in man." Am J Anat :112: pp.141–151 (1963).

[186] Ajijola OA, Vaseghi M, Zhou W, et al. "Functional differences between junctional And extra junctional adrenergic receptor activation in mammalian ventricle." Am J Physiol Heart Circ Physiol ,304:H579–88 (2013).

[187] Shivkumar K, Ajijola OA, Anand I, et al. "Clinical neurocardiology defining the value of neuroscience-based cardiovascular therapeutics".J Physiol;594:3911–54, (2016).

[188] Wang HJ, Wang W, Cornish KG, Rozanski GJ, Zucker IH. "Cardiac sympathetic Afferent denervation attenuates cardiac remodeling and improves cardiovascular dysfunction in rats with heart failure.", Hypertension ;64: pp.745–755 (2014).

[189] Vaseghi M, Zhou W, Shi J, et al. "Sympathetic innervation of the anterior left ventricular wall by the right and left stellate ganglia." Heart Rhythm ,9: pp.1303–9(2012).

[190] Vaseghi M, Yamakawa K, Sinha A, et al. "Modulation of regional dispersion of repolarization and T-peak to T-end interval by the right and left stellate ganglia." Am J Physiol Heart Circ Physiol , 305:H1020–30 (2013).

[191] Randall DC, Brown DR, McGuirt AS, Thompson GW, Armour JA, Ardell JL. "Interactions within the intrinsic cardiac nervous system contribute to chronotropic regulation." Am J PhysiolRegulIntegr Comp Physiol , 285: R1066–75 (2003).

[192] Ulphani JS, Cain JH, Inderyas F, et al. "Quantitative analysis of parasympathetic innervation of the porcine heart." Heart Rhythm, 7: pp. 1113–9(2010).

[193] Yamakawa K, Rajendran PS, Takamiya T, et al. "Vagal nerve stimulation activates vagal afferent fibers that reduce cardiac efferent parasympathetic effects." Am J Physiol Heart Circ Physiol ,309:H1579–90 (2015).

[194] Yamakawa K, So EL, Rajendran PS, et al. "Electrophysiological effects of right and left vagal nerve stimulation on the ventricular myocardium." Am J Physiol Heart Circ Physiol, 307:H722–31 (2014).

[195] Ardell JL, Rajendran PS, Nier HA, KenKnight BH, Armour JA. "Central-peripheral neural network interactions evoked by vagus nerve stimulation: functional consequences on control of cardiac function." Am J Physiol Heart Circ Physiol 309:H1740–52 (2015).

[196] Lewis, M. J., Short, A. L. "Autonomic nervous system control of the cardiovascular and respiratory systems in asthma." Respir. Med. 100(10), 1688–1705 (2006).

[197] Shaffer, F., McCraty, R., Zarr, L. "A healthy heart is not a metronome: an integrative Review of the heart's anatomy and heart rate variability." Front. Psychol. 5, 1040 (2014).

[198] Ursino, M. "Interaction between carotid baroregulation and the pulsating heart: a mathematical model." AMJ Physiol. 275(5), H1733–H1747 (1998).

[199] McCraty, R., Shaffer, F. "Heart rate variability: new perspectives on physiological mechanisms, assessment of self-regulatory capacity, and health risk." Glob. Adv. Health Med. 4(1), 46–61 (2015).

[200] Jang, A., Hwang, S.K., Padhye, N.S., Meininger, J.C. "Effects of cognitive behavior therapy on heart rate variability in young females with constipation-predominant irritable bowel syndrome: a parallel-group trial." J. Neurogastroenterol. Motil. 23(3), 435 (2017).

[201] Sowder, E. "Restoration of vagal tone, a possible mechanism for functional abdominal pain." Appl. Psychophysiol. Biofeedback 35(3), 199–206 (2010).

[202] Reardom, M., Malik, M. "Changes in heart rate variability with age." Pacing Clin. Electrophysiol., 19(11), 1863–1866 (1996).

[203] Elsenbruch, S., Harnish, M.J. "Heart rate variability during waking and sleep in healthy males and females." Sleep 22(8), 1067–1071 (1999).

[204] Cerutti, C., Barres, C., Paultre, C. "Baroreflex modulation of blood pressure and heart rate variabilities in rats: assessment by spectral analysis." Am. J. Physiol. 266(5), H1993–H2000, (1994).

[205] Cacioppo, J.T., Berntson, G.G. "The affect system architecture and operating Characteristics." Curr. Dir. Psychol. Sci. 8(5), 133–137 (1999).

[206] Berntson, G.G. "Heart rate variability: origins, methods, and interpretive caveats." Psychophysiology, 34(6), 623–648 (1997).

[207] Billman, G.E. "The LF/HF ratio does not accurately measure cardiac sympatho-vagal balance." Front. Physiol. 4, 26 (2013). PMC. Web. 29 (Nov 2017).

[208] Taylor, S. "Tend and befriend, "Biobehavioral bases of affiliation under stress", Curr. Dir.Psychol Sci. 15(6), 273–277 (2006).

[209] McFarland, D.J., Wolpaw, J.R. "Brain-computer interfaces for communication and control" Commun. ACM 54(5) (2011).

[210] Fazel-Rezai, R., et al. "P300 brain computer interface: current challenges and emerging trends." Frontiers Neuroeng. 5, 14 (2012).

[211] Kübler, A, and N Birbaumer. "Brain-computer interfaces and communication in paralysis: extinction of goal directed thinking in completely paralysed patients?" Clinical neurophysiology: official journal of the International Federation of Clinical Neurophysiology vol. 119,11: 2658-66 (2008).

[212] Neuper, C., Muller-Putz, G.R., Scherer, R. "Motor imagery and EEG-based control of spelling devices and neuroprostheses." Prog. Brain Res. 159, 393–409 (2006).

[213]Muller-Putz, G.R., Scherer, R., Neuper, C. "Steady-state somatosensory evoked potentials: suitable brain signals for brain-computer interfaces?" IEEE Trans. Neural Syst. Rehabil. Eng.14(1) (2006).

[214]Kaufmann, T., Herweg, A., Kübler, A. "Toward brain-computer interface based wheelchair control utilizing tactually-evoked event-related potentials." J. Neuro Eng. Rehabil. 11(1), 7(2014).

[215]Kaongoen, N., Jo, S. "A novel hybrid auditory BCI paradigm combining ASSR and P300." J. Neurosci. Methods 279, 44–51 (2017).

[216]Waisbourd, Michael et al. "Short-duration transient visual evoked potentials and color reflectivity discretization analysis in glaucoma patients and suspects." International journal of ophthalmology vol. 10, 2 254-261. (2017).

[217]Matthias M. Müller, Wolfgang Teder-Sälejärvi and Steven A., Hillyard. "The time course of cortical facilitation during cued shifts of spatial attention." Nature Neuroscience, Vol 1, Issue 7, pp 631- 634 ,1998.

[218]Ding, Jian, George Sperling, and Ramesh Srinivasan. "Attentional Modulation of SSVEP Power Depends on the Network Tagged by the Flicker Frequency." Cerebral Cortex , 1016–1029 (2006).

[219]XiaogangChen,ZhikaiChen,Shangkai Gao &Xiaorong Gao. "A high- ITR SSVEP-based BCI speller" Brain Computer Interfaces – Taylor& Francis Online, Vol 1 Issue 4 (2014).

[220]Rahib H. Abiyev, NurullahAkkaya,ErsinAytac,IrfanGünsel,and Ahmet Çağman. "Computer Interface for Control of Wheelchair Using Fuzzy Neural Networks" Biomed Research International, Volume 2016 (2016).

[221]Minjue Wang, Ian Daly, Brendan Z. Allison, Jing Jin,YuZhanga, Lanlan Chena, Xingyu Wang. "A new hybrid BCI paradigm based on P300 and SSVEP." Journal of Neuroscience Methods 244: 16–25 (2015).

[222]Lenis Meriño, Tapsya Nayak, Prasanna Kolar, Garrett Hall, Zijing Mao, Daniel J. Pack &Yufei Huang. "Asynchronous control of unmanned aerial vehicles using a steady-state visual evoked potential-based brain computer interface." Brain-Computer Interfaces, 4:1-2, 122-135 (2017).

[223]Richard W. Homan."The 10-20 Electrode System and Cerebral Location." American Journal of EEG Technology ,Volume 28,Issue 4 (1988)

[224] Yohei Tomita, Franc¸ois-Benoˆıt Vialatte, G´erard Dreyfus, Yasue Mitsukura, Hovagim Bakardjian, and Andrzej Cichocki, Bimodal. " BCI Using Simultaneously IRS and EEG." IEEE TRANSACTIONS ON BIOMEDICAL ENGINEERING, VOL. 61, NO.4, APRIL 2014.

[225] Zifkin, B.G., Inoue, Y. "Visual reflex seizures induced by complex stimuli." Epilepsia 45, 27–29 (2004).

[226] Lin, Z., Zhang, C., Wu, W. "Frequency recognition based on canonical correlation analysis for SSVEP-based BCIs." IEEE Trans. Biomed. Eng. 54(6), 1172–1176 (2007).

[227] Nakanishi, M., et al. "A comparison study of canonical correlation analysis based methods for detecting steady-state visual evoked potentials." Yao, D. (ed.) PLoSONE 10(10) (2015).

[228] Wu, Z. "SSVEP extraction based on the similarity of background EEG." Di Russo, F. (ed)PLoS ONE 9(4) (2014).

[229] Vapnik. "The Nature of Statistical Learning Theory." Springer, N.Y., ISBN- 0-387-94559-8 (1995).

[230] Yuanqing Li, Jinyi Long, Tianyou Yu. "An EEG-Based BCI System for 2-D Cursor Control by Combining Mu/Beta Rhythm and P300 Potential." IEEE Transactions on Biomedical Engineering, Vol 1 Issue 10 (2010.)

[231] Rahib H. Abiyev, Nurullah Akkaya, Ersin Aytac, Irfan Günsel, and Ahmet Çağman. "Computer Interface for Control of Wheelchair Using Fuzzy Neural Networks" Biomed Research International Volume 2016 (2016).

[232] Mike Cohen. "Comparison of different spatial transformations applied to EEG data: A case study of error processing." International Journal of Psychophysiology 97, pp. 245– 257 (2015).

[233] Howard, Marc W. "Temporal and spatial context in the mind and brain." Current opinion in behavioral sciences vol. 17: pp. 14-19 (2017).

[234] Naruhito Hironaga, Takako Mitsudo, Mariko Hayamizu, Yoshitaka Nakajima, Hiroshige Takeichi , ShozoTobimatsu . "Spatiotemporal brain dynamics of auditory temporal assimilation" Scientific Reports volume 7, Article number: 11400 (2017).

[235] A. A. Ioannides. "Dynamic functional connectivity." Current Opinion Neurobiol., vol. 17, pp. 161–170, (2007).

[236] B. He, Y. K. Dai, L. Astolfi, F. Babiloni, H. Yuan, and L. Yang. "eConnectome: A MATLAB toolbox for mapping and imaging of brain functional connectivity." J. Neurosci. Methods, vol. 195, pp. 261–269, (2011).

[237] C. W. J. Granger. "Investigating causal relations by econometric models and cross-spectral methods." Econometrica, vol. 37, no. 3, pp. 414–417, (1969).

[238] Byoung-Kyong Min, Sven Dähne, Min-HeeAhn, Yung-Kyun Noh & Klaus-Robert Müller. "Decoding of top- down cognitive processing for SSVEP-controlled BMI", Scientific Reports, Nature (2016).

[239] F. Babiloniet al. "Estimation of the cortical functional connectivity with the multimodal integration of high-resolution EEG and fMRI data by directed transfer function." Neuroimage, vol. 24, no. 1, pp. 118–131, (2005).

[240] L. Astolfiet al. "Comparison of different cortical connectivity estimators for high-resolution EEG recordings" Human Brain Mapping, vol. 28, pp. 143–157, (2007).

[241] R. Kus, M. Kaminski, and K. J. Blinowska. "Determination of EEG activity propagation: Pair-wise versus multichannel estimate." IEEE Trans. Biomed. Eng., vol. no. 9, pp. 1501–1510, (2004).

[242] C. W. J. Granger. "Investigating causal relations by econometric models and cross-spectral methods." Econometrica, vol. 37, no. 3, pp. 414–417 (1969).

[243] T. Schneider and A. Neumaier, "Algorithm 808: ARfit—A MATLAB package for the estimation of parameters and eigenmodes of multivariate autoregressive models,"ACM Trans. Math. Softw., vol. 27, pp. 58–65, (2001).

[244] L. Ding, G. A. Worrell, T. D. Lagerlund, and B. He. "Ictal source analysis: Localization and imaging of causal interactions in humans." Neuroimage, vol. 34, pp. 575–586, (2007).

[245] Chih-Wei Hsu and Chih-Jen Lin "A comparison of methods for multiclass support vector machines." in IEEE Transactions on Neural Networks, vol. 13, no. 2, pp. 415-425, (2002).